NUMERICAL MODELING OF THE FLOW FIELD FOR INDOOR THERMAL COMFORT OF A BUILDING UNDER STACK EFFECT

P. H. Viraj Nimarshana

(108015N)

Thesis submitted in partial fulfilment of the requirements for the degree Master of Science

Department of Mechanical Engineering

University of Moratuwa

Sri Lanka

April 2015

DECLARATION

I declare that this is my own work and this thesis does not incorporate without acknowledgement any material previously submitted for a Degree or Diploma in any other University or institute of higher learning and to the best of my knowledge and belief it does not contain any material previously published or written by another person expect where the acknowledgment is made in text.

Also, I hereby grant to University of Moratuwa the non-exclusive right to reproduce and distribute my thesis, in whole or in part in print, electronic or other medium. I retain the right to use this content in whole or part in future works (Such as articles or books)

....

P.H. Viraj Nimarshana Date

The above candidate has carried out research for the Masters Dissertation under my supervision.

....

Prof. R.A. Attalage Date

....

Prof. K.K.C.K. Perera Date

To My Beloved Parents

ACKNOWLEDGEMENT

On the successful completion of my thesis, I would like to express my regards and thoughts, to acknowledge the contributions of all those, who stood beside me and supported me towards the completion of my MSc.

First and foremost, I would like to express my deep sense of gratitude and extend my heartfelt thanks towards my supervisor, Prof. R.A. Attalage who guided me to become a thinking researcher. His deep insight into the subject, scientific attitude and skills to troubleshoot the problems has been vital in the completion of this thesis. Despite his extremely busy schedule, he has always been available for discussions and to provide me with guidance. I feel blessed and extremely lucky to have a guide and mentor like him early in my career.

I am extremely grateful to my co-supervisor, Prof. K.K.C.K. Perera. His valuable suggestions from time to time have been of great value.

Special thanks to Kasun Anjana, Amal Senevirathne and Thiwanka Wickramasooriya in Department of Mechanical engineering for all their unconditional support. Sincere thanks goes also to all members of Department of Mechanical engineering, University of Moratuwa, for their valuable suggestions and co-operation.

I also express my deep sense of gratitude towards my beloved parents, brothers and my wife for their unflinching care and encouragement.

Last but not the least, the financial help from Department of Mechanical Engineering, University of Moratuwa is duly acknowledged.

P.H. Viraj Nimarshana

Abstract

In recent years natural ventilation is widely recognised as excellent contributing towards in design low energy buildings. The main challenge in natural ventilation is identified as lack of knowledge in providing acceptable thermal comfort in an occupied space to meet the internal requirements against the prevailing climatic conditions variations. Numerical investigations of the indoor thermal comfort condition in a simple office space governed by the solar chimney stack effect have been undertaken using CFD techniques. A mathematical model was developed based on the relevant analytical framework governing the phenomena to simulate the velocity flow field and temperature distribution on the designated plane within the indoor space. Boussinesq approximation was incorporated to numerical scheme with realistic boundary conditions for flow simulation. The model was enriched by incorporating a sufficient fluid volume to represent environment surrounding the space and thereby eliminating the entry effect to the flow. Hexahedral cells were used in a non-uniform grid distribution to minimise numerical diffusion. A fine mesh is used near the walls to enhance the resolution and accuracy resolving the problems under the turbulent flow conditions. Grid independence analysis was carried out to ensure the accuracy of the numerical results. Under-relaxation factors 0.3, 1, 2, 0.8, 0.8, 1, 0.9 for pressure, density, momentum, turbulence kinetic energy, turbulence dissipation rate, turbulent viscosity, energy respectively were used. The model outputs were compared with the available experimental measurements taken under the same condition to calibrate the numerical scheme. A parametric study was carried out using the calibrated model to assess the distribution of thermal comfort index against the changes in geometrical and solar radiation parameters. The values of activity, metabolic rate for seated activity and clothing insulation were selected as 0, 60 W/m^2 and 0.5 Clo respectively for thermal performance analysis. The effect of each input parameter was investigated in terms of mean value and standard deviation corresponding to the flow velocity and the PPD_{NV} value. It can be concluded that the present model is capable of predicting the indoor thermal performance of a building under stack effect.

Keywords: *Natural ventilation, Solar chimney, Thermal comfort, CFD, Tropical climate*

TABLE OF CONTENTS

LIST OF FIGURES

LIST OF TABLES

LIST OF ABBREVIATIONS

(ACH) - Air Changes per Hour

(ASHRAE) - American Society of Heating, Refrigerating and Air-conditioning Engineers

(ASM) - Algebraic Stress Model

(CFD) - Computational Fluid Dynamic

(DNS) - Direct Numerical Simulation

(LEED) - Leadership in Energy and Environmental Design

(LES) - Large Eddy Simulation

(MET) - Metabolic Rate

(MRT) - Mean Radiant Temperature

(PCG) - Preconditioned Conjugate Gradient

(PD) - Percentage of Dissatisfied

(PMV) - Predicted Mean Vote

(PMV_{NV}) - Predicted Mean Vote Natural Ventilation

(PPD) - Predicted Percentage of Dissatisfied

(PPM) - Parts Per Million

(PPD_{NV}) - Predicted Percentage of Dissatisfied under Natural Ventilation

(RANS) - Reynolds Averaged Navier-Stokes

(RNG) - Renormalisation Group

(RSM) - Reynolds Stress Model

(SIMPLE) - Semi-Implicit Method for Pressure-Linked Equations

(TMY2) - Typical Metrological Year 2

(USGBC) - United State Green Building Council

1 INTRODUCTION

1.1 Problem Statement

Thermal comfort, where a majority of the people will feel reasonably comfortable is an essential requirement to make a comfort zone in most indoor workplaces for safety and health. Depending on the environmental and individual factors, the thermal comfort zone varies from workplace to workplace. Most of the office buildings use active methods to establish and control thermal comfort. But the cost increases due to price of equipment and accessories required installing, maintenances and steadily increasing world market prices of all forms of primary and secondary energy sources. Leadership in Energy and Environmental Design (LEED) certificate is a market tool introduced by United State Green Building Council (USGBC) to take building designers, contractors and operators towards energy efficiency and sustainability of green architecture, green operations and maintenance strategies. Therefore different green certification schemes are followed to implement green building design and construction to reach internationally accepted certification for commercial, industrial and institutional building such as LEED.

In this regard natural ventilation can play an important role specially in climates such as Sri Lanka where the temperatures do not go to extreme high values and extreme low values. Adopting stack effect to achieve/envisage required levels of thermal comfort in buildings could save energy and money. Therefore, investigation of internal flow fields of buildings under natural ventilation is not only timely due to energy scenario but also useful.

1.2 Study Objectives

- Study the thermal comfort aspects of commercial buildings under natural ventilation.
- Develop a mathematical model to simulate the velocity field and temperature distribution of naturally ventilated buildings under stack effect using Computational Fluid Dynamic (CFD) techniques.
- Validation of the numerical scheme by means of the experimental results.
- Establish governing parameters of stack effect and study their influence using simulated results.

1.3 Research Methodology

A literature survey is carried out to identify the thermal comfort aspect in commercial buildings and American Society of Heating, Refrigerating and Air-conditioning Engineers (ASHRAE) standards related to it. Different mathematical modelling techniques available for analysing natural ventilation systems under stack effect are investigated and one of them suit for the research is to be selected. Based on selected CFD simulating tool, a natural ventilation model under stack effect is developed to identify the velocity field and temperature distribution in using the realistic boundary conditions. Then the model is validated using the available experimental results. Finally, validated model is used to analysis the indoor thermal comfort of the different configuration adopting predicted mean vote and predicted percentage of dissatisfaction model developed for naturally ventilated spaces.

1.4 Expected Contribution

A background should be developed to understand the governing parameters which influence the thermal performance of a naturally ventilated building under stack effect. Further, mathematical framework is developed to visualize the temperature distribution and velocity field of indoor space. Thermal performance analysis is carried out based on the variation of environmental parameters helps to identify potential areas for natural ventilation. Outcomes of the analysis can be used to select suitable location to construct naturally ventilated buildings. Finally, it is expected to use this knowledge to design green buildings and extend the same for green building certification.

2 LITERATURE REVIEW

2.1 Introduction

It is necessary to provide buildings with adequate ventilation to ensure both removals of stale air and the supply of fresh air for occupants. This can be provided in different ways, which include: mechanical ventilation, in which fans and ducts are used to move large volume of air with or without heating the air; air conditioning, in which the temperature and humidity of air supplied via fans and ducts is fully controlled: and natural ventilation which harnesses the naturally occurring driving forces of wind and buoyancy. It is also possible to use a hybrid approach which uses both natural forces and mechanical means (usually fans and blowers). These are known as mixed-mode systems.

The main disadvantages of air conditioning are: cost, in terms of capital, running and maintenance; and the large amount of space required to house the necessary equipment. Furthermore, there is evidence to suggest that air conditioning systems are more likely to cause occupants health complaints than natural or mechanical ventilation (Wilson and Hedge 1987).

Given today's efforts to reduce energy usage and CO_2 emissions, there is an increasing trend to move away from air conditioned buildings. Consequently, many architects and building designers have turned their attention towards naturally ventilated or mixed mode techniques. Although such buildings use innovative techniques, many have been completed with a high degree of success (Jones et al 1998).

Due to the non-predetermination nature of natural ventilation systems, much care is needed at the design stage to ensure that the ventilation strategy will perform successfully under foreseeable climatic and occupancy scenarios. In particular that acceptable air change rates will be obtained. Predictions of such parameters are much easier in a mechanically driven system since the designer knows, to a high degree of accuracy, the volume flow rates produced by the various components that make up the system. When designing natural ventilation strategies however, the only way to predict the flow rates is by means of either a physical or mathematical model. This thesis concerns mathematical model with criteria used to select appropriate numerical schemes and solution techniques for such problems.

Physical modelling has been carried out successfully by researchers at Cambridge University using the salt bath modelling technique whereby Perspex models of a building are inverted and submerged in a tank of fresh water with brine solution used to represent temperature differences (Lame-Serff et al. 1991). The brine is dyed to enable flow visualisation. This technique enables air change rates and temperature differences to be predicted.

Since the advent of more powerful, affordable, desk top computers, another tool has become accessible to designers called Computational Fluid Dynamics. This technique considers the air flow in a space by dividing the space in to small cells and solving the equations which govern the airflow and temperature distribution. This offers the immediate advantage over the salt bath modelling approach of being able to provide information about the flow at many positions throughout the domain interest. It also enables changes to the geometry and operating conditions to be made more easily, offering an ideal tool for investigating many ventilation options early in the design process.

In the thesis, reference cited point to limitations in the CFD technique for reliably modelling buoyancy driven flows. These can be attributed to the small forces responsible for bringing about buoyancy driven flows in buildings which can cause instabilities in the solution process, knowledge still lacking in how to accurately model turbulence, and the best way of solving the set of governing equations. Consequently, there is still much scope for validation and improvements of CFD codes in the buoyancy driven force.

2.2 The Need for Natural Ventilation

Without ventilation, a building's occupants will initially be troubled by odours and other possible contaminants and heat. Sometime, humidity may rise because of indoor moisture sources such as the occupants, laundry activities, cooking and plants respiration; thus enhancing moisture hazards such as mould growth and condensation. The purpose of ventilation is to eliminate airborne contaminants, which are generated both by human activity and by the building itself. These are:

- bad odours, to which people entering the room are very sensitive
- moisture, which increases the risk of mould growth
- carbon dioxide (CO_2) gas, which may induce lethargy at high concentrations

- dust, aerosols and toxic gases resulting from human activity, as well as from the building materials. in principle, 'clean' materials should be chosen for internal use, but this is not always possible.
- excessive heat - The airflow rate required to ensure good indoor air quality depends upon the contaminant sources' strengths and on their maximum acceptable
- Concentration - larger the contaminant sources' strengths or the smaller the maximum acceptable concentration, then it leads to greater the required ventilation rate.

During the heating season in well-designed and clean buildings, the occupants are the main source of contaminants and the contaminant level will increase because of mostly odours and water vapour. The airflow rate should then be between 22 cubic metres per hour (m^3/h) per person, which limits the CO_2 concentration to about 1000 parts per million (ppm) above the outdoor concentration, and 54 m^3/h per person, which limits the CO_2 concentration to about 400 ppm above the outdoor concentration. It means that less than 10 per cent of people entering the room will be dissatisfied by the odour (CEN, 2006). Airflow rates should be much greater in poorly insulated buildings because there is a risk of mould growth and water vapour condensation, or in spaces where there is a particular source of contamination, including spaces where smoking is allowed. In heating, the minimum airflow rate may be much greater than the hygienic airflow rate in order to evacuate heat or provide cooling draughts.

However, when the outdoor temperature exceeds indoor temperatures, it may be wise to reduce the ventilation rate, only allowing high levels of ventilation at night when the outdoor temperature is low. Ventilation is hence not only essential to ensure an acceptable indoor air quality, but is also often used to improve thermal comfort. For this air heating or cooling, air conditioning (including air humidity control) or free cooling in which increasing the outdoor airflow rate to cool down the building envelop are used. In order to achieve these goals, several conditions should be met:

- Airflow rates should be adapted to need: if too low, good air quality will not be achieved, or draughts, noise and energy waste may result from an excessive airing.

- The air should be well distributed: ideally, the fresh air should reach any occupied zones first and contaminated air should be quickly extracted.
- The air supply should not decrease comfort. It should not cause complaints about draughts, noise or poor air quality.
- The air supplied by ventilation systems should be clean and, where appropriate, should comply with the temperature and moisture requirements.

In addition, to comply with a sustainable development policy, the ventilation systems should be energy efficient and should perform as required using a minimum amount of energy.

2.3 Human Thermal Comfort

Thermal comfort, where a majority of people will feel reasonably comfortable is an essential requirement to make a comfort zone in most indoor workplaces such as offices, factories, shops and laboratories for safety and health. Depending on the environmental factors such as air temperature, air velocity, humidity and radiant temperature and individual factors such as clothing and activity, the thermal comfort zone varies from workplace to workplace. In addition to these parameters, local thermal discomfort can be occurred due to high vertical temperature difference between head and ankles or higher asymmetry of radiant temperature with the space.

2.3.1 Thermal comfort analysis in naturally ventilated space

CFD provides much more detailed information about velocity fields and temperature distributions. That allows to perform a comprehensive thermal comfort analysis in the regularly occupied areas of the buildings. The solution given by CFD techniques has more detailed and accurate results compared to the solution given by approximated analytical procedure (Oosthuizen and Lightstone 2009).

Lot of research has been done on thermal comfort analysis related to buildings during past decade and now these studies available as models, standards and procedures on Fanger (1970), ISO 7730 and ASHRAE Standard 55 2007 - Thermal comfort.

2.3.2 Thermal comfort indices

Thermal comfort indices are used to analyse the integrated effect of air, radiant temperature and relative humidity. Presently, the thermal comfort indices Predicted Mean Vote (PMV) and Predicted Percentage of Dissatisfied (PPD) of Fanger (1970) are adopted in ISO 7730 and are calculated by empirical equations given in ISO

7730. The PMV index predicts the mean response of a large group of people according to the ASHRAE thermal sensation scale and defined in terms of the heat load that would be required to restore a state of "Comfort". It is evaluated by PMV equation, which is based on steady-state heat balance for the human body. For air-conditioned buildings, it can be expressed as,

$$PMV = [0.303\ exp\ (-\ 0.036\ M\ ) + 0.028]\ L \tag{2.1}$$

Where, M is the metabolic rate (W/m^2)

L is the thermal load on the body.

Thermal load defined as follows:

L = [Internal Heat Production] – [Heat Loss to the Actual Environment]

Further, it expressed as,

$$L = M - W - \{3.96 \times 10^{-8} f_{cl} [(T_{cl} +273)^4 - (T_r+273)^4] + f_{cl} h_c (T_{cl} - T) + 3.05 \times 10^{-3} [5733 - 6.99 (M - W) - P_v] + 0.42 (M - W - 58.15) + 1.7 \times 10^{-5} M (5867 - P_v) + 0.0014M (34 - T)]\} \tag{2.2}$$

Where, W stands for active work or shivering (W/m^2)

f_{cl} is the garment insulation factor

(1 clo = 0.155 m^2 K/W)

f_{cl} is defined according to the conditions of the resistance to sensible heat transfer provided by a clothing ensemble, I_{cl} (clo)

$$f_{cl} = \begin{cases} 1.05 + 0.645\, I_{cl} & ;\ \text{for } I_{cl} > 0.078 \\ 1.05 + 1.291\, I_{cl} & ;\ \text{for } I_{cl} < 0.078 \end{cases} \tag{2.3}$$

The T_{cl} (^{o}C) term is defined as the cloth temperature and is determined below as:

$$T_{cl} = 35.7 - 0.028\ (M - W) - I_{cl}\ \{\ 3.96 \text{ x } 10 \text{ x } 10^{-8} f_{cl} [(T_{cl} +273)^4 - (T_r+273)^4] + f_{cl} h_c (T_{cl} - T)\} \tag{2.4}$$

Where, T (^{o}C) is local air temperature

h_c is the heat transfer coefficient between the cloth and air (W/m^{2}K)

T_r (^{o}C) is the mean radiant temperature

The heat-transfer coefficient h_c is calculated based on the relationship between local velocity, u and temperature difference between cloth and local air as follows:

$$f_{cl} = \begin{cases} h_c = 2.38\ (T_{cl} - T)^{0.25} & ;\ \text{for } (T_{cl} - T)^{0.25} > 12.1\ u^{0.5} \\ h_c = 2.38\ u^{0.5} & ;\ \text{for } (T_{cl} - T)^{0.25} < 12.1\ u^{0.5} \end{cases} \tag{2.5}$$

However, it has been proven that the traditional PMV index is inadequate for naturally ventilated buildings. Therefore, an optional thermal comfort model, also known as adaptive comfort standard is implemented in the new revised ASHRAE Standard 55. This model is used to determine thermal comfort in entirely naturally ventilated spaces by means of its indoor temperature and mean monthly outdoor temperature.

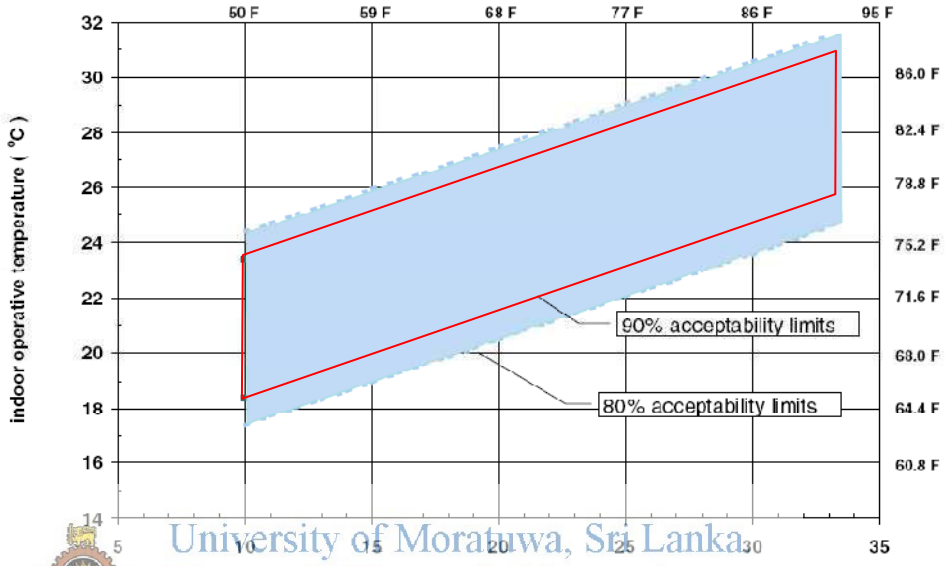

Figure 2.5: Adaptive comfort standard for naturally ventilated buildings - ASHRAE Standard 55

However, there are limitations (Fanger and Toftum, 2002) such as that it is only applicable to mean monthly temperatures from 10°C to 33°C and that only information of global thermal discomfort in large spaces is provided.

Fanger and Toftum (2002) introduced an extended PMV for natural ventilation (PMV_{NV}) comfort model more suitable for naturally ventilated buildings which can be considered consistent with the traditional PMV model. The PMV_{NV} index represents an extension of the traditional PMV model to account for the occupants 'expectancy factor' according to their habitat, as well as to the estimated activity. Further, the metabolic rate is reduced for every scale unit of PMV above neutral, a PMV of 1.5 corresponds to a reduction in the metabolic rate of 10% under hot and humid conditions. The expectancy factor is multiplied by the traditional PMV to give the mean thermal sensation vote of the occupants of a naturally ventilated building in a warm climate. The expectancy factor is estimated to vary between 1 and 0.5. If the weather is warm all year or most of the year, expectancy factor may be 0.5. In

regions with only brief periods of warm weather occur during the summer, the expectancy factor may be 0.9 - 1.0. It is 1.0 for the air-conditioned buildings. In this model, PMV and PPD (%) for natural ventilation are determined as follows:

$$PMV_{NV} = e\,[0.303 \exp(-0.036\, M_{red}) + 0.028]\, L \quad (2.6)$$

$$PPD\ (\%) = 100 - 95 \exp[-0.03353\,(PMV_{NV})^4 - 0.2179\,(PMV_{NV})^2] \quad (2.7)$$

Where, e, is the expectancy factor and M_{red} is reduced metabolic rate.

The PPD equation indicates the variance in the thermal sensation of a group of persons exposed to the same thermal conditions. Dissatisfaction with the thermal environment, discomfort was defined by participants using the 7 point scale: cool (–2), cold (–3), warm (+2) or hot (+3). Under optimal thermal conditions (PMV = 0), 5% of persons will be dissatisfied assuming identical activity level, clothing, and environmental conditions.

The PMV and PPD are calculated from six basic variables: activity, clothing, air temperature, air velocity, mean radiant temperature (MRT), and relative humidity. The values of the variables for the activity (metabolic rate) and clothing (ensemble insulation) are determined from ASHRAE Fundamentals. In order to quantify thermal comfort in naturally ventilated buildings, the models discussed above may be integrated into a CFD model.

For draft assessment, the Percentage Dissatisfied (PD) index may be used to calculate the risk of thermal discomfort due to draft. The thermal comfort empirical equation for Percentage of Dissatisfied (PD) of Fanger (1970) adopted in ISO 7730 is normally used and is given below:

$$PD = (34 - Ta)(V\text{-}0.05)^{0.62} \times (0.37\, Tu + 3.14) \quad (2.8)$$

This equation requires the values of three parameters; velocity, V, air temperature, Ta, and turbulence intensity, Tu as a percentage.

Some other studies have developed models which could enhance the study of thermal comfort in the indoor environment (Stavrakakis et al. (2008), Fanger and Toftum (2002), Dear and Brager (1998)). Stamou et al. (2007) used a CFD code to calculate the airflow and temperature fields for the evaluation of the thermal comfort conditions in the indoor Galatsi Arena. The calculated mean velocities and temperatures were used to determine the thermal comfort indices PMV and PPD and

to evaluate the thermal conditions in the various regions of the Arena. It was found that the thermal conditions in the Galatsi Arena were satisfactory.

Kavgic et al. (2008) evaluated the thermal comfort and indoor air quality in a mechanically ventilated theatre based on monitoring air speed, temperature, relative humidity and heat flux by using CFD modelling. It was shown that for most of the monitored periods, the environmental parameters were within the standard limits of thermal comfort. The authors pointed out that the theatre was over-ventilated and the ventilation system employed led to higher complaints of cold discomfort. Li and Pitts (2006) carried out thermal comfort and environmental modelling in atrium buildings and developed a tool for the evaluation of thermal comfort level in atrium spaces. The temperature field was obtained from CFD modelling and a code was developed based upon the combination of solar radiation and radiant heat transfer from the walls to calculate mean radiant temperature.

Cheong et al. (2003) evaluated the thermal comfort conditions of an air-conditioned theatre in a tertiary institution using CFD modelling and subjective assessment. It was found that the predicted results showed good distributions of air flow characteristics and temperature gradients and were in fair agreement with empirical measurements. The overall comfort vote, predicted mean vote and predicted percentage dissatisfied indices found that the occupants were slightly uncomfortable and dissatisfied.

From the literature survey it is noted that the thermal sensation experienced by the occupants in a building space is known to be affected by four environmental factors such as air temperature, air velocity, mean radiant temperature and relative humidity. Modern buildings performance standards create a need for accurate and flexible simulation models that can contribute to a better design and increased use of low energy, naturally driven cooling systems. The ultimate aim of the evaluation of thermal comfort conditions inside a building is to provide a comfortable and healthy indoor environment for the occupants.

2.4

2.5

Wind is the second most influential climatic parameter, as it can create positive or negative pressures at the outlet of the solar chimney and thus obstruct or enhance the airflow. In the outdoor experiments by Arce (2009) at a full-scale solar chimney, the highest airflow rates coincided with the highest recorded wind velocity, while Afonso and Oliveira (2000) altered their model to include wind effects which proved significant error between model predictions and measurements was then lower than 10%. In the analytical study of Mathur et al. (2006) the large error of 23% was attributed to wind effects, which were neglected in the model. In practice, devices can be incorporated at the outlet of the solar chimney so that wind of all directions creates negative pressures.

2.6 Turbulence Modelling Techniques for Numerical Modelling of Flow Field

Most fluid flows occurring in nature are turbulent. Turbulence can be described as a state of continuous instability in the flow, where it is still possible to separate the fluctuations from the mean flow properties. It is characterised by irregularity in the flow, increased diffusivity and energy dissipation (Tennekes and Lumley 1972). Turbulent flows are always three-dimensional and time dependent, even if the boundary conditions of the flow do not change in time. A comprehensive review of simulation techniques for turbulent flows was done by Ferziger, J.H. (1987).

There are several possible approaches to simulate the turbulent flows. The first, Direct Numerical Simulation (DNS) (Eswaran V. and Pope S.B 1988, Rogallo R.S. and Moin P. 1984, Rogallo R.S. and Moin P. 1987) numerically integrates the governing equations over the whole range of turbulent scales. The requirements on mesh resolution and time-step size put very high demands on the computer resources, rendering it unsuitable for engineering applications.

The second approach is generally known as Large Eddy Simulation (LES). In order to separate different length scales in a turbulent flow field, a spatial filter is applied. Large scale structures that can be resolved by the numerical method on a given mesh are called the super-grid scales. The influence of all other (sub-grid) scales to the super-grid behaviour is modelled. The rationale behind this principle lies in the fact that the small scales of turbulence are more homogeneous and isotropic and therefore easier to model. As the mesh gets finer, the number of scales that require modelling becomes smaller, thus approaching the Direct Numerical Simulation. Examples of

this DNS approach can be found in Deardorff J.W 1970, Givi, P 1989 and Moin and Kim 1982.

An alternative approach to the simulation of turbulent flows is statistical. Separating the local value of the variable into the mean and the fluctuation around the mean, it is possible to derive the equations for the mean properties themselves. The selection of averaging methods depends on the characteristics of turbulent flow, and according to Hinze (1975), the following three averaging method can be distinguished:

1. Time averaging in a fixed point of space, for stationary turbulence,
2. Space averaging for a fixed moment in time in the case of homogeneous turbulence,
3. Ensemble averaging for a series of identical experiments. This is the most general form of averaging.

All these methods can appear in two versions, unweighted (Reynolds) and weighted such as density-weighted Favre averaging (Favre A. 1965). The Reynolds averaging technique operates as follows:

$$\phi_{(x,t)} = \bar{\phi}_{(x,t)} + \phi'_{(x,t)} \tag{2.9}$$

Where, $\phi'_{(x,t)}$ denotes the fluctuation about the mean value, defined as:

$$\bar{\phi}_{(X,t)} = \lim_{n\to\infty} \frac{1}{N} \sum_{i=1}^{N} \phi_{i(X,t)} \tag{2.10}$$

and N is the number of identically performed experiments.

Applying the above averaging procedure to the incompressible Navier-Stokes equations, the following form of the averaged equations can be obtained:

$$\nabla \circ \bar{U} = 0 \tag{2.11}$$

$$\frac{\partial \bar{U}}{\partial t} + \nabla \circ (\bar{U}\bar{U}) = g - \nabla \bar{P} + \nabla \circ (\nu \nabla \bar{U}) + \overline{U'U'} \tag{2.12}$$

In the case of compressible flows, Favre averaging is usually applied (Favre (1965), Cebeci and Smith (1974)). The term $\overline{U'U'}$ is called the Reynolds stress tensor. In order to close the system, further modelling is necessary.

The task of Reynolds averaged turbulence modelling is to express the Reynolds stress tensor in terms of the known quantities. There are two widely accepted approaches. The first approach formulates and solves the transport equation for the Reynolds stress tensor (and higher moments, depending on the order of the closure). It is, however, still necessary to model some of the terms, since the number of

unknowns increases faster than the number of equations (Rotta (1951), Launder et al. (1975) and Hanjalic and Rodi (1972)). The second and more popular approach prescribes a relationship between the Reynolds stress and mean velocity gradient. Although models prescribing non-linear relations have been proposed recently (Speziale (1987) and Shih et al. (1994)), the most popular approach is to use the Boussinesq approximation (Boussinesq (1987)), which prescribes a linear relation of the form:

$$\overline{U'U'} = \nu_t[\nabla U + (\nabla U)^T] + \frac{2}{3}\,\mathrm{k}\,\mathbf{I} \tag{2.13}$$

Where,

$$\mathrm{k} = \frac{1}{2}\,\overline{U'\,U'} \tag{2.14}$$

The kinematic eddy viscosity ν_t can be evaluated in many different ways, ranging from algebraic relations and local equilibrium assumptions to the solution of transport equations. The most popular approach is to express ν_t as a function of the turbulent kinetic energy *k* and its dissipation rate ϵ, leading to a "two-equation'' and named because k and ϵ are obtained by the solution of their respective transport equations. The first model of this kind has been proposed by Harlow and Nakayama (1968). turbulence model:

$$\nu_t = C_\mu \frac{k^2}{\epsilon} \tag{2.15}$$

$$\epsilon = \nu\,\overline{U'\,U' : \nabla U'} \tag{2.16}$$

Derivation of the transport equations for *k* and ϵ can be found in Launder and Spalding (1974). In fact, a wide variety of $\mathrm{k}-\epsilon$ models exists, the most noteworthy being the standard $\mathrm{k}-\epsilon$ model by Launder and Spalding (1974) and the RNG $\mathrm{k}-\epsilon$ variant by Yakhot and Orszag (1986) Yakhot and Orszag (1992). The physics of turbulence in the vicinity of impermeable no-slip walls is considerably different from the other parts of the flow. It is therefore necessary to use appropriate turbulence models in the near-wall region. For the most general and detailed treatment, low-Re versions should be used (Lam and Bremhorst (1981), Launder and Sharma (1974)). However, in order to resolve the near-wall details well, the computational mesh needs to be very fine in this region. It is possible to compensate for the existence of the wall without resolving the near-wall region, albeit at the expense of considerable

approximation and, as will be shown later, also with adverse effects on numerical resolution. Wall-functions (Launder and Spalding (1974)) represent a simplified model of turbulence, which mimics the near-wall behaviour of the velocity, k and ϵ. It assumes that the flow near the solid wall behaves like a fully developed turbulent boundary layer. In numerical simulations, this model is used to bridge the regions of high gradients near the wall and couples with the high-Re $\mathrm{k}-\epsilon$ model in the rest of the domain. For the details of its derivation and implementation, the reader is referred to Launder and Spalding (1974) and Gosman and Ideriah (1983).

2.6.1 Zero-equation model

In order to represent the eddy viscosity ν_t, an empirical formula was introduced by Prandtl (1925) in which a mixing length scale l_m was introduced:

$$\nu_t = \rho l_m u_t \tag{2.17}$$

Where, u_t is a lateral turbulence velocity, assumed to be proportional to the mixing length and the time-mean velocity gradient, expressed by

$$u_t = l_m \left|\frac{\partial u}{\partial y}\right| \tag{2.18}$$

and

$$\nu_t = \rho l_m^2 \left|\frac{\partial u}{\partial y}\right| \tag{2.19}$$

The only unknown remaining here is the mixing length scale l_m. In general it is assumed to be proportional to the distance from the nearest wall or the width of a shear layer, a wake, a jet, etc. There are no extra transport equations introduced, this model is therefore called zero-equation model or mixing length model.

In the zero equation model, the way of representing the turbulence velocity $u_t = l_m \left|\frac{\partial u}{\partial y}\right|$ lacks generality. For example, a turbulent flow at the centre of a pipe where the velocity gradient $\frac{\partial u}{\partial y}$ is zero, which would lead to a zero u_t, whereas in fact u_t is very large. Another drawback of the zero equation models is the difficulty of assigning a value for l_m in complex turbulence problems which are occurred when the flow involves separation and recirculation.

2.6.2 One-equation model

Before introducing the one equation model, it is first necessary to define the turbulent kinetic energy k. Similar to other transport variables the instantaneous kinetic energy $K(t)$ is defined as the sum of the mean kinetic energy and the turbulent kinetic energy:

$$K(t) = K + k \tag{2.20}$$

$$\text{Where, } K = \frac{1}{2}(u^2 + v^2 + w^2) \tag{2.21}$$

$$\text{And } k = \frac{1}{2}(u'^2 + v'^2 + w'^2) \tag{2.22}$$

The one-equation model suggested by Kolmogorov (1942) uses the turbulent kinetic energy k to represent the turbulence velocity v_t ($v_t = \sqrt{k}$).

The turbulent viscosity is then given by

$$\mu_t = C_D' \rho \, l_s \sqrt{k} \tag{2.23}$$

where C_D' is an empirical constant (≈ 1.0) and l_s is a length scale. k is treated as a new dependent variable and can be transported by the governing equation. This model is a one step improvement over the zero-equation model in terms of representing the turbulence velocity, v_t, however, it still presents the same difficulty as the zero-equation model for determining the length scale l_s .

2.6.3 Two-equation models

In the one-equation model, the turbulence velocity v_t is represented by turbulent kinetic energy k which can be transported by the governing equation, while for two-equation models, efforts have been made to represent the length scale by some quantity which could be similarly transported in the same way as k. The dissipation rate of the turbulent kinetic energy ε, was introduced by Launder & Spalding (1974) and the length scale l is expressed by a combination of k and ε.

$$l = \frac{C_\mu \, k^{\frac{2}{3}}}{\epsilon} \tag{2.24}$$

where C_μ is a constant. The turbulent viscosity μ_t is therefore defined by

$$\mu_t = \frac{C_\mu \, \rho k^2}{\epsilon} \tag{2.25}$$

The transport equations for turbulent kinetic energy k and its dissipation rate ε are given as follows (Launder & Spalding 1974):

$$\frac{\partial(\rho k)}{\partial t}+\frac{\partial(\rho u_j k)}{\partial x_j}=\frac{\partial}{\partial x_j}\left[\left(\mu+\frac{\mu_t}{\sigma_k}\right)\frac{\partial k}{\partial x_j}\right]+P_k-\rho\varepsilon \tag{2.26}$$

$$\frac{\partial(\rho\varepsilon)}{\partial t}+\frac{\partial(\rho u_j \varepsilon)}{\partial x_j}=\frac{\partial}{\partial x_j}\left[\left(\mu+\frac{\mu_t}{\sigma_\varepsilon}\right)\frac{\partial \varepsilon}{\partial x_j}\right]+C_{1\varepsilon}P_k\frac{\varepsilon}{k}-\rho C_{2\varepsilon}\frac{\varepsilon^2}{k} \tag{2.27}$$

where the P_k is the production of turbulent kinetic energy due to shear stresses, expressed by:

$$P_k=(\mu+\mu_t)\left[\frac{\partial u_i}{\partial x_j}+\frac{\partial u_j}{\partial x_i}\right] \tag{2.28}$$

The model introduced above is the standard k –ε model, the most widely used and validated turbulence model for engineering applications (Kato et al (1992), Shankar et al (1995)). There are five adjustable constants used in this model for $C_\mu, \sigma_k, \sigma_\varepsilon, C_{1\varepsilon}$ *and* $C_{2\varepsilon}$ as 0.09, 1.0, 1.3, 1.44 and 1.92 respectively.

These values were determined by substantial investigation of experimental data and have been found to be applicable over a wide range of turbulent flows. However, if these constants are sensitive to a numerical solution for a specific turbulent flow, the values can be adjusted. For example, the constant C_μ was changed from 0.09 to 0.11 by Kulmala (1997) in order to accurately predict the mean velocity in a thermal plume.

One improvement to the standard k -ε model was made by Yakhot et al (1992) in which a complex mathematical procedure termed the Renormalisation Group (RNG) Theory was applied. The following model equations are taken from Yakhot et al (1992).

$$\frac{\partial(\rho k)}{\partial t}+\frac{\partial(\rho u_j k)}{\partial x_j}=\frac{\partial}{\partial x_j}\left[\left(\mu+\frac{\mu_t}{\sigma_k}\right)\frac{\partial k}{\partial x_j}\right]+P_k-\rho\varepsilon \tag{2.29}$$

$$\frac{\partial(\rho\varepsilon)}{\partial t}+\frac{\partial(\rho u_j \varepsilon)}{\partial x_j}=\frac{\partial}{\partial x_j}\left[\left(\mu+\frac{\mu_t}{\sigma_\varepsilon}\right)\frac{\partial \varepsilon}{\partial x_j}\right]+(C_{1\varepsilon}-C_{1\varepsilon}^*)P_k\frac{\varepsilon}{k}-\rho C_{2\varepsilon}\frac{\varepsilon^2}{k} \tag{2.30}$$

Where, P_k is the same as in the standard k –ε model.

2.6.4 Reynolds stress model

In the Reynolds Stress Model (RSM) (Launder et al (1975)), the individual Reynolds stresses/fluxes (have six Reynolds stresses and three Reynolds fluxes) are represented by exact transport equations rather than using the eddy viscosity

assumption. The derivation of these Reynolds stresses/fluxes equations can be found in relevant literatures such as Launder & Spalding (1972), or Leschziner (1990).

Compared with two-equation turbulence models, RSM is a more accurate way to model fluid flows due to its rigorous and detailed mathematical formulation. However, a great deal of computational cost is added for solving the nine extra transport equations for Reynolds stresses/fluxes. For complicated turbulent flows it is still very difficult to handle even using modern computers. In order to reduce the computational cost, Rodi (1985) tried to simplify the transport equations by approximating the convection and diffusion terms into algebraic expressions, to give what is known as the Algebraic Stress Model (ASM). Although ASM is not as well validated as the $k-\varepsilon$ models it can be used in flows where the isotropic assumption of eddy viscosity is not appropriate.

2.6.5 Large eddy simulation

In the large-eddy simulations (LES) model (Deardorff (1970)) small eddies are filtered from the instantaneous motions and are modelled using some simple models. The LES model can be used to resolve the unsteady, three dimensional evolution of the large scale turbulent flow field and monitor the flow at any moment in time and if mean flow quantities are required the calculations must be done over a sufficient large time scale. Although its computational cost is less than the direct numerical simulations (Murakamni (1997) of turbulence, it still requires impractical amounts of computing to be a model that can be recommended for engineering applications. This model has been used to investigate cases such as isothermal flows in channels (Deardorff (1970)) or over a cube (Murakami et al (1987)).

3 CFD TECHNIQUES FOR NUMERICAL MODELLING OF FLOW FIELD

The physical properties of fluid flows are governed by three fundamental conservation laws namely the conservation of mass, momentum and energy. These laws can be interpreted in terms of partial differential equations. Computational Fluid Dynamics is a numerical method of determining a solution to the governing equations of a fluid flow by advancing the solution through space and/or time to obtain a numerical description of the whole flow field of interest.

3.1 Governing Equations of Continuum Mechanics

The problems relevance to continuum mechanics has significantly interaction with characteristic length scale and time scales compared to the scales of the discrete structure of the matter. Therefore, any physical property of the matter can describe as a continuous function in a space-time coordinate system. The rate of change of the intensive physical property ϕ in time can be written in material derivative form as:

$$\frac{d}{dt}\int_{V_M(t)} \rho\phi_{(X,t)}dV = \frac{\partial}{\partial t}\int_{V_M(t)} \rho\phi dV + \oint_{\partial V_M(t)} dS.\rho\phi U \tag{3.1}$$

Where, ρ is density, U is the velocity vector, t is the time, V_M is the material volume and dS is the outward pointing unit normal on $\partial V_M(t)$.

The rate of change of ϕ in V_M is equal to its volume and surface sources. It can be written in differential form:

$$\frac{\partial\rho\phi}{\partial t} + \nabla\circ(\rho\phi U) = Q_V(\phi) + \nabla\circ Q_s(\phi) \tag{3.2}$$

Where, Q_V is the volume source and Q_s is the surface source.

The above form can be used to represent all the governing equations of continuum mechanics, valid for any continuum (Aris 1989).

In the present study attention has been focused on the modelling of solar induced buoyancy driven natural convective flows in an enclosure with one horizontal opening and one vertical opening to identify the suitable geometrical parameters for occupants' thermal comfort. According to the problem definition, conservation laws for a Newtonian fluid: the continuity equation, the momentum equations and the energy equation can be written as:

Conservation of mass:

$$\frac{\partial \rho}{\partial t} + \nabla \circ (\rho U) = 0 \tag{3.3}$$

It represent the increase of mass within a finite control volume of a fluid should be equal to the difference between the mass inflow and mass outflow.

Conservation of linear momentum:

$$\frac{\partial \rho U}{\partial t} + \nabla \circ (\rho U U) = \rho g + \nabla \circ a \tag{3.4}$$

Newton's second law stated that the rate of change of momentum equals the sum of the forces acting on the fluid control volume considered.

Conservation of energy:

The rate of change of energy within a control volume is equal to the sum of the net heat exchange rate and the rate of net work done on the volume. This is the first law of thermodynamics and can be stated as:

$$\frac{\partial \rho e}{\partial t} + \nabla \circ (\rho e U) = \rho g U + \nabla \circ (\sigma U) - \nabla \circ q + \rho Q \tag{3.5}$$

However, the number of un-known quantities is, however, larger than the number of equations in the system, making the system indeterminate. In order to close the system, the following set of constitutive relations which depend on the properties of the continuous medium of interest is used:

For Newtonian fluids, internal energy defines as a function of pressure P and temperature T.

$$u = u_{(P,T)} \tag{3.6}$$

The total energy is calculated as the sum of the kinetic e_M and internal energy

$$e = e_M + u_{(P,T)} = \frac{1}{2} UU + u_{(P,T)} \tag{3.7}$$

The equation of state:

$$\rho = \rho_{(P,T)} \tag{3.8}$$

The Fourier's law of heat conduction:

$$q = -\lambda \nabla T \tag{3.9}$$

Generalised form of the Newton's law of viscosity:

$$\sigma = -\left(P + \frac{2}{3}\mu \nabla \circ U\right)\mathbf{I} + \mu[\nabla U + (\nabla U)^T] \tag{3.10}$$

These constitutive relations, together with the governing equations for a continuum create a closed system of partial differential equations for Newtonian fluids.

Continuity equation:

$$\frac{\partial \rho}{\partial t} + \nabla \circ (\rho U) = 0 \tag{3.11}$$

Navier-Stokes equations:

$$\frac{\partial \rho U}{\partial t} + \nabla \circ (\rho U U) = \rho g - \nabla\left(P + \frac{2}{3}\mu \nabla \circ U\right) + \nabla \circ \left[\mu\left[\nabla U + (\nabla U)^T\right]\right] \tag{3.12}$$

Energy equation:

$$\frac{\partial \rho e}{\partial t} + \nabla \circ (\rho e U) = \rho g U + \nabla \circ (P U) - \nabla \circ \left(\frac{2}{3}\mu(\nabla \circ \mathrm{U})U\right) + \nabla \circ \left[\mu\left(\nabla U + (\nabla U)^T\right)U\right]$$
$$+\nabla \circ \lambda \nabla T + \rho Q \tag{3.13}$$

The transport coefficients λ and μ are also functions of the thermodynamic state variables:

$$\lambda = \lambda_{(P,T)} \tag{3.14}$$

$$\mu = \mu_{(P,T)} \tag{3.15}$$

For incompressible and isothermal fluids (ρ = constant and $\lambda = \propto$), the system can be further simplified to:

$$\nabla \circ U = 0 \tag{3.16}$$

$$\frac{\partial U}{\partial t} + \nabla \circ (U U) = g - \nabla P + \nabla \circ (\upsilon \nabla U) \tag{3.17}$$

With these assumptions, the set of governing equations for conservation of mass, momentum and energy in Cartesian coordinates can be written as follows taking the y-direction being in the vertical direction.

Continuity:

$$\frac{\partial(\rho u)}{\partial x} + \frac{\partial(\rho v)}{\partial x} + \frac{\partial(\rho w)}{\partial x} = 0 \tag{3.18}$$

Momentum in x-direction:

$$\frac{\partial(\rho u)}{\partial t} + \frac{\partial(\rho u u)}{\partial x} + \frac{\partial(\rho v u)}{\partial y} + \frac{\partial(\rho w u)}{\partial z} = -\frac{\partial p}{\partial x} + \mu\left(\frac{\partial^2 u}{\partial x^2} + \frac{\partial^2 u}{\partial y^2} + \frac{\partial^2 u}{\partial z^2}\right) \tag{3.19}$$

Momentum in y-direction:

$$\frac{\partial(\rho v)}{\partial t} + \frac{\partial(\rho u v)}{\partial x} + \frac{\partial(\rho v v)}{\partial y} + \frac{\partial(\rho w v)}{\partial z}$$
$$= -\frac{\partial p}{\partial y} + \mu\left(\frac{\partial^2 v}{\partial x^2} + \frac{\partial^2 v}{\partial y^2} + \frac{\partial^2 v}{\partial z^2}\right) - \rho g \beta (T_\propto - T) \tag{3.20}$$

Momentum in z-direction:

$$\frac{\partial(\rho w)}{\partial t}+\frac{\partial(\rho u w)}{\partial x}+\frac{\partial(\rho v w)}{\partial y}+\frac{\partial(\rho w w)}{\partial z}=-\frac{\partial p}{\partial z}+\mu\left(\frac{\partial^2 w}{\partial x^2}+\frac{\partial^2 w}{\partial y^2}+\frac{\partial^2 w}{\partial z^2}\right) \quad (3.21)$$

Energy:

$$\frac{\partial}{\partial t}(\rho C_p T)+\frac{\partial(\rho u C_p T)}{\partial x}+\frac{\partial(\rho v C_p T)}{\partial y}+\frac{\partial(\rho w C_p T)}{\partial z} = k\left(\frac{\partial^2 T}{\partial x^2}+\frac{\partial^2 T}{\partial y^2}+\frac{\partial^2 T}{\partial z^2}\right)+q'' \quad (3.22)$$

3.2 Modelling Natural Convection

Natural convection flows in buildings are normally generated by thermal buoyancy. When a natural convection flow is influenced by other forces, e.g. pressure difference induced by wind effect, the convection flow becomes the combination of natural and forced convection. For engineering applications of these types of flows, where the temperature differences and compressibility effects are small, the flow is treated as incompressible and can be modelled using the Boussinesq approximation (Boussinesq (1903)). The fluid properties ρ, μ and Prandtl number (a relative measure of momentum diffusivity and thermal diffusivity) are treated as constants by the approximation except for the density in the momentum equations which is written as

$$\rho_o = \rho_o - \beta(T - T_o) \quad (3.23)$$

where ρ_o and β are the density and the thermal expansion coefficient at a reference temperature T_o . Normally, $T_o$is taken as the ambient temperature in a natural convection boundary layer or the average temperature in an enclosure, and $\beta \approx \frac{1}{T_o}$.

Based on this approximation, the modelling equations for steady state, incompressible turbulent natural and forced convection flows are given by the following form.

$$\frac{\partial u_i}{\partial x_i} = 0 \quad (3.24)$$

When applying the Boussinesq approximation for modelling buoyancy-driven flows the temperature variation ΔT of the fluid domain should not be larger than 30ºC (Etheridge & Sandberg (1996)). Assuming density is constant may be inappropriate for large temperature variations. In building simulations, the temperature differences

in air are usually small and the density variation can be ignored. Therefore the Boussinesq approximation is assumed to be sufficient.

4 MODELLING AND VALIDATION OF MATHEMATICAL FRAMEWORK

4.1 Geometrical Modelling of the Experimental Framework

For CFD simulations, a geometrical model was prepared based on a simplified model of the office interior space as shown in Figure 3.1 and 3.2. The internal dimensions of the space are 1.8 m long, 1.65 m wide and 2 m high. The room has a 0.5 m by 0.6 m opening in the centre of one its face, and a 1.40 m wide inlet variable in height, on the opposite side which is open to the base of the cavity. 0.1 m uniform wall thickness was used in the model. For convenience of modelling, furniture and other obstructions inside the space were ignored. The mesh was generated using the blockMesh tool available in OpenFoam.

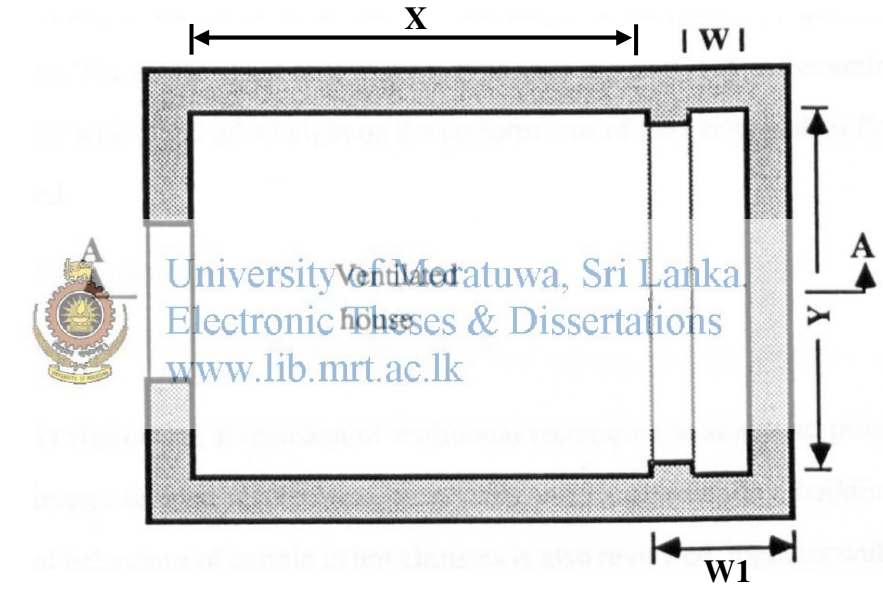

Figure 4.1: Plan view of the geometrical model

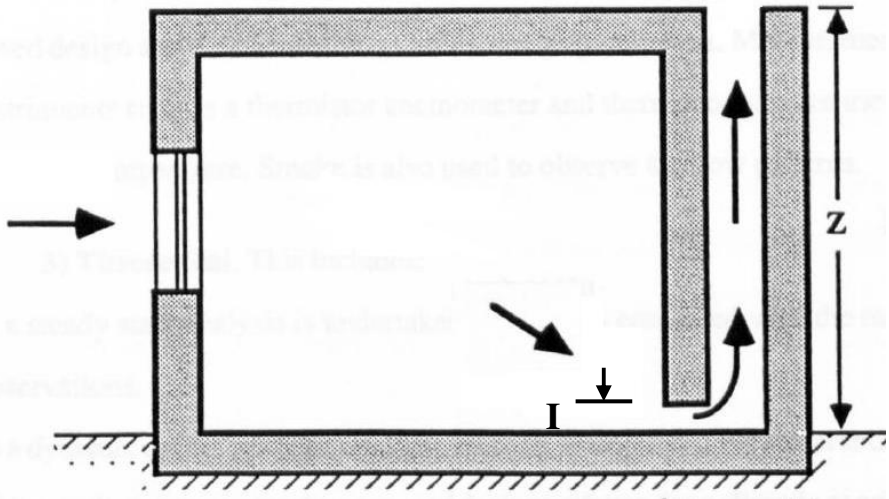

Figure 4.2: Sectional view (A-A) of the geometrical model

4.2 Boundary Conditions Used for Simulation

The boundary conditions were set to match conditions existing in the experimental setup which was used to collect actual data. The wall surfaces were assumed to be adiabatic and zero temperature gradient was employed except hot surfaces of the chimney walls. A constant temperature was applied on the hot surfaces of the chimney walls. Ambient temperature and pressure values were used to simulate the fluid walls of the free environment.

Wall function models are available in OpenFOAM applied as boundary conditions on individual patches and different wall function models were applied to different wall regions. Wall function models used for the properties of the flow regime are represented in Table 4.1

Table 4.1: Boundary field types and values used for each variable

Variable	Description	Boundary Field Type	Boundary Field Value
alphat	Thermal diffusivity	alphatWallFuntion	uniform 0
epsilon	rate of dissipation in turbulent kinetic energy	epsilonWallFuntion	uniform 0.01
k	rate of production in turbulent kinetic energy	kqRWallFunction	uniform 0.1
kappat	turbulent thermal conductivity	kappatJayatillekeWall Function	uniform 0 Prt 0.85
nut	turbulent kinematic viscosity	nutWallFunction	uniform 0
p	Pressure	calculated	$internalField
p_rgh	static Pressure	buoyantPressure	uniform 0
T	Temerature	fixedValue ZeroGradient	ambient , chimney wall T
U	Velocity	fixedValue	uniform (0 0 0)

4.3 Mesh Design

The purpose of the computational mesh is to allow the solution of the flow variables by tracking transport of mass, momentum and enthalpy. To do this accurately, it is important to place more grid nodes in areas where there may be large gradients in the flow variables, such as near solid boundaries and openings, in relation to other areas where the flow gradients are relatively low.

In the present study, hexahedral cells were created with fine mesh near the walls using OpenFoam. For a simple shape the hexahedral elements is the best because it usually results in less numerical diffusion (Fluent, Inc. 2006). A non-uniform grid distribution was used. Close to the heated walls, chimney inlet and chimney outlet areas, the number of grid points or control volumes were increased to enhance the resolution and accuracy. An appropriate modelling of the turbulence phenomena involved in the chimney space implies that the mesh should be designed properly to define minimum cell size to compute the turbulent mixing appropriately with the proposed geometry.

Mesh density depends on the near-wall modelling strategy adopted for resolving the problem under turbulent flow conditions, and is determined by the y+ characteristic parameter. The parameter, y+ termed as the dimensionless wall distance, and defined by the relation , where *y* represents the distance of the cell centre to the wall and ,U was used to find a suitable correct grid size near the walls T where represents shear stress near the wall.

Nielsen et al. (2007) provided a correlation for choosing the initial cell count for the mesh. The correlation used is $N = 44400 \times V^{0.38}$ where N is the number of cells and V is the volume in m^3. It is important to emphasize that there can't be a truly universal correlation of volume and cell count, due to the fact that complexities of the flows in buildings can greatly differ and therefore influence the number of cells required. The volume of the chimney considered is varies from 0.3 to 1.5 m^3 which according to Nielsen's correlation, corresponds to roughly 28,100 to 51,800 cells. Keeping in view this correlation, y+ requirements near walls and computational capability of available computers, the cell count in the range of 28,000 - 52,000 cells respectively was used in chimney regime for the CFD simulations. The wall adjacent cells had to be very small to obtain the required values. A fine mesh near the walls

and coarser mesh away from wall was generated to avoid excessive computational effort as shown in figure 4.3.

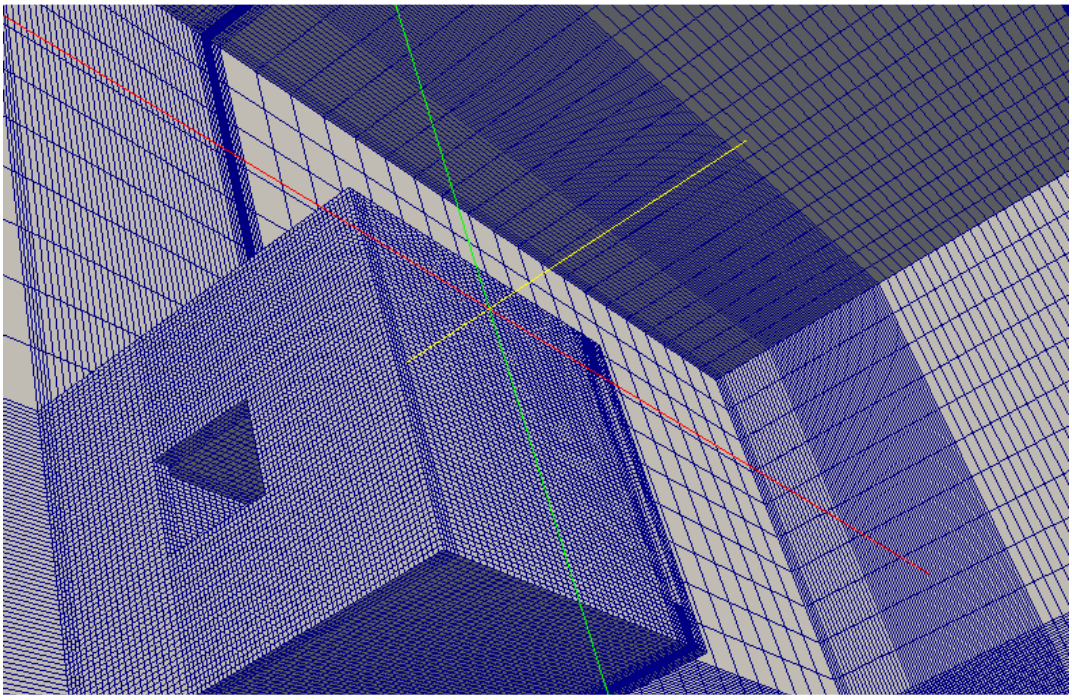

Figure 4.3: 3 - dimensional view of mesh generated using openFOAM

4.4 Mesh Sensitivity of the Numerical Results

To ensure the accuracy of the numerical results, a grid independence study was carried out. Different grid sizes in the x, y and z-coordinate directions used to determine the influence of grid size on the results. A mesh sensitivity test was performed to examine the mesh independence of the numerical results. Three mesh densities employed for whole confined domain were investigated as 854,156, 1,018,632 and 1,535,244 number of cells respectively.

Typical effect of grid density on the mean mass flow rate at window, chimney inlet and outlet were obtained using the Standard k-ε turbulence model and results are shown in table 4.2.

Table 4.2: Effect of grid density on predicted average mass flow rate

Mesh No.	No. of Cells	Average air mass flow rate (kg/m^3)		
		at window	Chimney inlet	Chimney outlet
Mesh-1	854,156	0.1131	0.1163	0.1164
Mesh-2	1,018,632	0.1156	0.1164	0.1176
Mesh-3	1,535,244	0.1160	0.1164	0.1177

There is a difference of less than 1% between the predicted results obtained by three meshes thereby indicating the results are essentially mesh independent.

4.5 Numerical Solution Procedure

The validated CFD model based on the use of the Reynolds Averaged Navier-Stokes (RANS) modelling approach with the Standard k-ε turbulence model was utilized using the steady-state solver for buoyant, turbulent flow of incompressible fluids called "buoyantBoussinesqSimpleFoam" in OpenFOAM. In dealing with the buoyancy forces in the momentum equations the Boussinesq approach was adopted. In addition, the rate of dissipation term (ε) in the energy equation was assumed to be 0.01 kg/ms due to the low velocities involved.

For buoyant pressure discretization, preconditioned conjugate gradient (PCG) solver was employed while U, T, k and epsilon was discritized using Preconditioned (bi-) conjugate gradient (PBiCG) solver. PCG is used for symmetric matrices and PBiCG is used for asymmetric matrices. Pressure-velocity coupling discretization was done by using Semi-implicit method for pressure-linked equations (SIMPLE) algorithm. Second order upwind scheme was used to discretize the momentum and other equations in the numerical simulations.

4.6 Solution Convergence Criteria

The equations for mass and momentum conservation were iteratively solved to get a converged solution, until the sum of the absolute normalized residuals for all the cells in flow domain became less than 10^{-4} while the energy equation was iterated until the residual fell below 10^{-6}, the solution then being considered to be converged. Under-relaxation factors 0.3, 1, 2, 0.8, 0.8, 1, 0.9 for pressure, density, momentum, turbulence kinetic energy, turbulence dissipation rate, turbulent viscosity, energy respectively were used. In all the cases considered, the convergence criteria were met after about 9,000 iterations using a mesh size of approximately 1,018,000 cells.

4.7 CFD Model Validation

Bouchair (1987) has studied performance of a full-scale 1.5 m wide and 2 m high solar chimney that was part of a 3.6 m^3 room under laboratory conditions. A series of CFD simulations were run using the identified mesh density for the model which was experimentally tested by Bouchair (1987). Numerical results were obtained when the

convergence criteria were met after approximately 9,000 iterations. The results are presented here only for three configurations.

Figure 4.4 shows comparison of the air mass flow rate predicted by CFD model against experimental results available for the configuration: 0.1 m wide cavity and 0.1 m high cavity inlet. Average mass flow rate of the CFD model was calculated by introducing a probe array placed at the cavity inlet to measure flow velocities according to the arraignment and positions followed in the experiment performed.

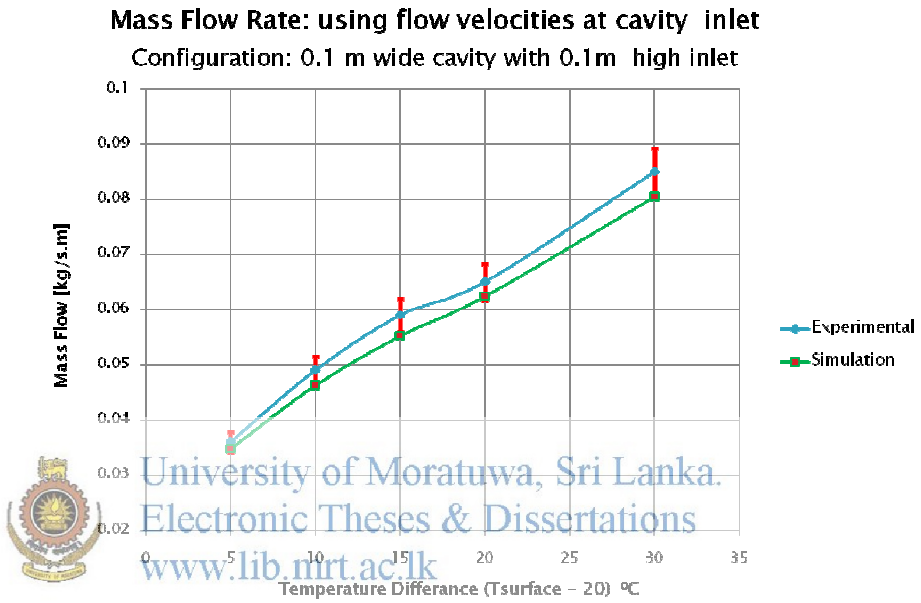

Figure 4.4: Mass flow rate calculated using flow velocities at chimney inlet

Average mass flow rate calculated at window for same configuration is presented in figure 4.5.

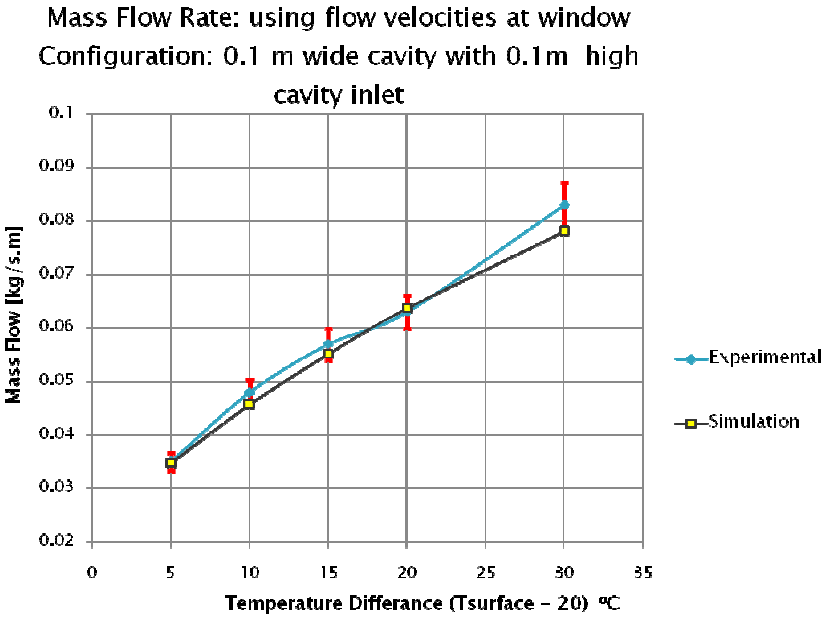

Figure 4.5: Mass flow rate calculated using flow velocities at window

Response of the CFD model for a different configuration was studied by changing the cavity dimension to 0.3 m and chimney inlet height to 0.4 m is illustrated in figure 4.6. Mass flow rate is increased gradually with the increase of temperature difference of 20^{o}C between surface and ambient temperature.

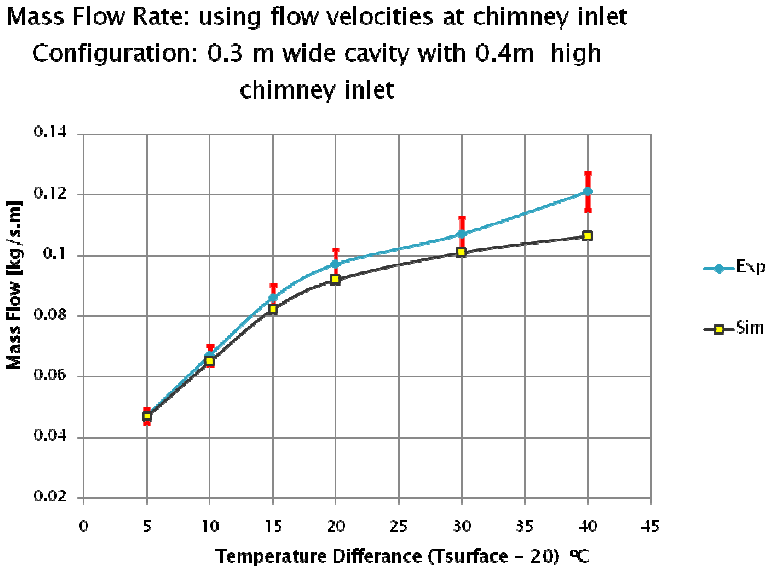

Figure 4.6: Mass flow rate calculated using flow velocities at chimney inlet for congiguration 3

From these results it can be seen that a good agreement between the experimental data and the CFD predictions was obtained. Further, it was noted that the relative percentage error between predictions and measurements was less than 10% for all the models used. However, with the increase of temperature difference between hot surface of the chimney and ambient air, CFD prediction tends to deviate from the experimental results. This may be caused by boussinesq approximation used in the simulation.

5 NATURAL VENTILATION POTENTIAL IN LOCAL CLIMATE FOR THERMAL COMFORT PREDICATION

It is necessary to identify the influence of the environmental factors to evaluate the conditions of thermal comfort of a particular space. The analysis was carried out for the buildings located in Colombo using Typical Metrological Year 2 (TMY2) weather data available for Colombo, Sri Lanka (Longitude/ Latitude 7.025˚ North 80.0˚ East). TMY2 weather file consists of hourly data for solar radiation, dry bulb and wet bulb temperature and wind speed throughout the year. Solar assisted buoyancy driven displacement ventilation can effectively use during the daytime. Therefore, hourly weather data available for the daylight hours from 6.00 a.m. to 6.00 p.m. were used in the present analysis.

5.1 Influence of the Temperature and Relative Humidity

The variation of weather conditions during the daytime were investigated by plotting weather data on the psychrometric chart as shown in figure 5.1. The results of the analysis were illustrated more than 99% of the data confine to the space bounded by dry bulb temperature range of 22˚C - 33˚C and relative humidity range of 40% - 100%. In the figure 5.1 the data plotted in green color indicates the comfort zone defined by adaptive comfort model in ASHRAE 55-2004 and 44% of the daytime falls into the comfort zone.

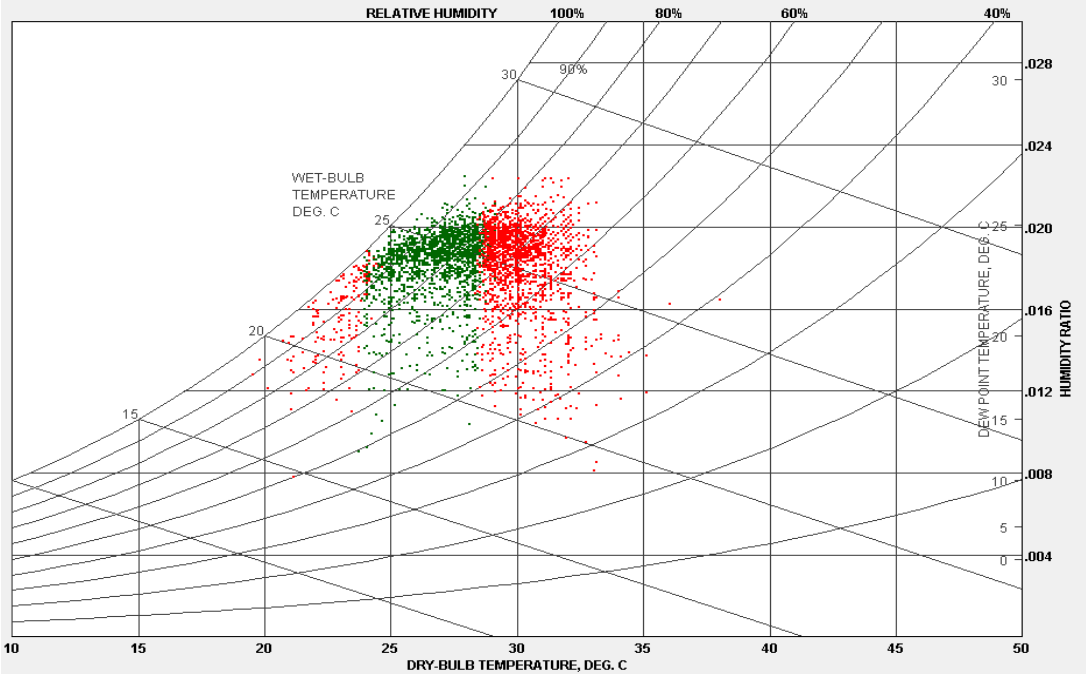

Figure 5.1: Psychrometric chart for Colombo climate during daylit from 6.00 a.m. to 6.00 p.m.

In naturally ventilated spaces where the occupant can open and close windows, their thermal response depend in part on the outdoor climate. Many occupants have wider comfort range than in the buildings with mechanical cooling systems. Further, adaptive comfort model assumes occupants adopt their clothing to thermal conditions. However this model does not apply if a mechanical cooling or heating system is in operation.

According the significance of hourly variation in the outdoor climate during daytime throughout the year, the analysis can further be improved by classifying data under two periods such that Period-1from November to April and Period-2 from May to October. As illustrated in figure 5.2, only 37% of the daytime was comfortable during the Period-1 if ASHARE 55-2004 adoptive comfort model is used.

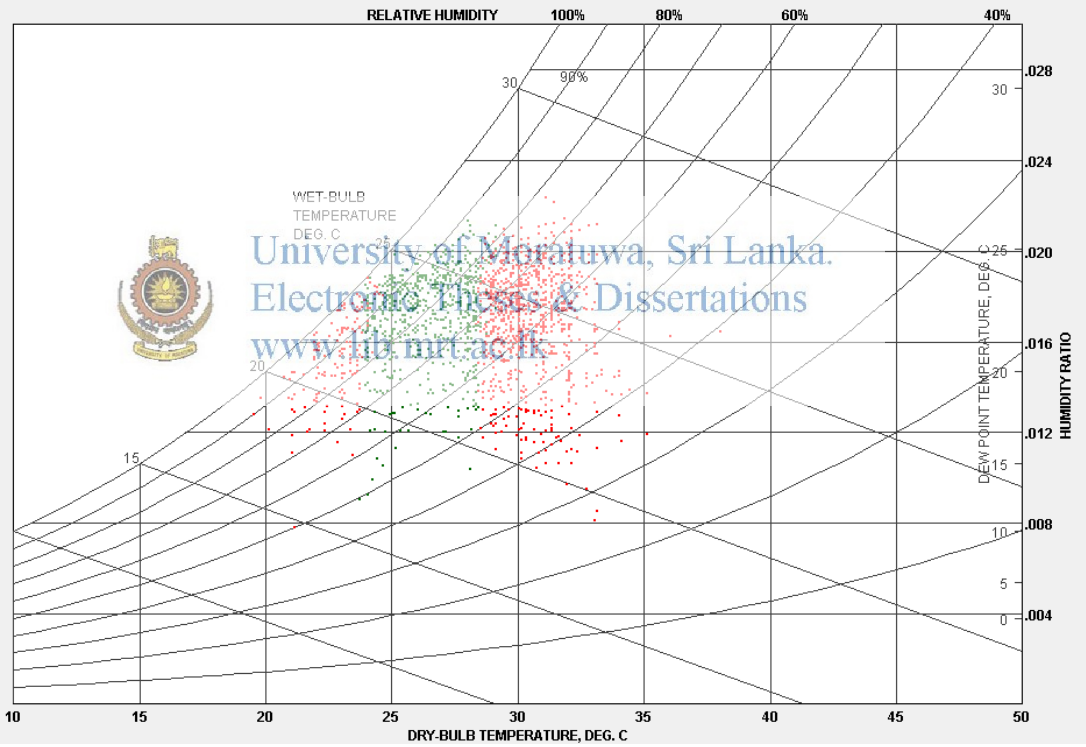

Figure 5.2: Psychrometric chart for the Period-1 of Colombo climate during daytime

Due to the significant variation observed in mean hourly climate data, the investigation was further extended by plotting the daily minimum and daily maximum values reported for the dry bulb and wet bulb temperatures. Figure 5.3 illustrates the results of the investigation carried out for the Period-1. This can be used to identify the daily maximum and daily minimum conditions recorded for the outdoor climate of the months during the period of November to April. It was observed that during the months of January, February and March, the variation

between the maximum and minimum values are significantly high compared to the other months of the year.

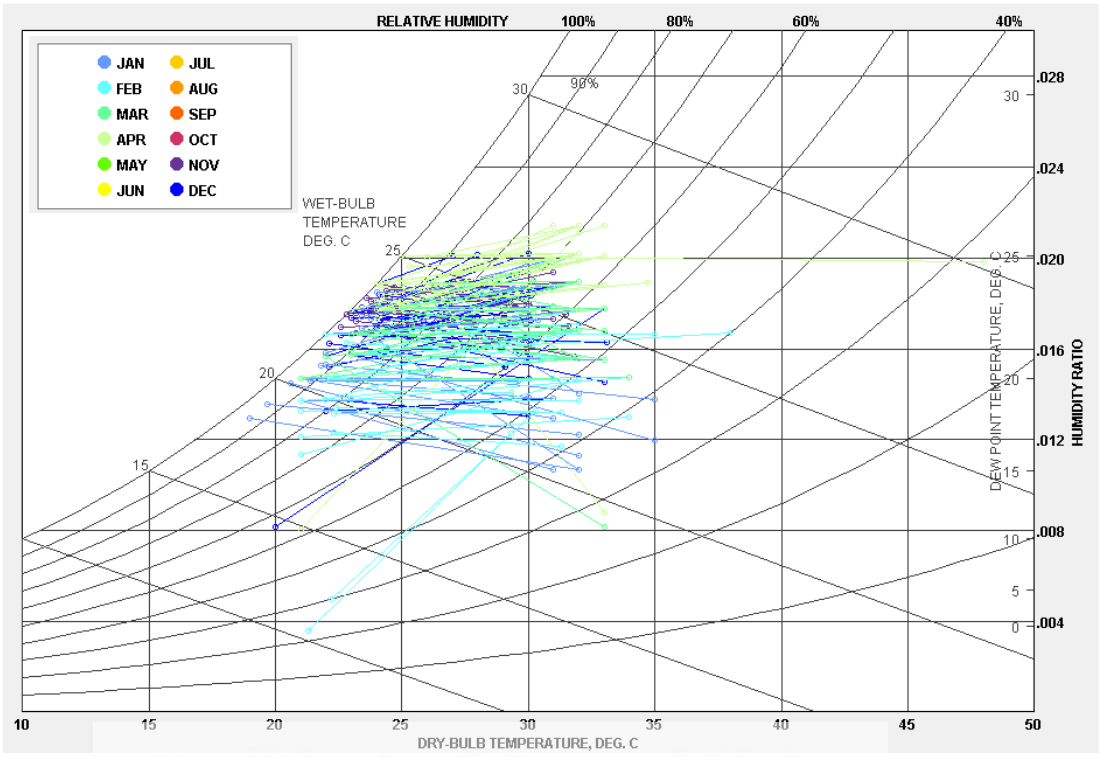

Figure 5.3: Outdoor climate variation for the Period-1 with daily minimum-maximum

Outdoor climate conditions plotted on the psychrometric chart for the Period-2 is shown in figure 5.4 which illustrates 52% of the daytime falls into the comfort zone.

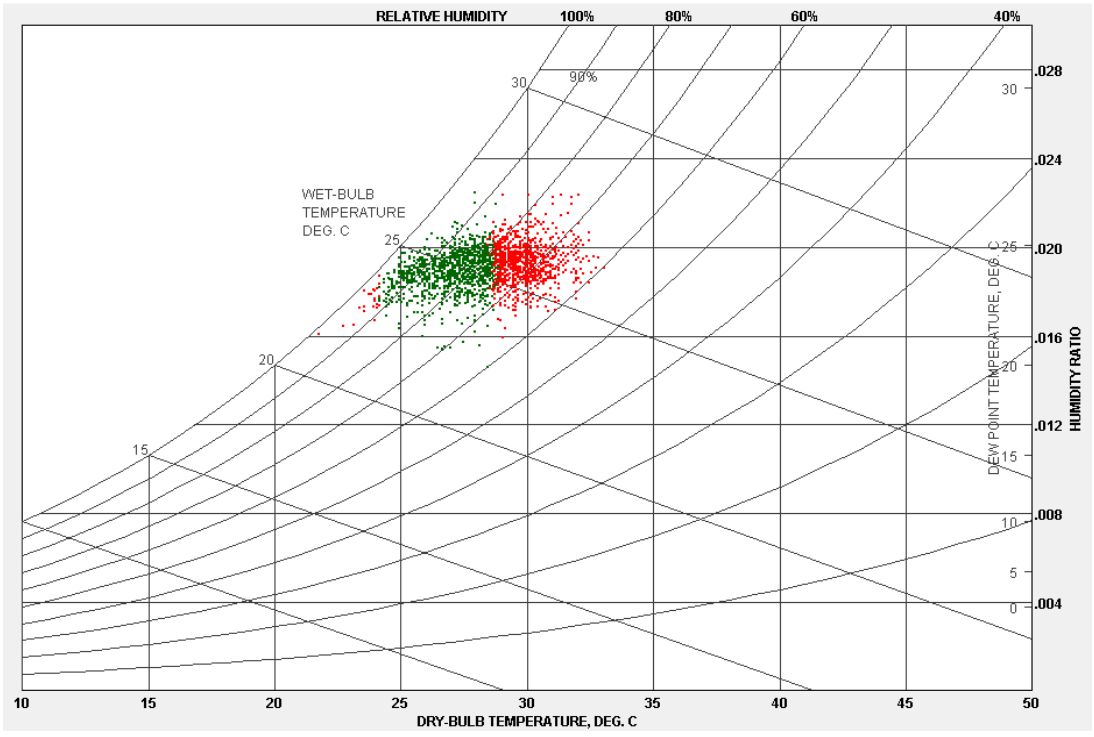

Figure 5.4: Psychrometric chart for the Period-2 of Colombo climate during daytime

Corresponding daily maximum and daily minimum conditions recorded for the outdoor climate of the months during the period of May to October were shown in figure 5.5. During the Period-2, relative humidity is varied in between 65% and 95% more than 95% of the daytime. Therefore, humid climate conditions can be expected during the daytime of the Period-2.

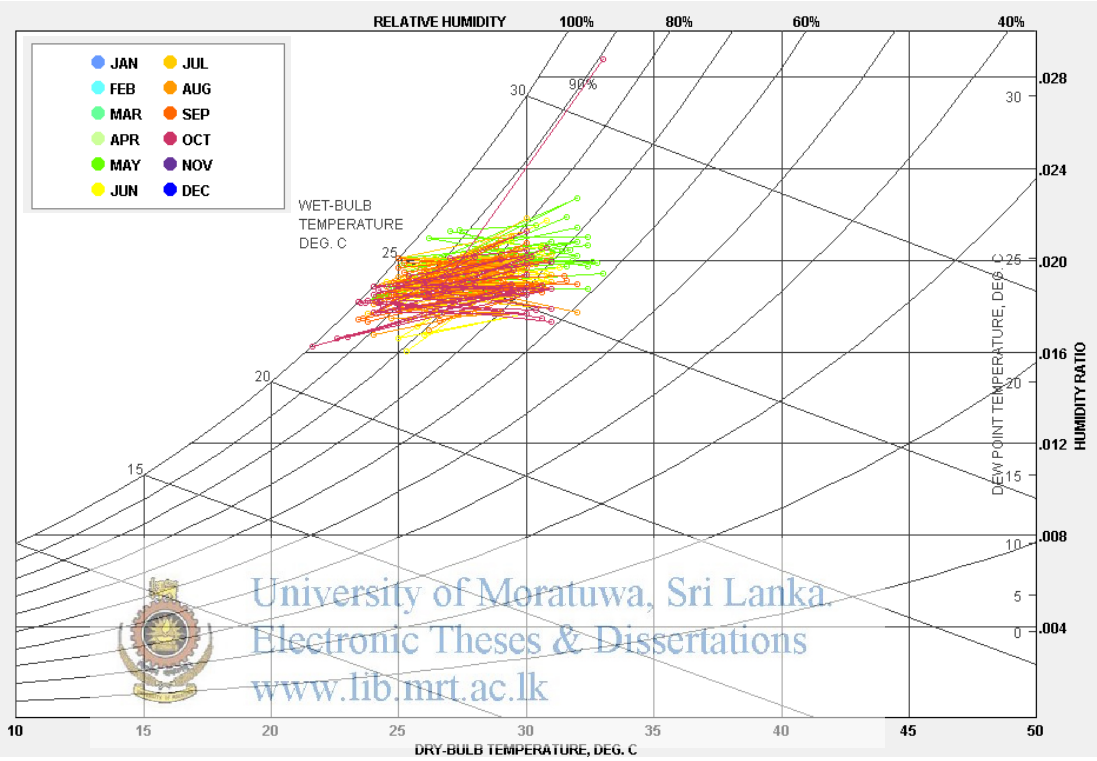

Figure 5.5: Outdoor climate variation for the Period-2 with daily minimum-maximum

Indoor thermal condition is highly influenced by dry bulb temperature of the climate. Therefore, monthly average dry bulb temperature variation during the daytime was studied to choose an appropriate value for dry bulb temperature to evaluate the thermal comfort condition and this variation is represented in figure 5.6. Maximum monthly average value of the dry bulb temperature was reported as 33.28˚C while minimum was recorded as 24.21˚C during daytime.

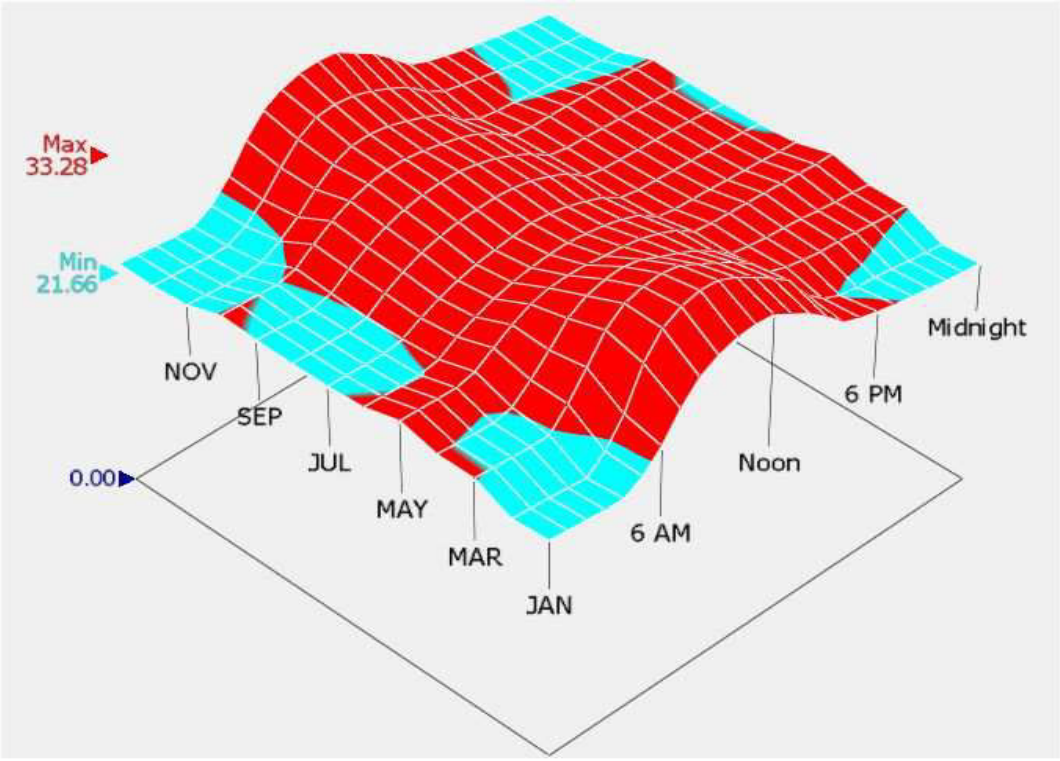

Figure 5.6: Monthly average dry bulb temperature variation

Further, variation of the monthly mean dry bulb and wet bulb temperature during 24 hours of the day was analyzed and results for each month are respectively represented in figure 5.7 and 5.8. This information was used to predict the amount of ventilation rate required for months throughout year.

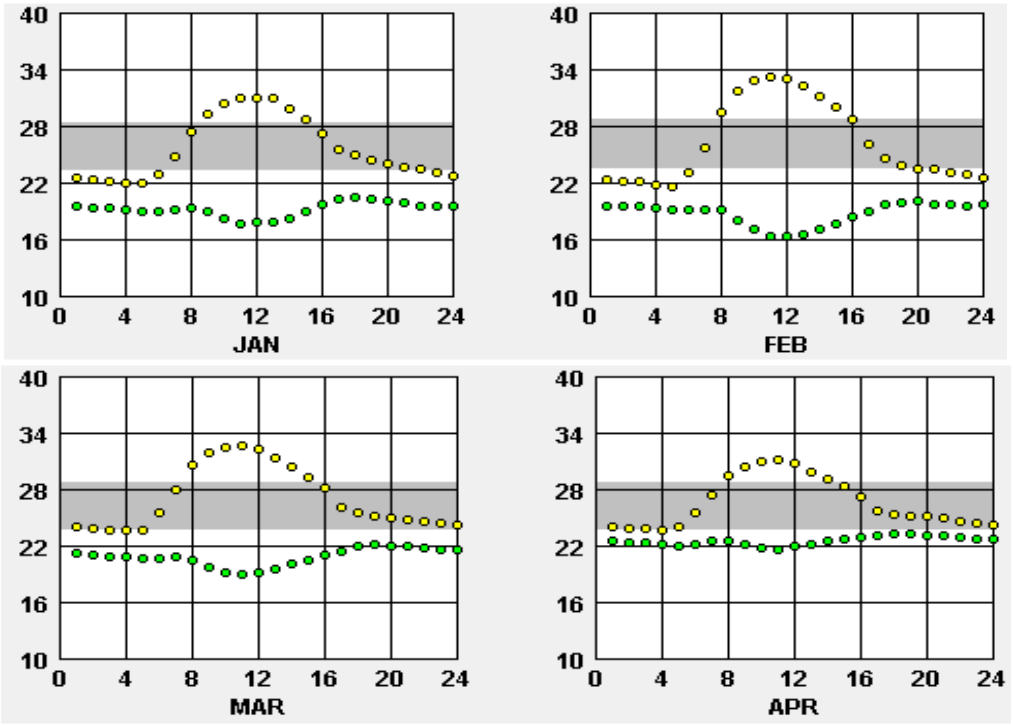

Figure 5.7: Variation of the dry bulb and wet bulb temperature from January to April

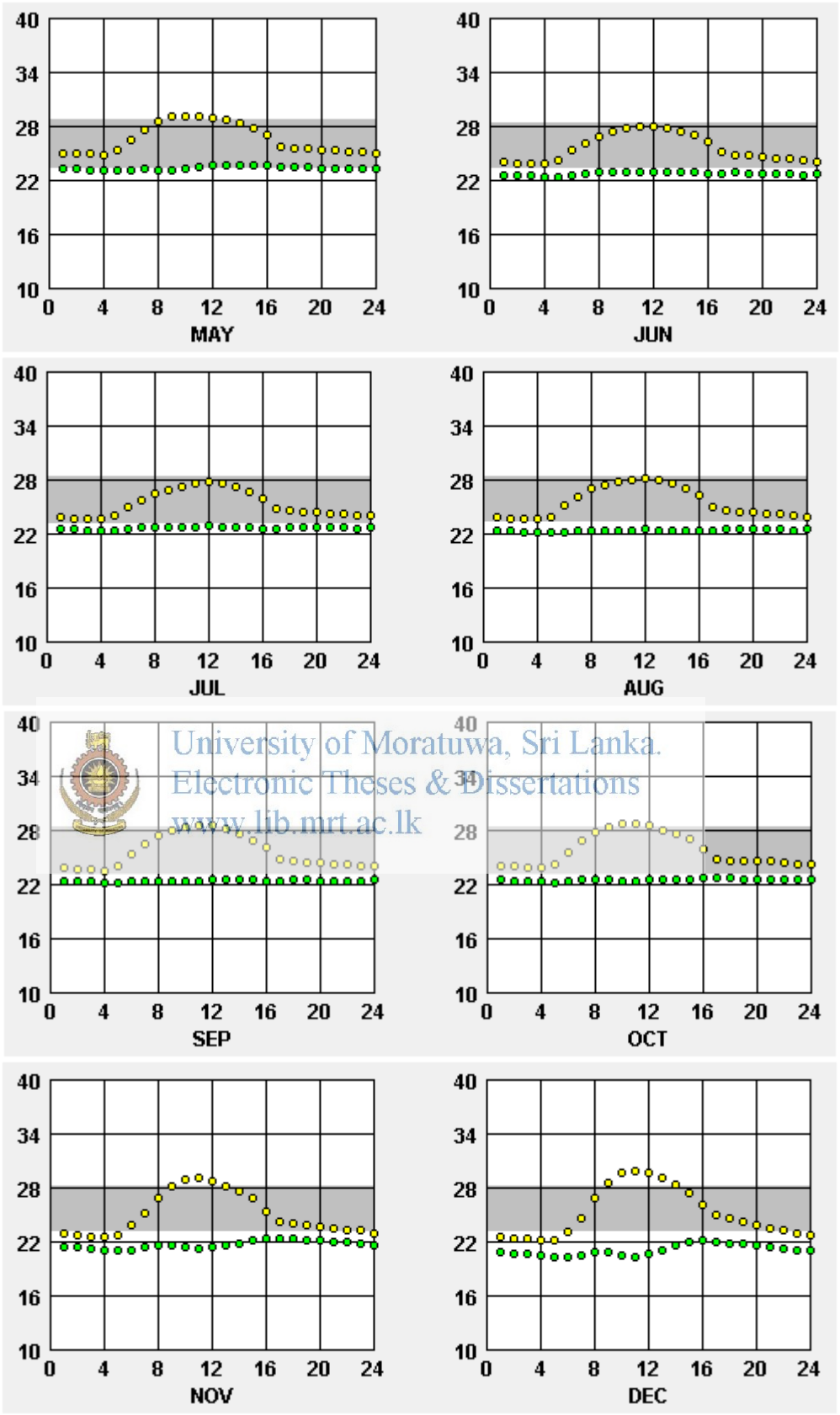

Figure 5.8: Variation of the dry bulb and wet bulb temperature from May to December

5.2 Influence of the Solar Irradiation

Factors influence air flow thorough the solar chimney are the location and orientation of the building, size of ventilated space and internal heat generation. The chimney induces airflow through the space when solar radiation impinges on it. Solar radiation is absorbed at the wall surface of the chimney then the air in the chimney is heated by convection and radiation heat transfer from inner wall of the chimney. The decrease in density experienced by the air causes it to rise, whereupon it is replaced by air from adjacent space attached to it. The air flow rate drawn through the space depends upon the buoyancy force experienced, the resistance to flow through the chimney and the resistance to the entry of fresh air into the room. Therefore, air flow through ventilated space can be maximized by increasing the buoyancy force while reducing the other resistance to the flow. The buoyancy force depends upon the temperature difference between heated air and the fresh air. For a given set of weather conditions, airflow through the space can be improved thereby increasing the solar radiation incidents on the chimney wall. However, fluctuation of solar radiation during the daytime changes air flow rate through the building thereby providing the importance to feasibility study on solar radiation for a chosen climate.

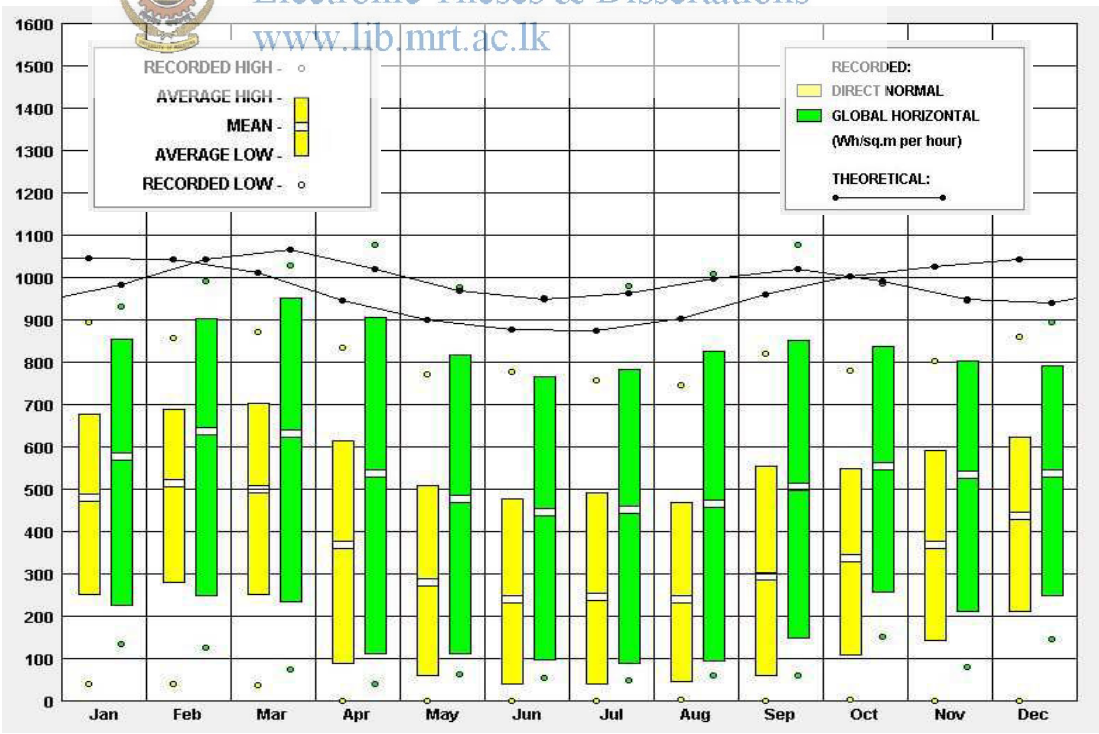

Figure 5.9: Solar irradiation based on hourly average values with its theoretical variation

Figure 5.9 shows the recorded solar irradiation of the direct normal and global horizontal valued generated on hourly average values with its theoretical variation.

Maximum value for the direct normal is recorded in March as 700 Wh/m^2 per hour.

Figure 5.10 show the variation of hourly average direct, diffuse and total irradiation with corresponding dry bulb and wet bulb temperatures during the daytime. The maximum peak value of the total solar irradiation recorded as 900 Wh/m^2 at noon during the month of March while minimum value recorded as 700 Wh/m^2 in June.

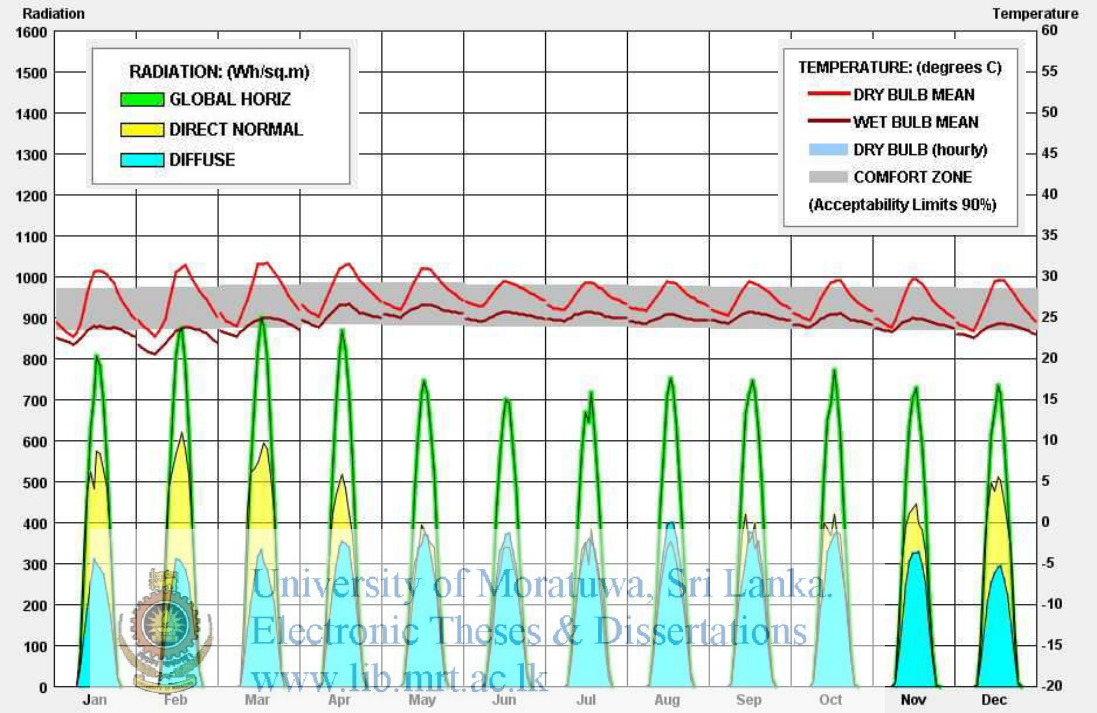

Figure 5.10: Variation of hourly average direct, diffuse and total irradiation with corresponding dry bulb and wet bulb temperatures

6 RESULTS AND DISCUSSION

Thermal comfort is defined in ISO 7730 as "the condition of mind that expresses satisfaction with the thermal environment". It is now normal practice to express the thermal comfort conditions in term of indices such as Predicted Mean Vote (PMV) and Predicted Percentage of Dissatisfied (PPD). These indices are adopted in ISO 7730 and are calculated by empirical equations as described in Chapter two, Section 2.3.2.

In the present work, the PPD values in the occupied region of the simplified office space were calculated from six basic variables: activity, clothing, air temperature, air velocity, mean radiant temperature (MRT) and humidity. The values of the activity (metabolic rate) and clothing (ensemble insulation) were determined using ASHRAE 55 (2007) as applicable to tropical climate condition. The mean radiant temperature was taken as same as dry bulb temperature because the space is located in a tropical climate and the space does not have any cold source. The mean value of the air flow velocities (V) in the area of interest was determined from the CFD simulations applying realistic boundary conditions. Mean air temperature inside the space was taken as ambient temperature assuming walls are adiabatic except the heated wall of the chimney.

In natural ventilation, the stall air within the space is frequently displaced by the air surround the building to naturally condition the space by means of wind driven ventilation or buoyancy driven ventilation. Therefore, the condition of indoor thermal comfort is highly depended on the condition of the environment surround the building. Thus, it is essential to identify the limitations imposed by the environmental factors on thermal comfort to evaluate the possibility of employing natural ventilation in the chosen climate zone.

6.1 Feasibility of the Climatic Conditions to Employ Natural Ventilation

The variation of PPD value with ambient temperatures and air flow velocities were analyzed under the different relative humidity levels. For the analysis, the humidity levels were selected considering the weather details of the different climatic locations and its variation throughout the year. The upper limit of air flow velocity was determined according to the maximum attainable flow velocity under the solar assisted buoyancy driven ventilation studied in the research. The range of the dry

bulb temperature was limited by its variation during daytime and the acceptable level of PPD value corresponding to the natural ventilation. The results of the analyses present in table 6.1. In the calculations, the values of metabolic rate (met) and clothing insulation (clo) were taken as 1.1 and 0.65 respectively considering the sedentary activity-light office work.

Table 6.1: Variation of PPD_{NV} with ambient temperatures and air flow velocities under different relative humidity levels

	RH = 50%					**RH = 60%**				
	Velocity [m/s]					Velocity [m/s]				
DBT[°C]	0.1	0.2	0.3	0.4	0.5	0.1	0.2	0.3	0.4	0.5
28	6.4	5.5	5.1	5.0	5.0	7.1	5.9	5.4	5.1	5.0
29	9.4	7.8	7.0	6.4	6.1	10.6	8.8	7.8	7.1	6.7
30	14.2	12.3	11.1	10.3	9.7	16.0	13.9	12.6	11.7	11.0
31	20.9	18.9	17.6	16.7	16.0	23.4	21.2	19.9	18.9	18.1
32	29.3	27.5	26.4	25.6	25.0	32.4	30.6	29.5	28.6	27.9
33	39.2	38.1	37.4	36.9	36.5	43.0	41.9	41.1	40.6	40.2

	RH = 70%					**RH = 80%**				
	Velocity [m/s]					Velocity [m/s]				
DBT[°C]	0.1	0.2	0.3	0.4	0.5	0.1	0.2	0.3	0.4	0.5
28	7.8	6.4	5.7	5.4	5.2	8.8	7.1	6.2	5.7	5.4
29	12.0	10.0	8.8	8.0	7.5	13.5	11.2	9.9	9.0	8.4
30	18.0	15.7	14.3	13.3	12.5	20.2	17.7	16.1	15.0	14.2
31	26.1	23.8	22.3	21.2	20.4	28.9	26.5	24.9	23.8	22.9
32	35.8	33.9	32.7	31.8	31.1	39.3	37.3	36.0	35.1	34.3
33	46.9	45.7	45.0	44.4	44.0	50.8	49.7	48.9	48.4	47.9

	RH = 90%					**RH = 100%**				
	Velocity [m/s]					Velocity [m/s]				
DBT[°C]	0.1	0.2	0.3	0.4	0.5	0.1	0.2	0.3	0.4	0.5
28	9.8	7.9	6.9	6.2	5.8	11.0	8.8	7.6	6.9	6.4
29	15.1	12.7	11.2	10.2	9.4	16.9	14.2	12.6	11.5	10.6
30	22.5	19.8	18.1	16.9	16.0	25.0	22.1	20.3	19.0	18.0
31	31.9	29.3	27.7	26.5	25.5	35.0	32.3	30.6	29.3	28.3
32	42.9	40.8	39.5	38.6	37.8	46.5	44.5	43.1	42.1	41.3
33	54.8	53.7	52.9	52.4	51.9	58.8	57.7	56.9	56.4	55.9

The predicted percentage dissatisfied under the different combustions of environmental factors confined the standalone use of a natural ventilation system to make a naturally conditioned space. The value of PPD with more than 20% is forced designer to use either a mechanical ventilation system or a mechanical cooling

system to maintain the required indoor thermal comfort level. Further, these results will be helped to predict the time duration which required to operate an alternative system when natural ventilation system cannot meet the specified requirement.

6.2 Effect of Geometric Parameters on Thermal Comfort

The thermal performance of the buildings is depended on many factors. Therefore, a parametric analysis is required to quantify the effect of the various parameters on its thermal comfort. Further, the analysis helps to explore and understand the mechanisms controlling the thermal performance of the space. The present study has been focused only on the use of solar assisted buoyancy driven natural ventilation in an office space and an investigation of the effect of the main parameters influencing the solar chimney and the thermal performance of the space.

The most influential geometrical parameters have been identified as chimney inlet height and width, the gap between chimney walls and the height and width of the inlet window. In addition, construction material and structural design of the space and the chimney and solar intensity, radiation properties of the building surfaces and shading are also influenced on the thermal performance. The selected parameters were varied one by one in a certain range with some variations from the chimney design specifications selected to determine the sensitivity of the thermal performance to each parameter. Some typical results are presented in this section concerning the effect of these parameters on the thermal performance of the space. The effect of each input parameter was examined in terms of four output performance parameters such as mean value and standard deviation corresponding to the flow velocity and the PPD value.

For the purpose of simulation, the ambient temperature was taken as 29.6°C considering the results obtained by climatic data analysis while relative humidity level was taken as 80% based on the annual mean value calculated for daytime period. The values of activity, metabolic rate for seated activity and clothing insulation were selected as 0, 60 W/m^2 and 0.5 Clo respectively. The air flow velocities in the area of interest were determined from the simulated results of CFD. These values were used to calculate the value of PPD_{NV} for the evaluation of the thermal comfort conditions in the occupied area of the space. The velocity flow field on a horizontal plane at 0.6 m above the floor level has been selected to investigate

the thermal performance for the seated activity. Therefore, CFD simulations were carried out to investigate the influence of chimney wall temperature on the air flow field in the space by varying the geometric parameters of the chimney with its wall temperature. The temperature difference between inside surface of the chimney wall and ambient air changed from 5˚C to 30˚C at 5˚C intervals. The width of chimney was changed from 0.1 m to 0.5 m while chimney inlet height was changed from 0.1 m to 0.4 m. The results obtained for the mean velocity and mean PPD_{NV} with corresponding standard deviation values for seated activity are given in Tables 6.2.

Table 6.2: PPD_{NV} and flow velocity variation with the temperature difference between ambient air and chimney surface for diffenernt geomerical configurations

Case A: Cavity width 0.1 m inlet height 0.1 m

	Temperature difference [˚C]					
	5	10	15	20	25	30
PPD% - Mean	19.7	15.3	12.9	11.5	10.9	10.5
PPD% - SD	2.2	2.6	2.6	2.6	2.6	2.6
V (ms^{-1}) – Mean	0.13	0.22	0.26	0.29	0.32	0.36
V (ms^{-1}) – SD	0.10	0.17	0.21	0.23	0.26	0.28

Case B: Cavity width 0.2 m inlet height 0.1 m

	Temperature difference [˚C]					
	5	10	15	20	25	30
PPD% - Mean	19.2	14.7	12.3	10.9	10.3	9.9
PPD% - SD	2.4	2.8	2.8	2.7	2.7	2.7
V (ms^{-1}) - Mean	0.15	0.27	0.33	0.37	0.40	0.44
V (ms^{-1}) - SD	0.12	0.21	0.26	0.29	0.32	0.35

Case C: Cavity width 0.3 m inlet height 0.1 m

	Temperature difference [˚C]					
	5	10	15	20	25	30
PPD% - Mean	19.3	14.8	12.4	11.0	10.4	10.0
PPD% - SD	2.3	2.8	2.8	2.7	2.6	2.7
V (ms^{-1}) - Mean	0.15	0.26	0.32	0.36	0.40	0.43
V (ms^{-1}) - SD	0.12	0.21	0.25	0.28	0.31	0.34

Case D: Cavity width 0.5 m inlet height 0.1 m

	Temperature difference [˚C]					
	5	10	15	20	25	30
PPD% - Mean	19.4	15.0	12.5	11.0	10.4	10.1
PPD% - SD	2.3	2.7	2.7	2.7	2.6	2.6
V (ms^{-1}) - Mean	0.14	0.25	0.31	0.36	0.39	0.42
V (ms^{-1}) - SD	0.11	0.19	0.24	0.28	0.30	0.33

The graphical representations of the statistical analysis tabulated for each case in the table 6.2 are shown respectively from figure 6.1 to 6.8 to illustrate the velocity variation and the PPD_{NV} variation separately.

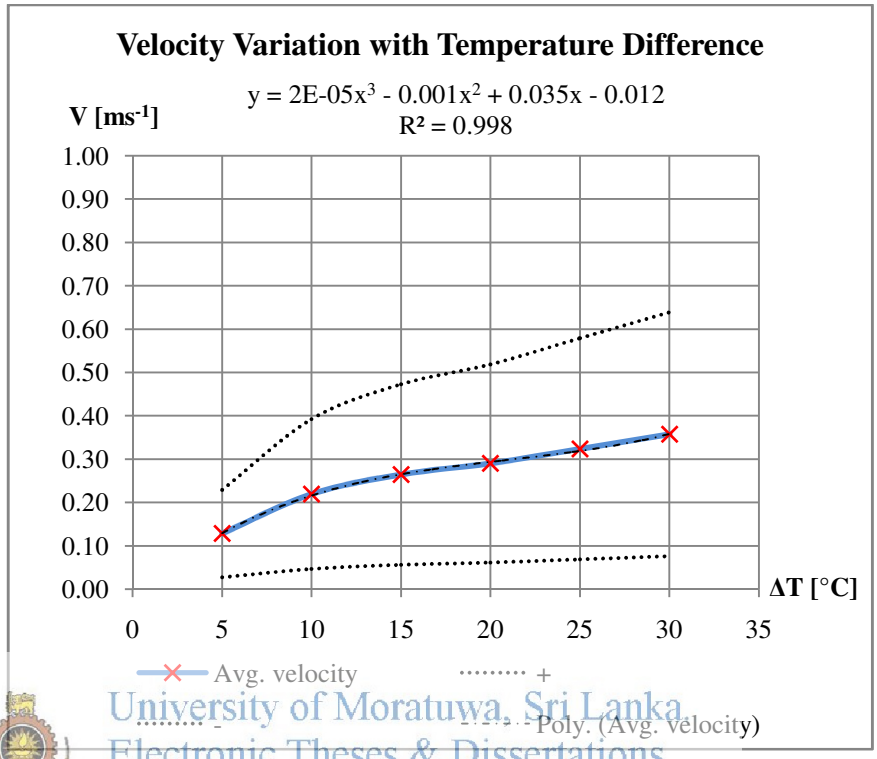

Figure 6.1: Average velocity variation with temperature difference for Case A

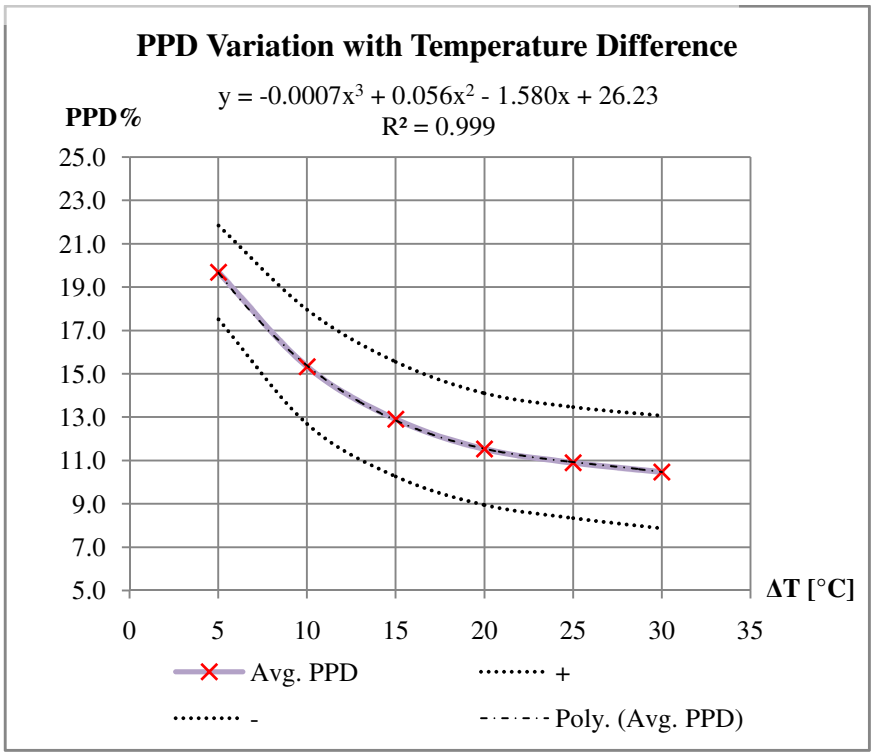

Figure 6.2: Average PPD_{NV} variation with temperature difference for Case A

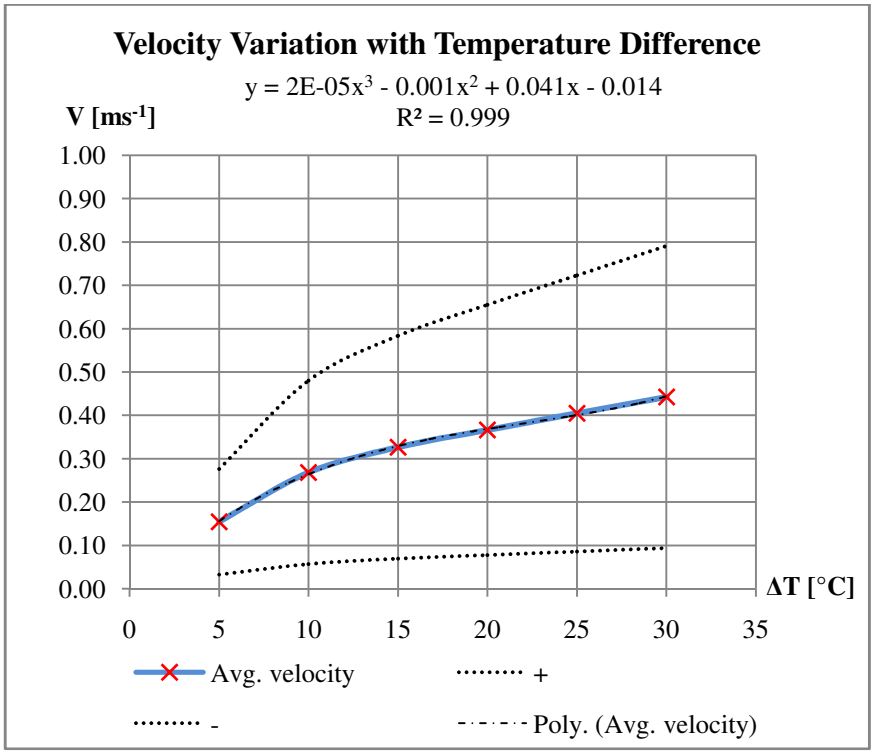

Figure 6.3: Average velocity variation with temperature difference for Case B

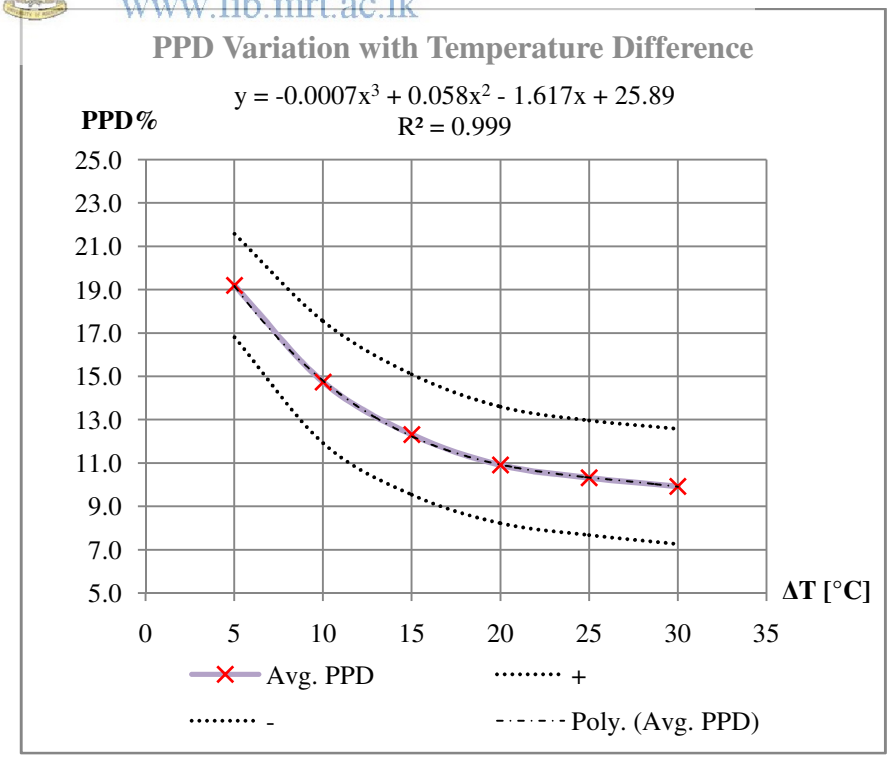

Figure 6.4: Average PPD_{NV} variation with temperature difference for Case B

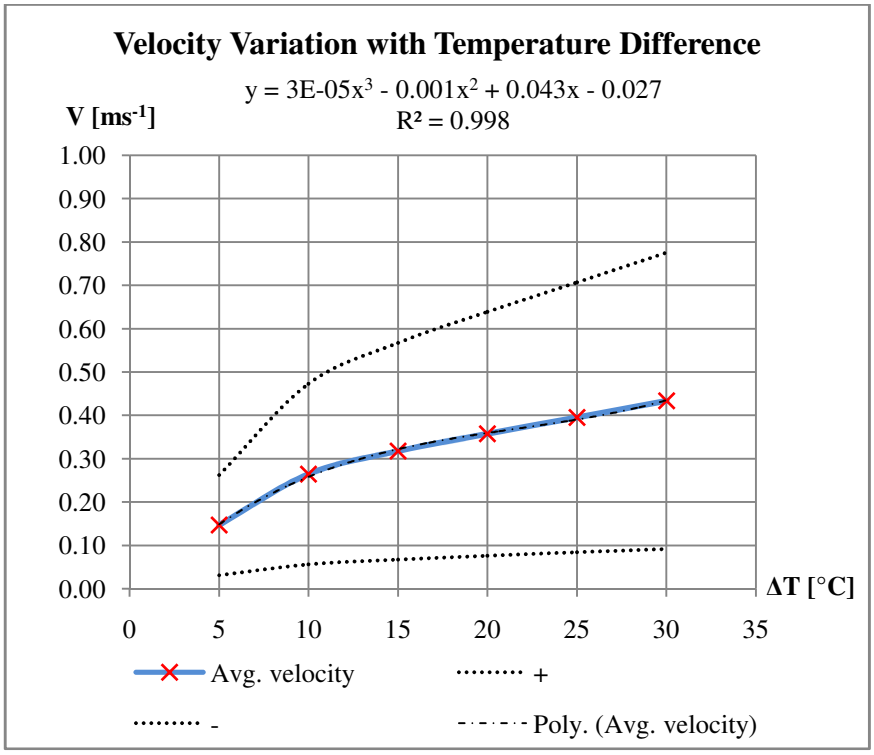

Figure 6.5: Average velocity variation with temperature difference for Case C

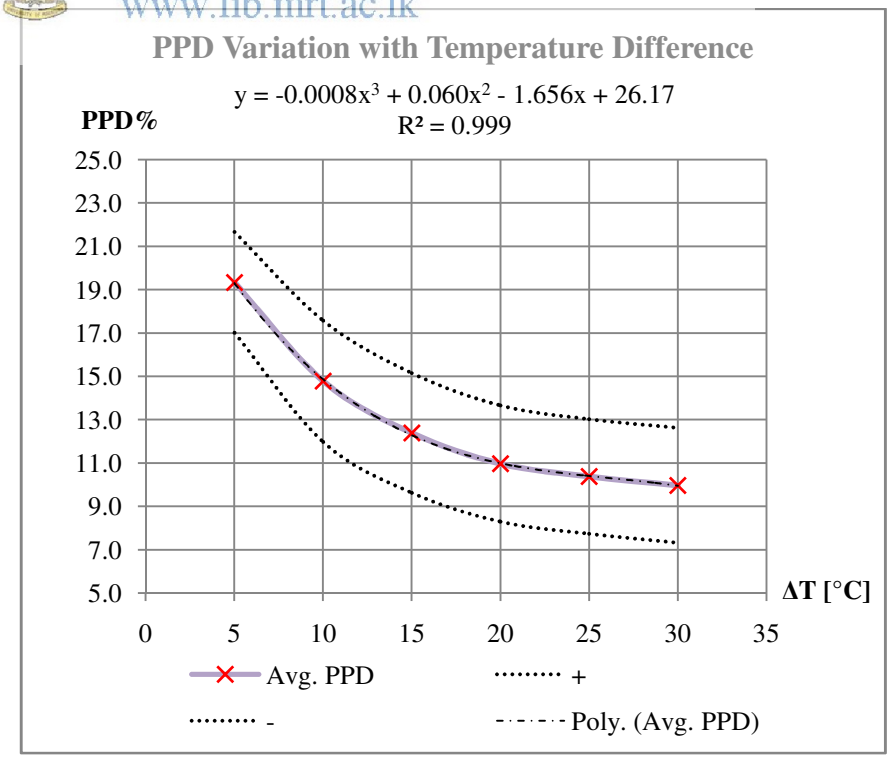

Figure 6.6: Average PPD_{NV} variation with temperature difference for Case C

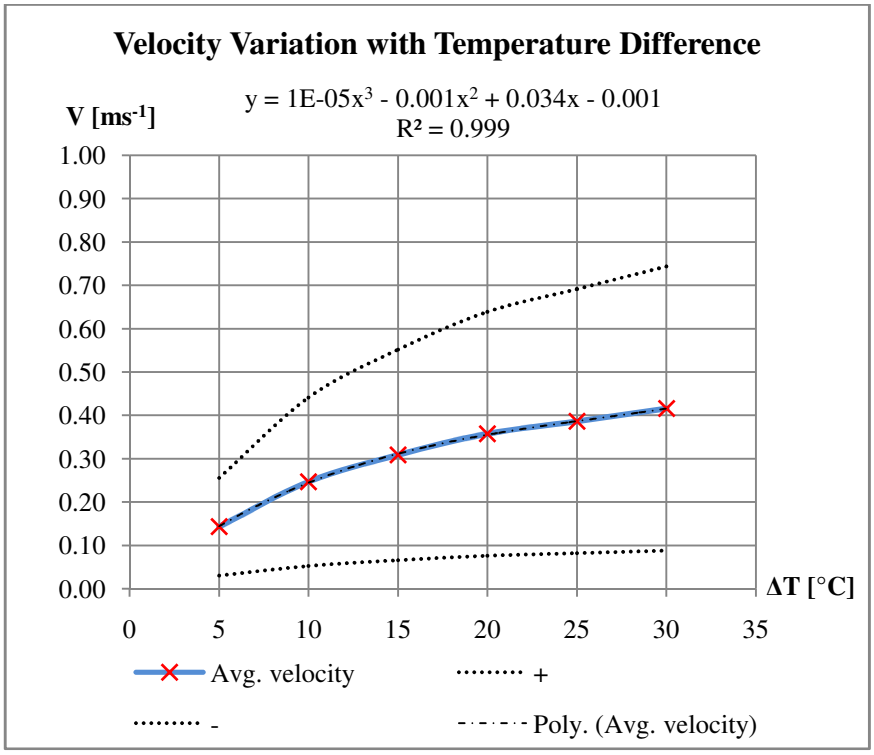

Figure 6.7: Average velocity variation with temperature difference for Case D

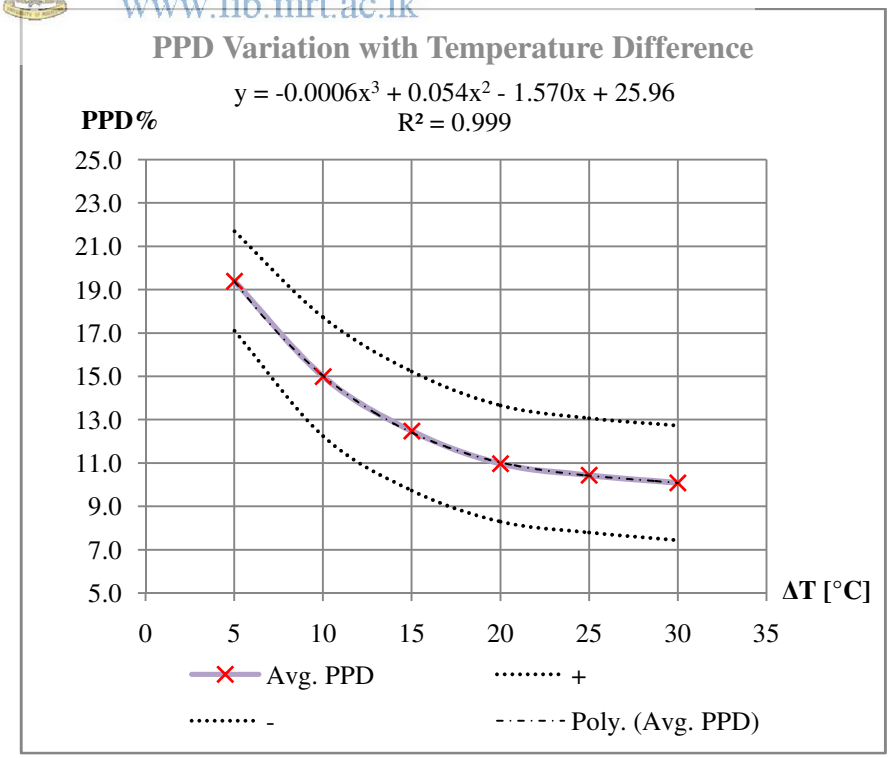

Figure 6.8: Average PPD_{NV} variation with temperature difference for Case D

Further, mean values of the velocity and PPD_{NV} were plotted with corresponding standard deviation values thereby identifying the best fit regression equations and coefficient of correlation. Curves shown by the dotted lines are illustrated the upper bound and the lower bound of the standard deviation of the mean values of the velocity and predicted percentage of dissatisfies people on the horizontal plane selected for the analysis.

The air was supplied to these layers from the room through an inlet at the bottom of the cavity. Simulated results showed that the flow of air in the cavity takes place within layers near the heated wall surfaces. The thickness of each boundary layer at the top of the cavity varied slightly with the temperature difference between the heated wall surface of the cavity and the ambient air and the layer was thicker with the higher temperature differences. In addition, the analysis showed that the flow velocity is dependent upon the temperature difference between the heated cavity walls and the ambient air and thereby the convective heat transfer coefficient is also dependent on the cavity width and the velocity of the air flow. The temperature increase of the air as it travels along the cavity also was found to be a nearly 2nd order polynomial function of the said temperature difference.

The figures show that with the increase of temperature difference calculated mean velocity is also increased thereby reducing the number of occupants thermally dissatisfied within the space. However, the difference between the maximum and minimum values of the local velocities reported in the simulation increases with the temperature difference showing a drastically diverging behaviour. Further, that represents the velocity difference between air moving through the vertical centre plane of the room and air stagnated closer to the walls and corners of its space. This may be caused of boussinesq approximation used in the numerical scheme of the simulation.

A significant variation in the calculated values of the PPD_{NV} were identified when temperature difference varies from 5°C to 20°C but beyond that difference it was not much affected. For a fixed 0.1 m chimney inlet height, the mean velocity increases up to 0.2 m of the cavity width and then it decreases by confirming the optimum width for an effective cavity. This variation can be observed for all the identical temperature differences indicated in case A, B, C and D. According to the PPD_{NV} values calculated based on the simulations, almost 90% of the occupant can be

thermally satisfied in the space considered under case B, if the optimum cavity width is used as 0.2 m for 0.1 m effective chimney inlet height.

Similarly, another studied was carried out under the four distinct cases, to investigate the chimney inlet height on the thermal performance of the space. The results calculated for the geometric configurations of 0.4 m inlet height with its various cavity widths are represent in table 6.3.

Table 6.3: PPD_{NV} and flow velocity variation with the temperature difference between ambient air and chimney surface for different geometrical configurations

Case E: Cavity width 0.1 m inlet height 0.4 m

	Temperature difference [˚C]					
	5	10	15	20	25	30
PPD% - Mean	19.7	15.5	13.0	11.4	10.8	10.4
PPD% - SD	2.1	2.5	2.6	2.6	2.6	2.6
V (ms^{-1}) - Mean	0.13	0.21	0.25	0.30	0.33	0.36
V (ms^{-1}) - SD	0.10	0.16	0.19	0.23	0.25	0.27

Case F: Cavity width 0.2 m inlet height 0.4 m

	Temperature difference [˚C]					
	5	10	15	20	25	30
PPD% - Mean	18.3	13.8	11.5	10.0	9.6	9.3
PPD% - SD	2.4	2.8	2.7	2.6	2.6	2.5
V (ms^{-1}) - Mean	0.16	0.29	0.35	0.42	0.44	0.46
V (ms^{-1}) - SD	0.12	0.22	0.27	0.32	0.34	0.35

Case G: Cavity width 0.3 m inlet height 0.4 m

	Temperature difference [˚C]					
	5	10	15	20	25	30
PPD% - Mean	18.2	13.7	11.3	9.9	9.5	9.2
PPD% - SD	2.4	2.8	2.8	2.6	2.6	2.6
V (ms^{-1}) - Mean	0.17	0.30	0.38	0.43	0.46	0.48
V (ms^{-1}) - SD	0.13	0.23	0.30	0.33	0.35	0.37

Case H: Cavity width 0.5 m inlet height 0.4 m

	Temperature difference [˚C]					
	5	10	15	20	25	30
PPD% - Mean	17.9	13.5	11.0	9.8	9.3	9.1
PPD% - SD	2.5	2.9	2.8	2.6	2.6	2.6
V (ms^{-1}) - Mean	0.19	0.33	0.42	0.46	0.48	0.51
V (ms^{-1}) - SD	0.14	0.25	0.32	0.35	0.37	0.39

The graphical representations of the statistical analysis tabulated for each case in the table 6.3 are respectively presented from figure 6.9 to 6.16 to demonstrate the mean velocity variation and mean PPD_{NV} variation separately.

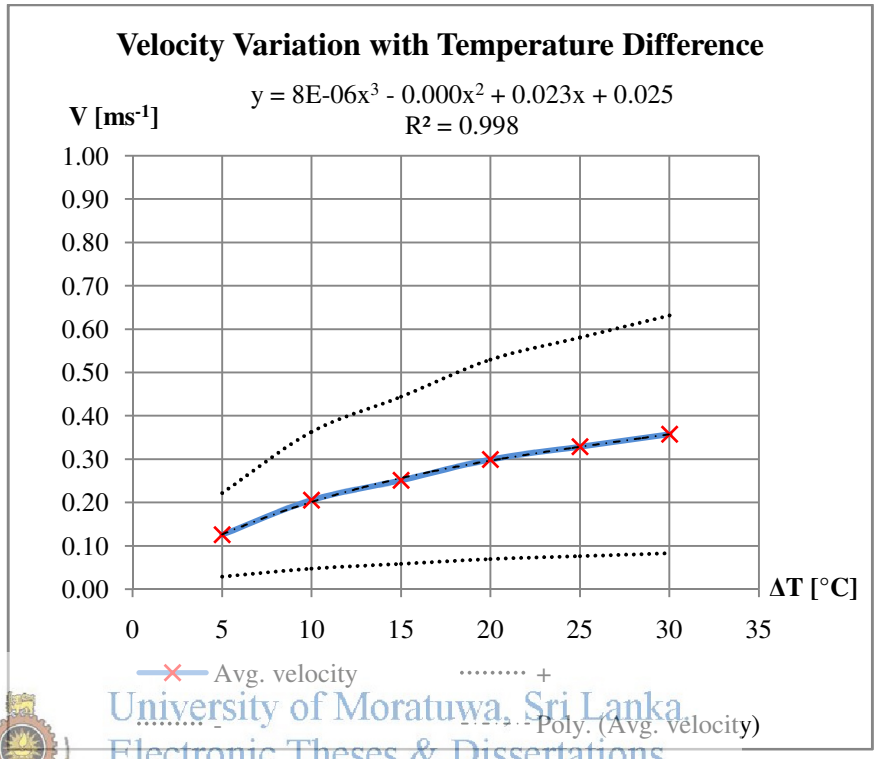

Figure 6.9: Average velocity variation with temperature difference for Case E

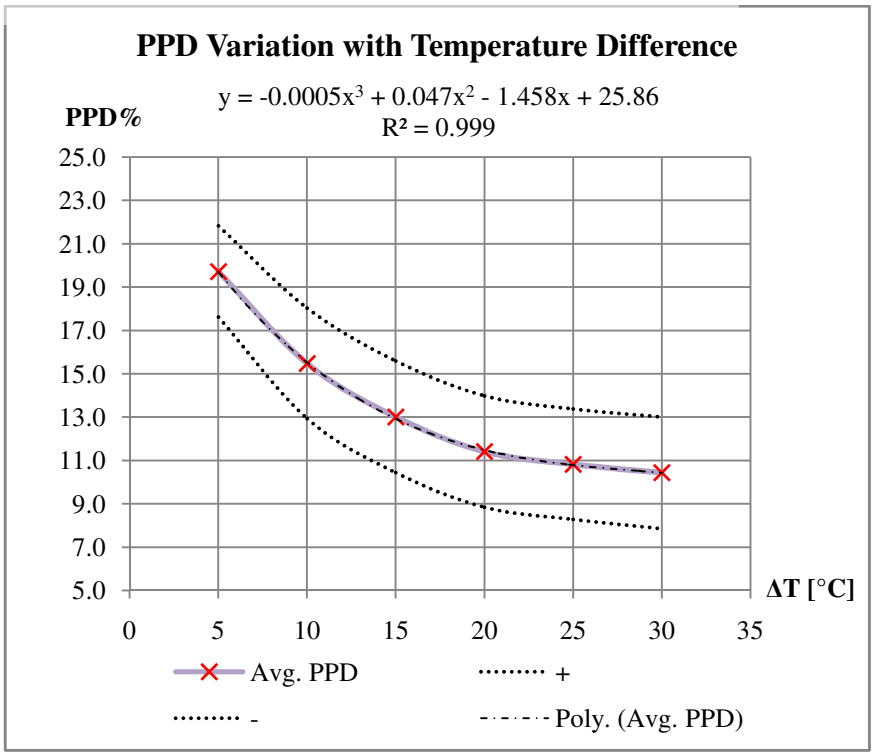

Figure 6.10: Average PPD_{NV} variation with temperature difference for Case E

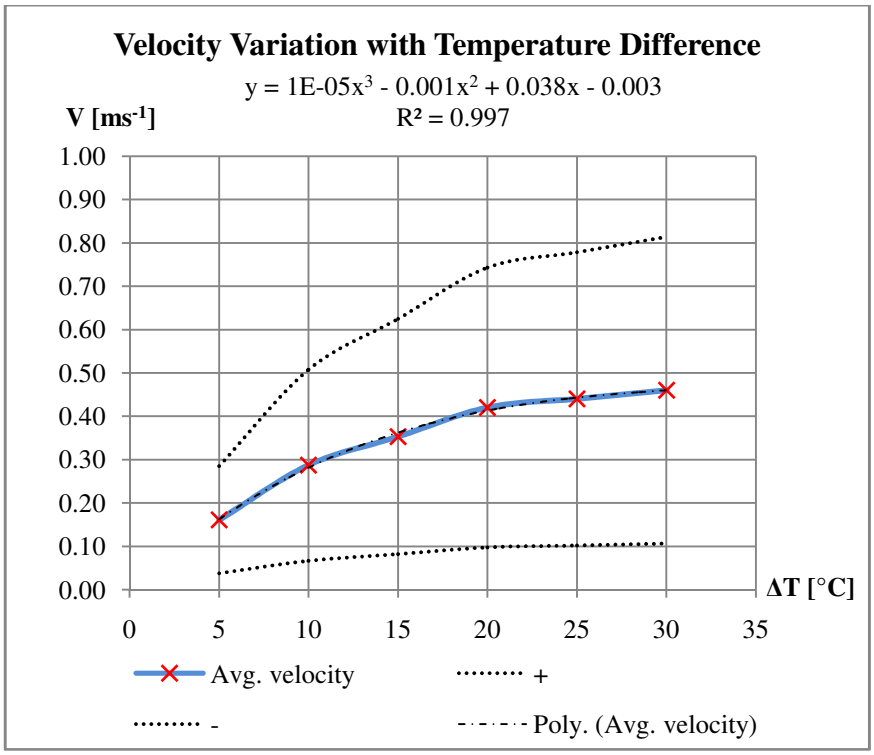

Figure 6.11: Average velocity variation with temperature difference for Case F

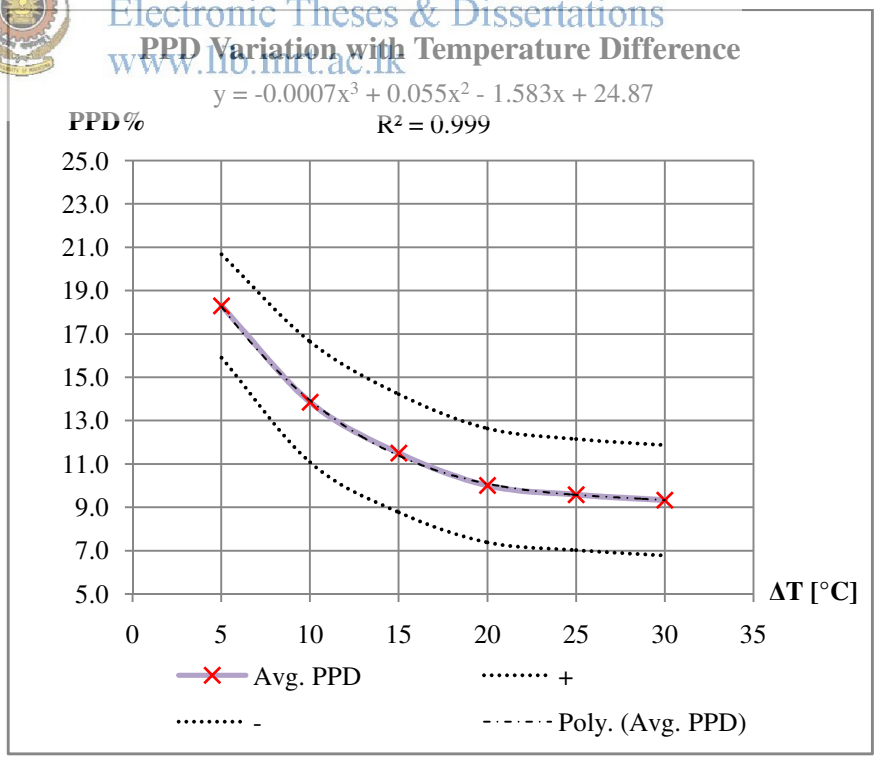

Figure 6.12: Average PPD_{NV} variation with temperature difference for Case F

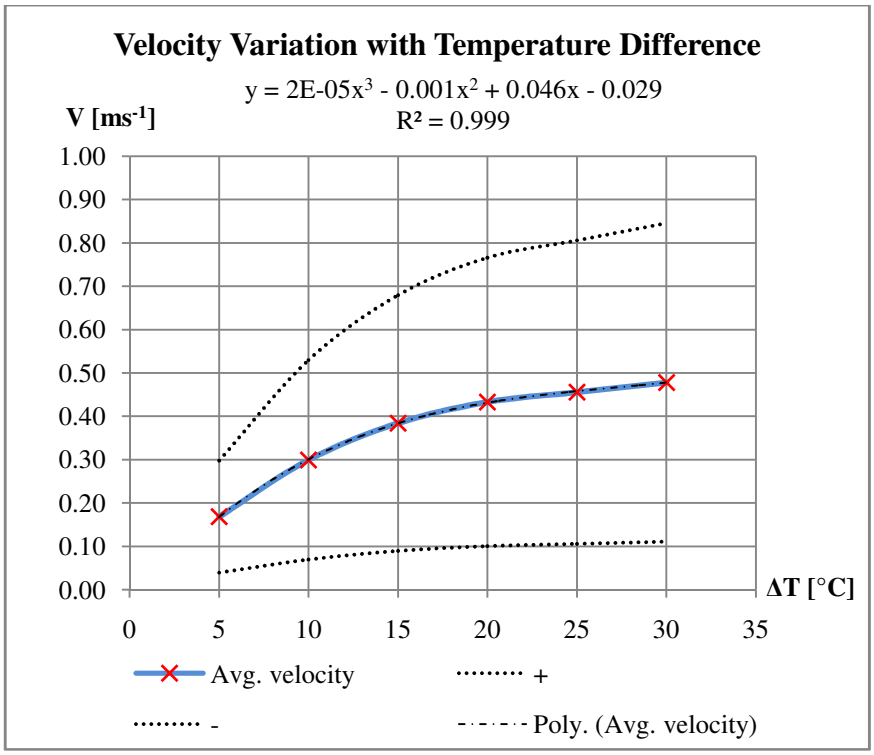

Figure 6.13: Average velocity variation with temperature difference for Case G

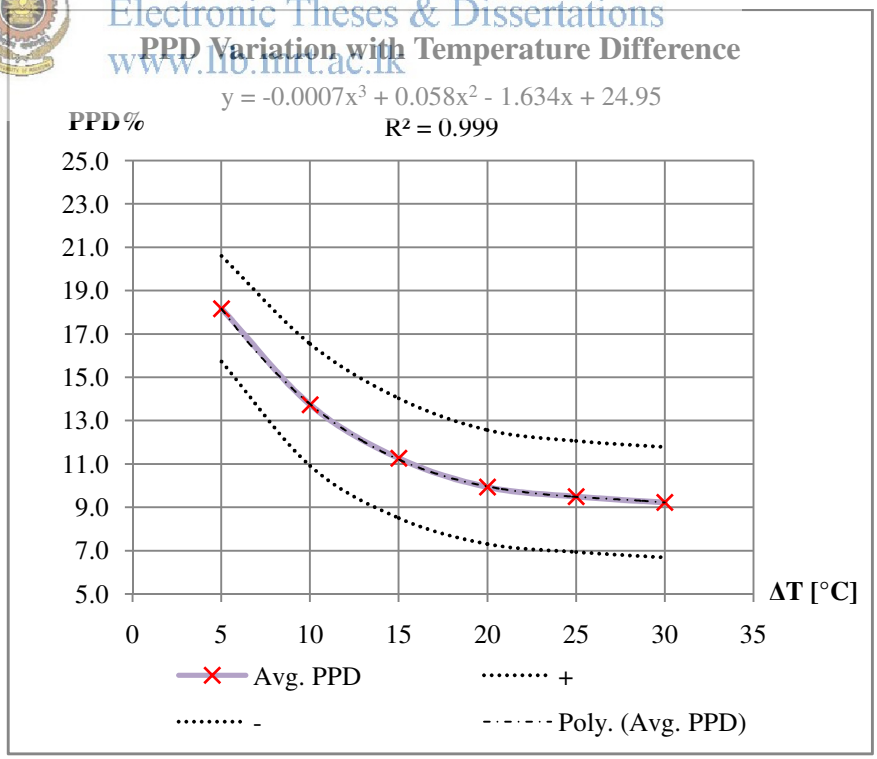

Figure 6.14: Average PPD_{NV} variation with temperature difference for Case G

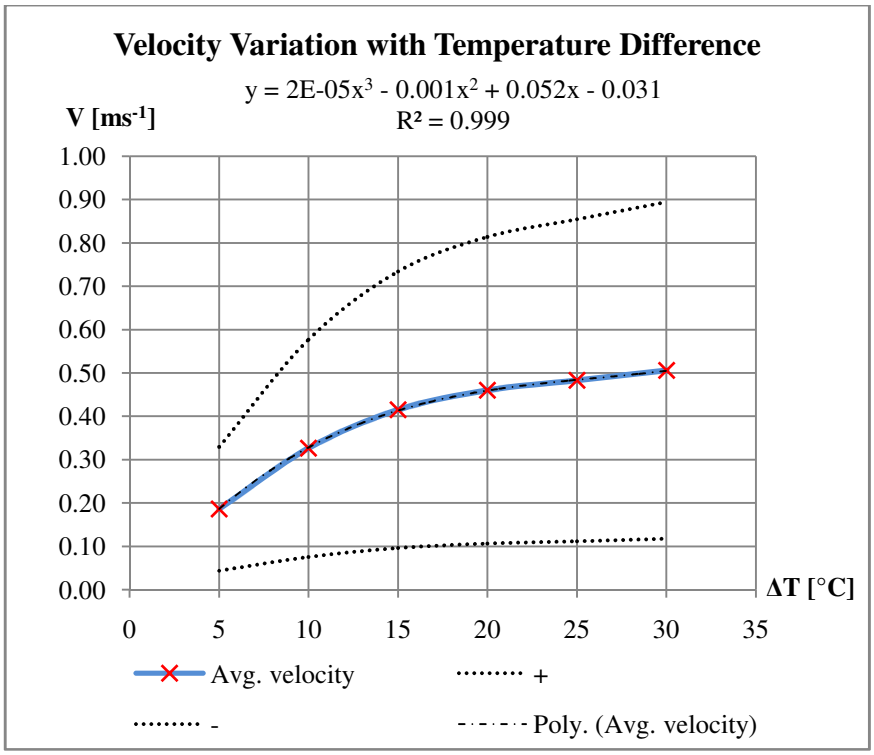

Figure 6.15: Average velocity variation with temperature difference for Case H

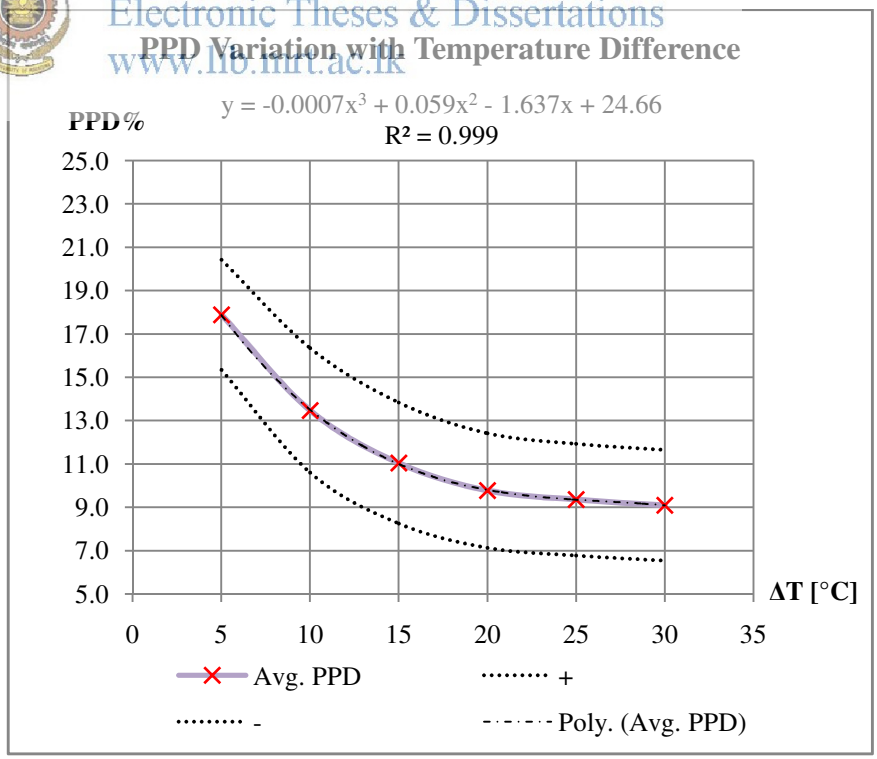

Figure 6.16: Average PPD_{NV} variation with temperature difference for Case H

As the inlet height increases the resistance to the air flow is decreased, thus the flow will increase. However increasing the inlet height will result in reducing the internal wall area, consequently heat storage will be less. It can be seen that results obtained under Case E for 0.1 m cavity width with 0.4 m inlet chimney height is nearly same as the results produced under the Case A for same cavity width with 0.1 m chimney height. Therefore, the air flow field on the selected horizontal plane at 0.6 m above ground is not affected by the chimney inlet height if cavity width is kept as narrow as possible. Further, chimney maintains the same gap between heated walls for the both cases. As a result, development and the growth rates of the thermal boundary layers and velocity boundary layers may be similar for both cases thereby establishing the same boundary layer thickness. However, for Case F, G and H investigated, it was found that mean velocities of the air flow are slightly greater than the values those are calculated under the respective geometric configurations in Case B, C and D. Similarly, number of occupants dissatisfied in the space also reduces compared to the corresponding cases investigated under the 0.1 m chimney inlet height.

It was also noticed that mean air velocity increases with the increase of temperature difference between heated surface of the chimney wall and ambient air for all cases investigated under the employed numerical scheme. The consequent PPD_{NV} values calculated for each case also reduces with increases of the temperature difference. The standard deviation values related to velocity of the flow in each case increases with the increase of temperature difference, thereby increasing the difference between the maximum and minimum value of the velocity. In Case G and Case H, a considerable variation can be recognized in the standard deviation values calculate for velocity compared to Case C and Case D respectively. Therefore, if width of the cavity is larger than 0.2 m, variations in the velocity field are greatly influenced by the chimney inlet height. Further, simulated results shows that more air tends to stagnate closer to the side walls and to the corners of the space providing a narrow down velocity field.

However, it is necessary to improve the thermal performance of the space for the design purpose by minimize the number of occupant dissatisfied and also maintaining the less fluctuation between maximum and minimum values of the velocities. The effect of the cavity width on the thermal performance of the space can be model with the 2^{nd} order polynomial as a function of temperature difference.

Simulated flow field indicates an air flow from the outside by downward flow through the top near the centre, if the cavity is wide enough.

The polynomial curves show that the calculated results for a cavity with an inlet 0.1 m high gives lower values than those given for 0.4 m inlet height, probably because of the increase of pressure loss with the narrow inlet. This consequently shows the optimum width for an effective cavity. If the cavity were taller, the optimum cavity width would be greater. For a 0.4 m high cavity, the optimum width to induce ventilation without down flow would be about 0.4 m.

In view of design aspect, it is necessary to identify the area which air being stagnant. Therefore, contours for velocity and corresponding PPD_{NV} distribution were plotted as shown in figure 6.17 and 6.18 respectively for Case B.

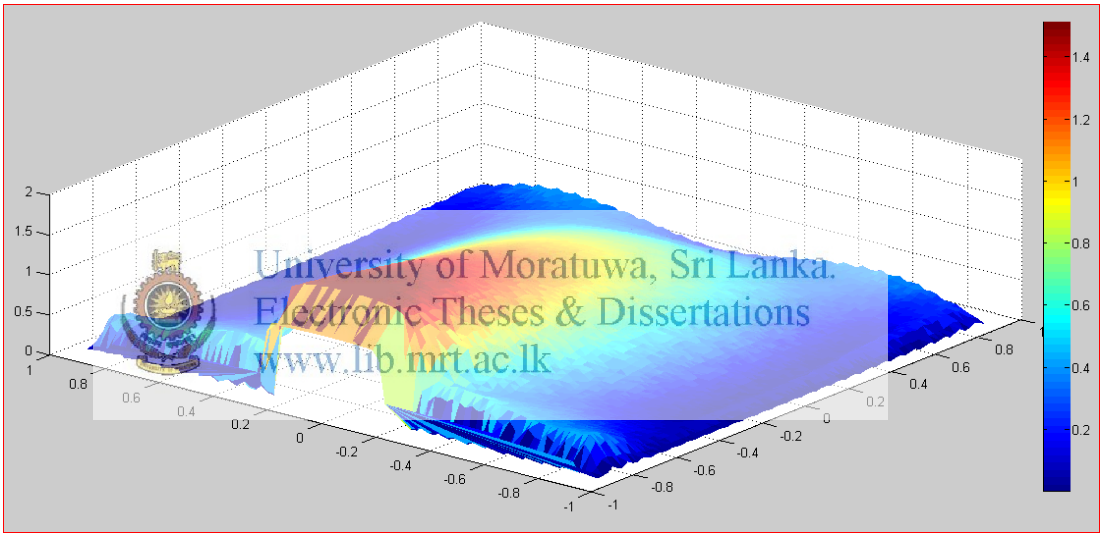

Figure 6.17: 3-D view of the velocity magnitude on the horizontal plane at 0.6 m above the floor

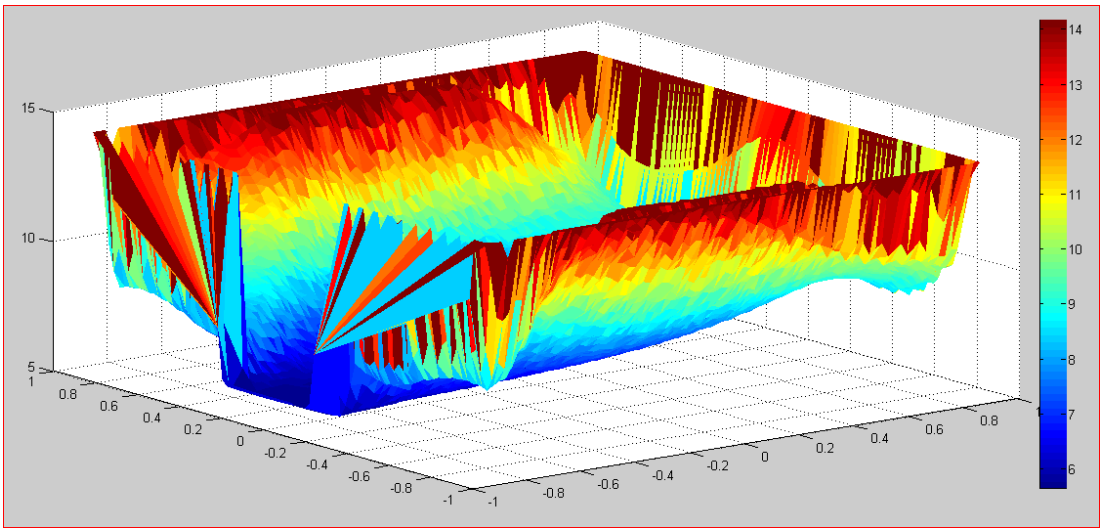

Figure 6.18: 3-D view of the PPD_{NV} distribution on the horizontal plane at 0.6 m above the floor

The velocity and PPD_{NV} plots would solve all the difficulties encountered in selecting a geometrical configuration based on their standard deviation values. Figure 6.19 to 6.28 show the velocity and PPD_{NV} plots for temperature differences simulated in a 0.1 m inlet height and 0.2 m cavity width specified in Case B.

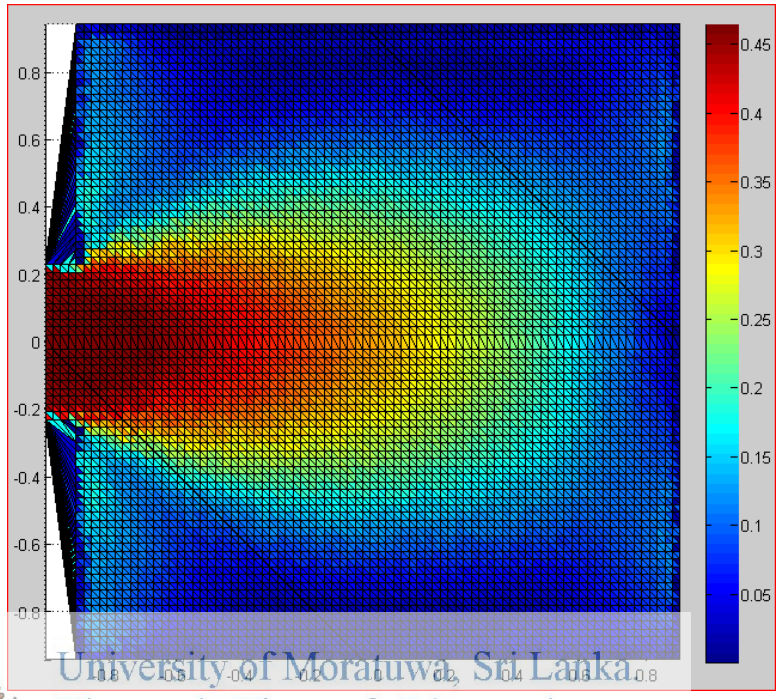

Figure 6.19: Magnitude of the velocity variation on the horizontal plane at 0.6 m above the floor for ΔT= 5°C of CASE B

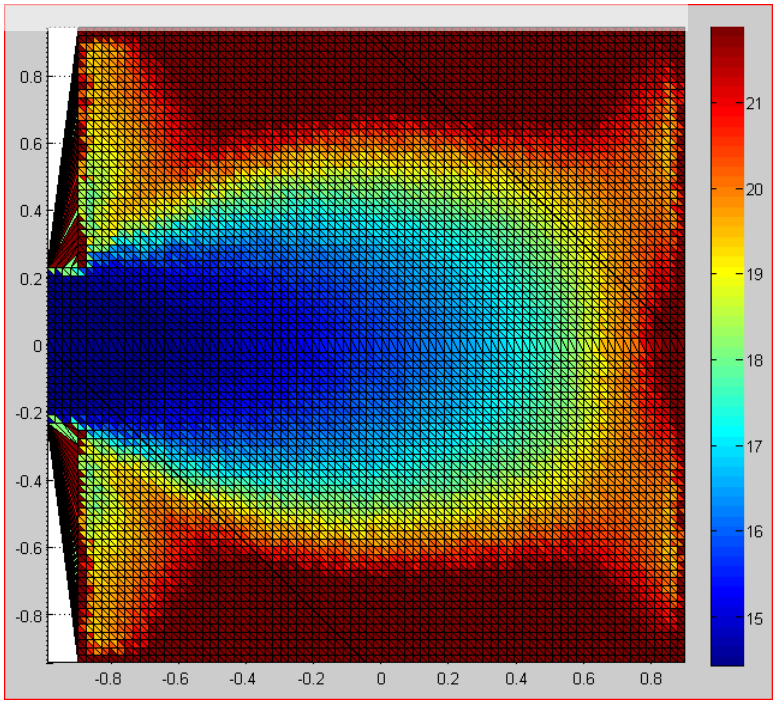

Figure 6.20: PPD_{NV} distribution on the horizontal plane at 0.6 m above the floor for ΔT= 5°C of CASE B

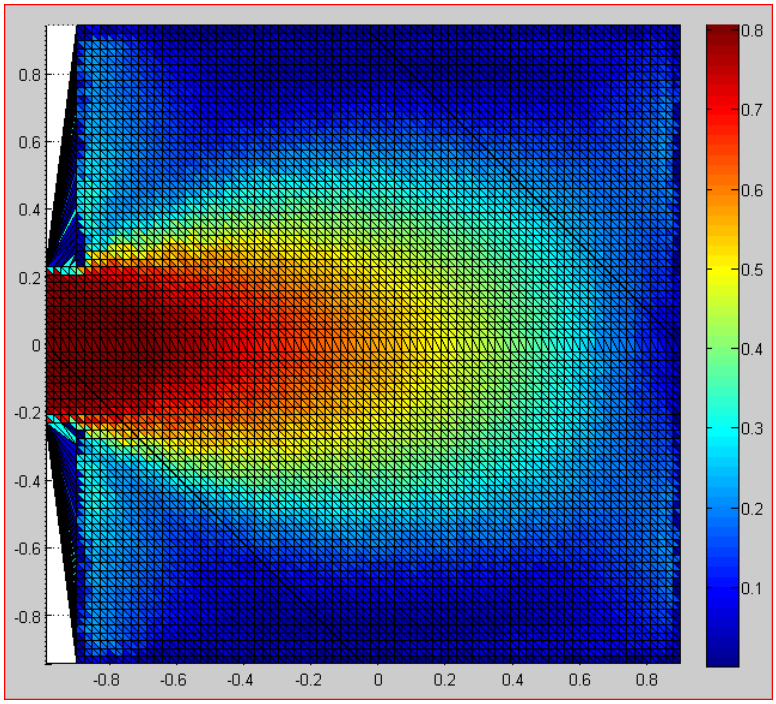

Figure 6.21: Magnitude of the velocity variation on the horizontal plane at 0.6 m above the floor for ΔT= 10°C of CASE B

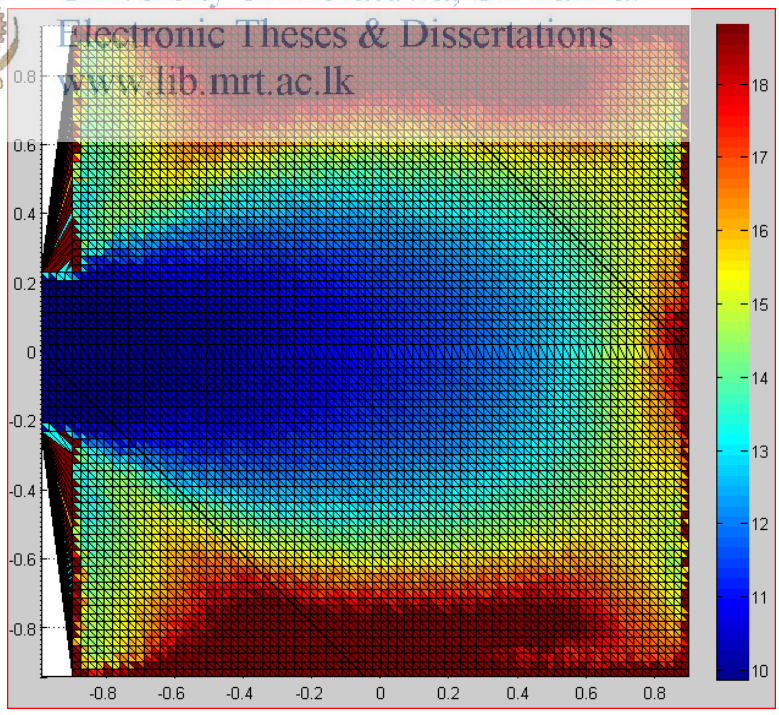

Figure 6.22: PPD_{NV} distribution on the horizontal plane at 0.6 m above the floor for ΔT= 10°C of CASE B

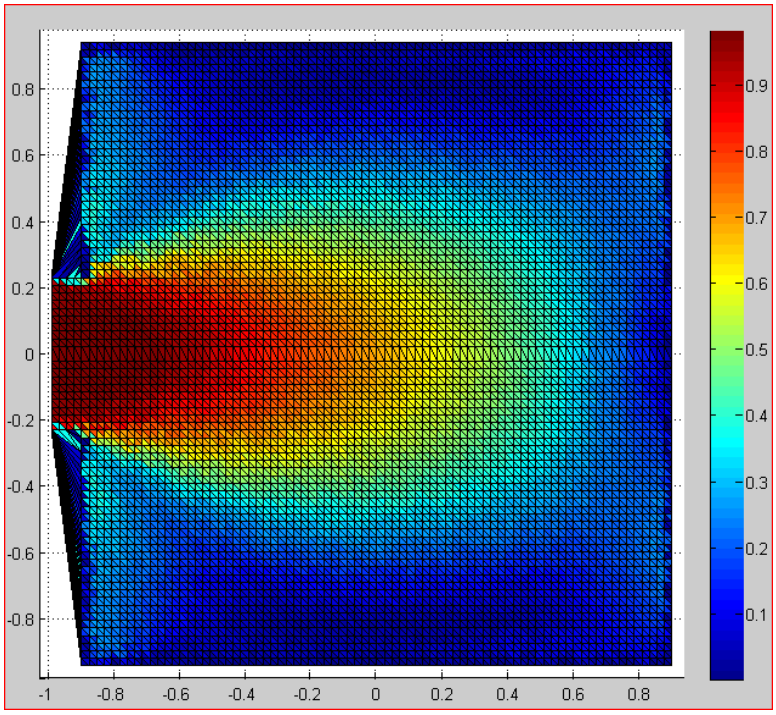

Figure 6.23: Magnitude of the velocity variation on the horizontal plane at 0.6 m above the floor for ΔT= 15°C of CASE B

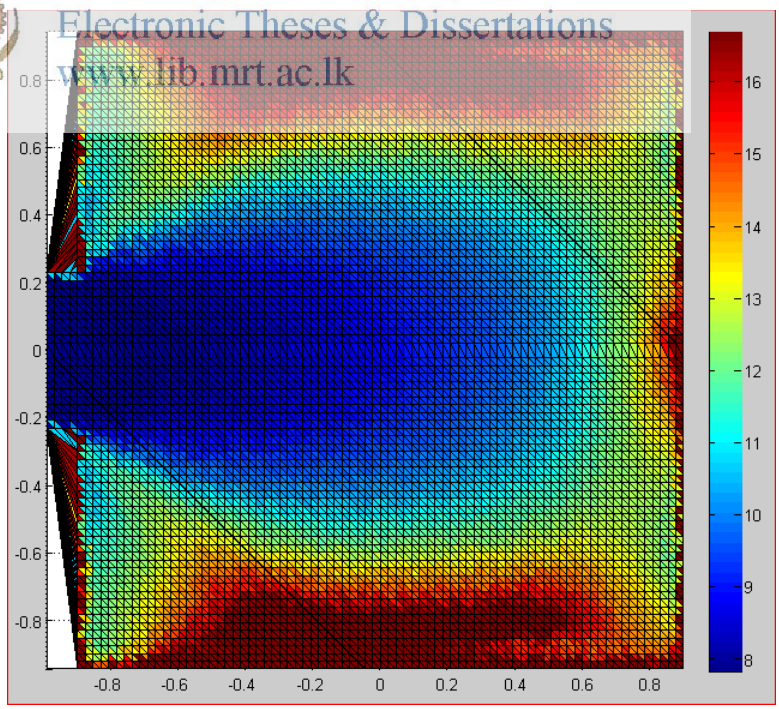

Figure 6.24: PPD_{NV} distribution on the horizontal plane at 0.6 m above the floor for ΔT= 15°C of CASE B

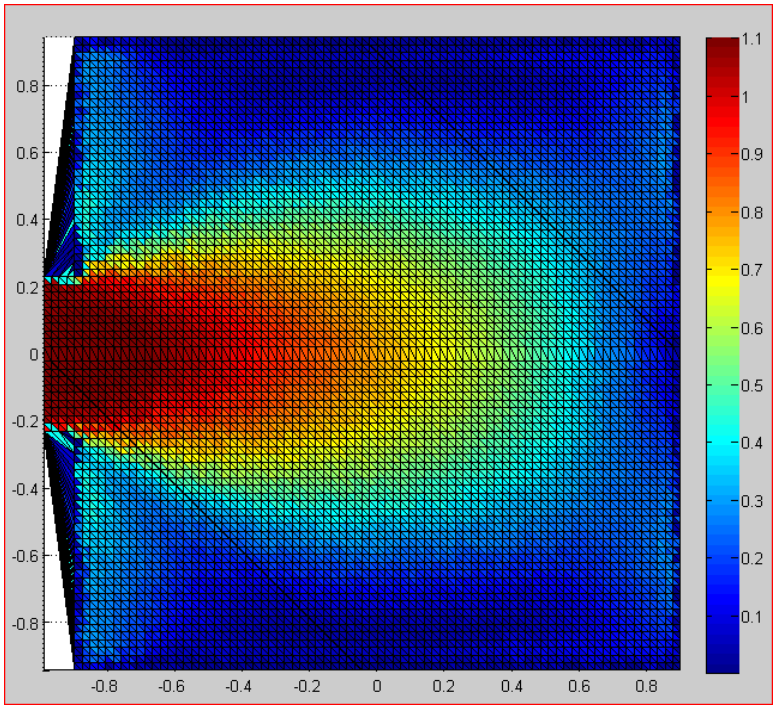

Figure 6.25: Magnitude of the velocity variation on the horizontal plane at 0.6 m above the floor for ΔT= 20°C of CASE B

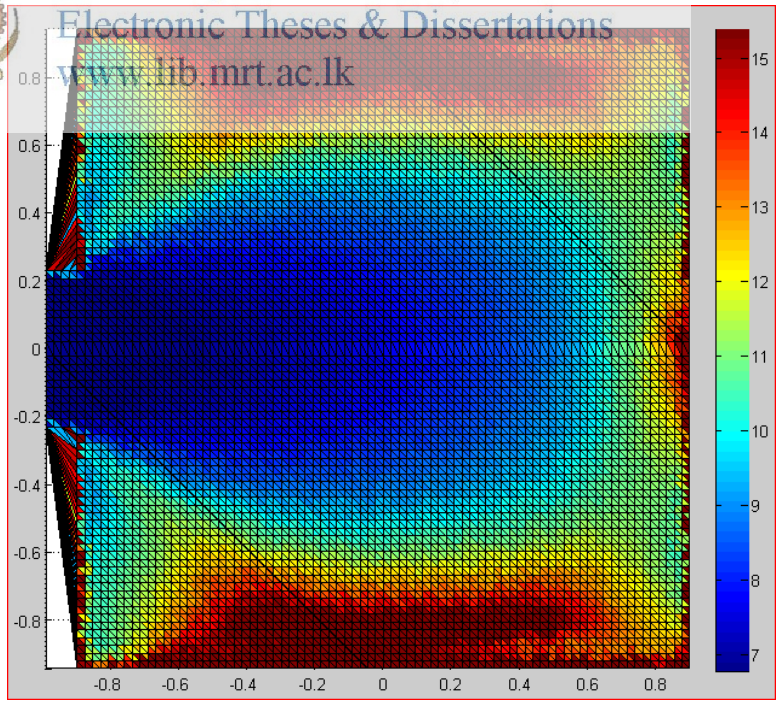

Figure 6.26: PPD_{NV} distribution on the horizontal plane at 0.6 m above the floor for ΔT= 20°C of CASE B

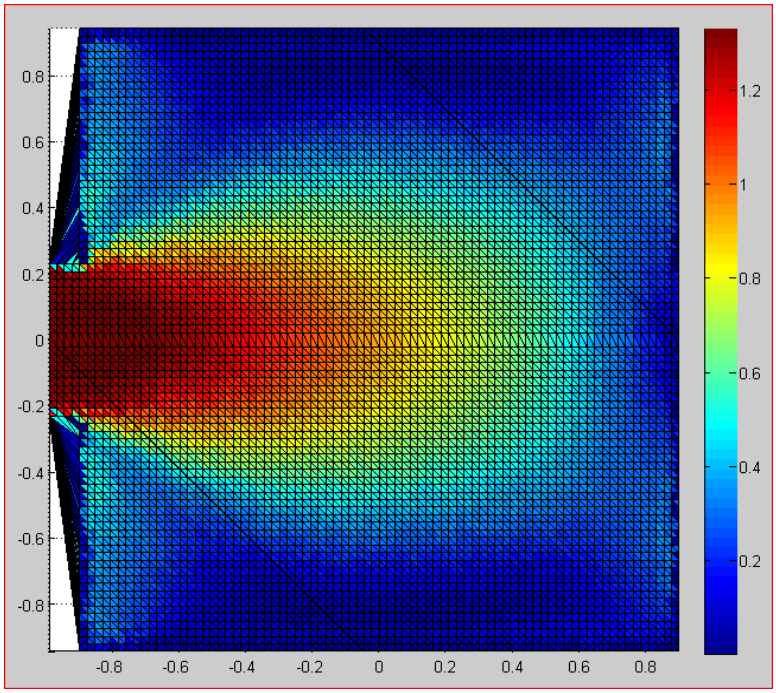

Figure 6.27: Magnitude of the velocity variation on the horizontal plane at 0.6 m above the floor for ΔT= 25°C of CASE B

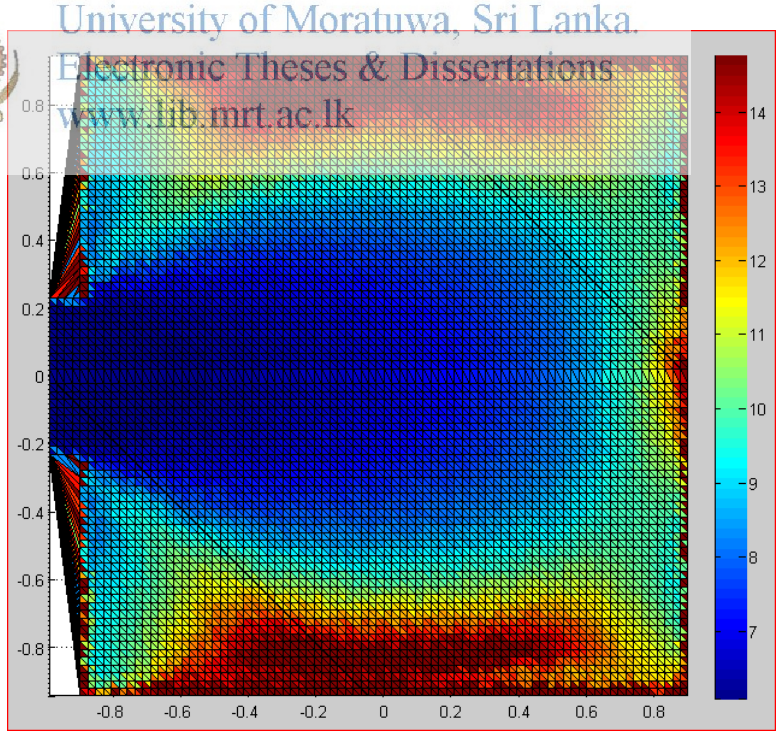

Figure 6.28: PPD_{NV} distribution on the horizontal plane at 0.6 m above the floor for ΔT= 25°C of CASE B

Figure 6.29 to 6.38 show the velocity and PPD_{NV} plots for temperature differences simulated in a 0.4 m inlet height and 0.5 m cavity width specified in Case H.

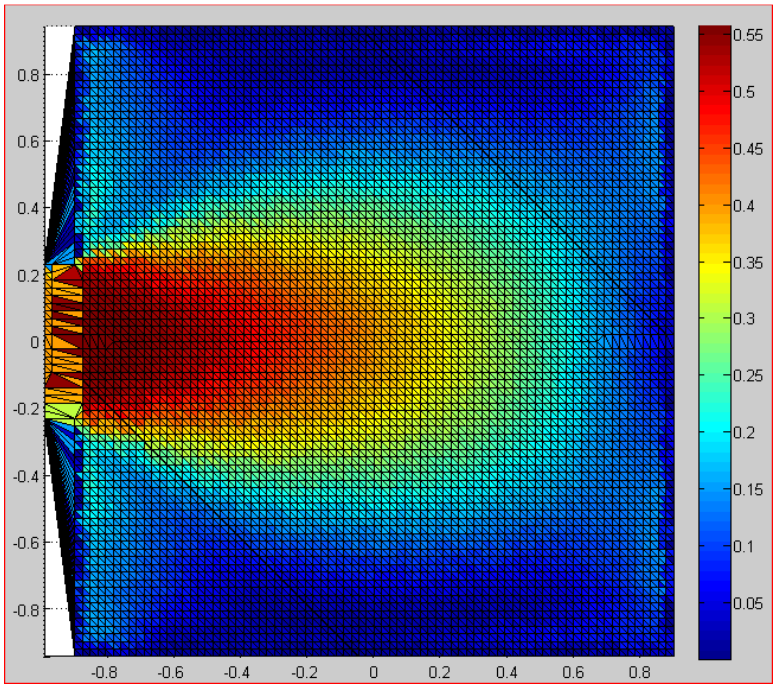

Figure 6.29: Magnitude of the velocity variation on the horizontal plane at 0.6 m above the floor for ΔT= 5°C of CASE H

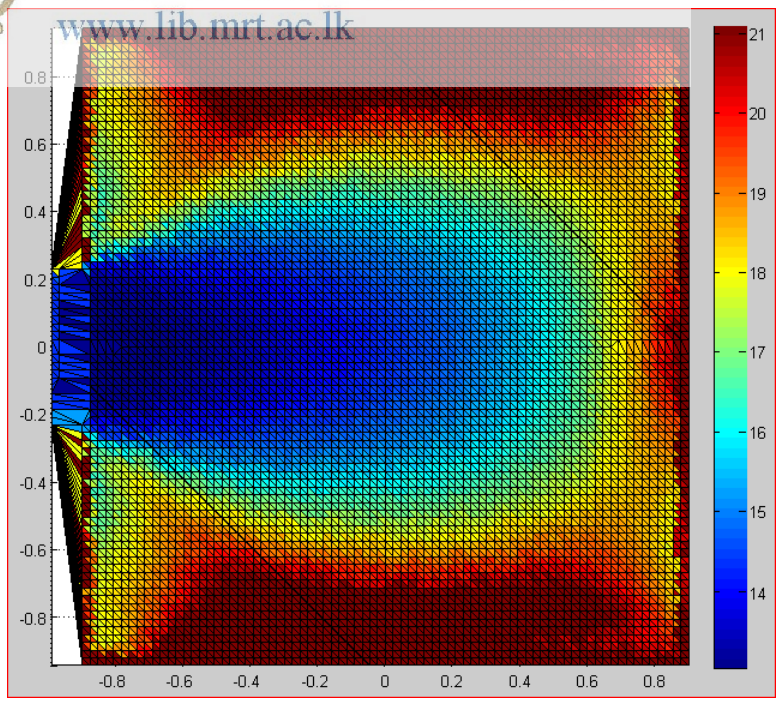

Figure 6.30: PPD_{NV} distribution on the horizontal plane at 0.6 m above the floor for ΔT= 5°C of CASE H

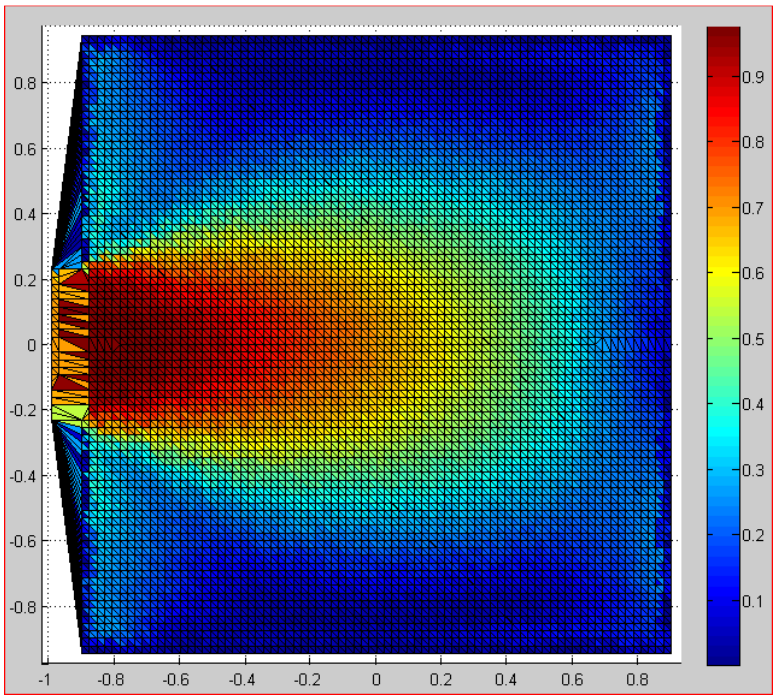

Figure 6.31Magnitude of the velocity variation on the horizontal plane at 0.6 m above the floor for ΔT= 10°C of CASE H

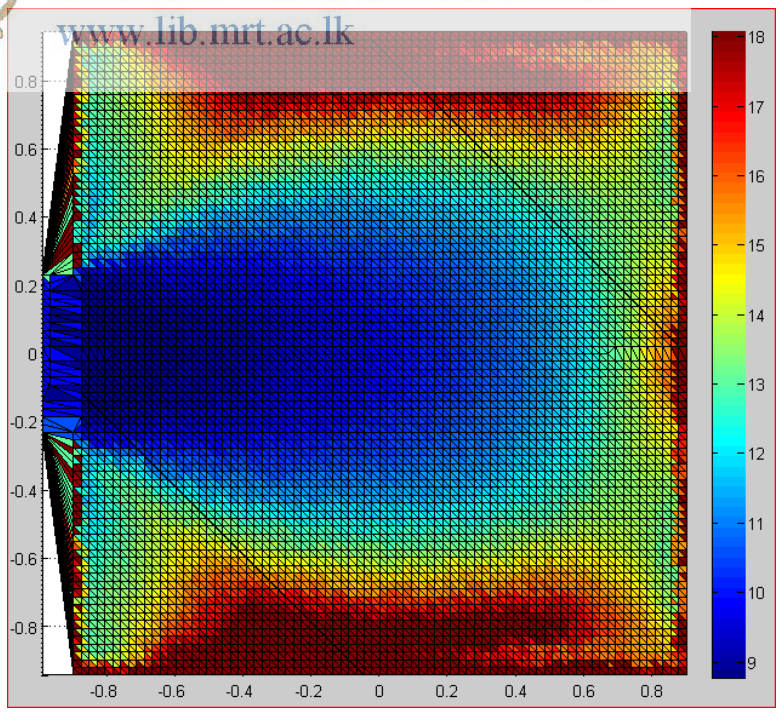

Figure 6.32: PPD_{NV} distribution on the horizontal plane at 0.6 m above the floor for ΔT= 10°C of CASE H

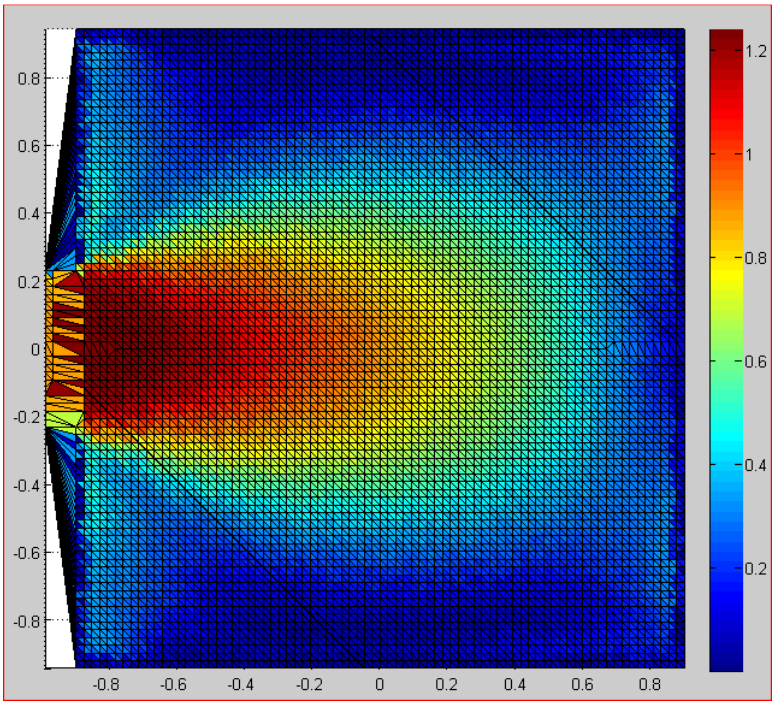

Figure 6.33Magnitude of the velocity variation on the horizontal plane at 0.6 m above the floor for ΔT= 15°C of CASE H

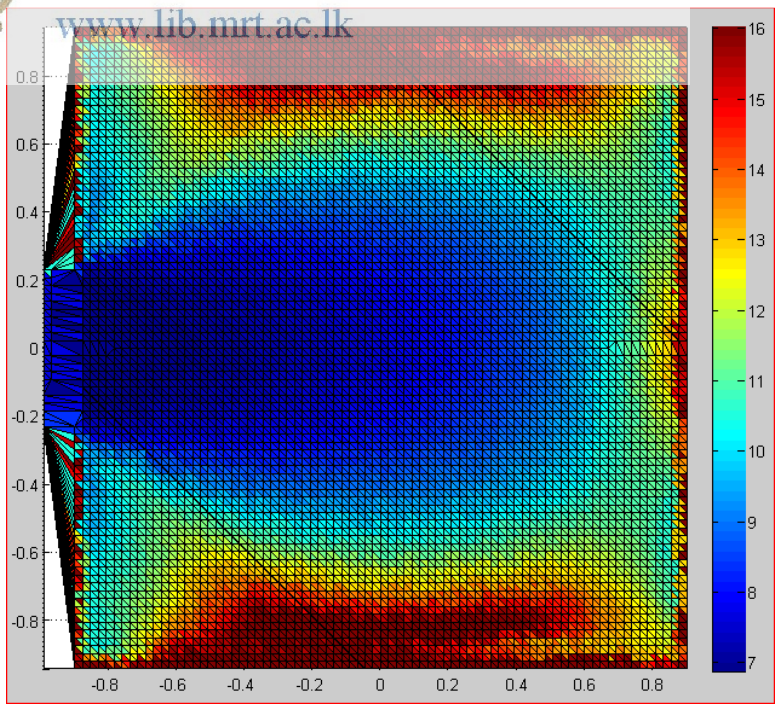

Figure 6.34: PPD_{NV} distribution on the horizontal plane at 0.6 m above the floor for ΔT= 15°C of CASE H

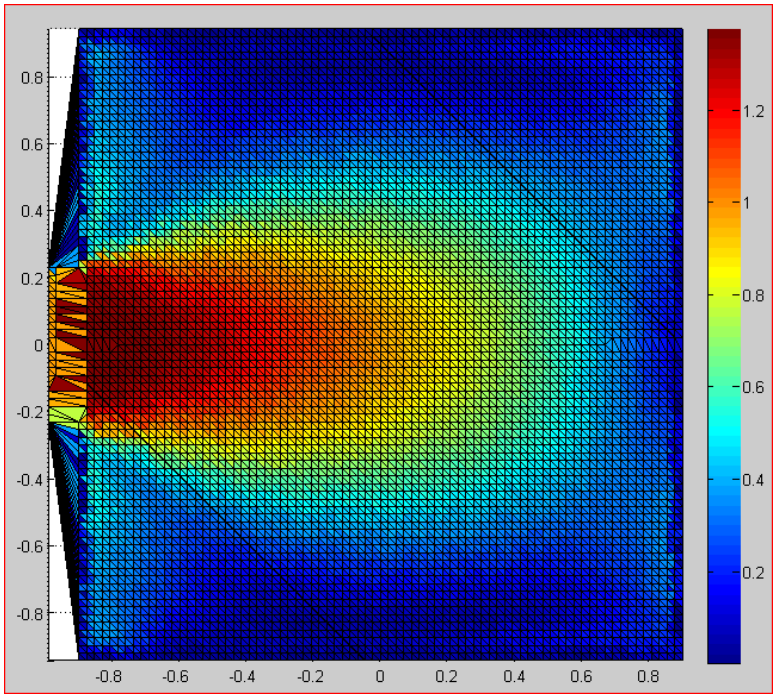

Figure 6.35Magnitude of the velocity variation on the horizontal plane at 0.6 m above the floor for ΔT= 20°C of CASE H

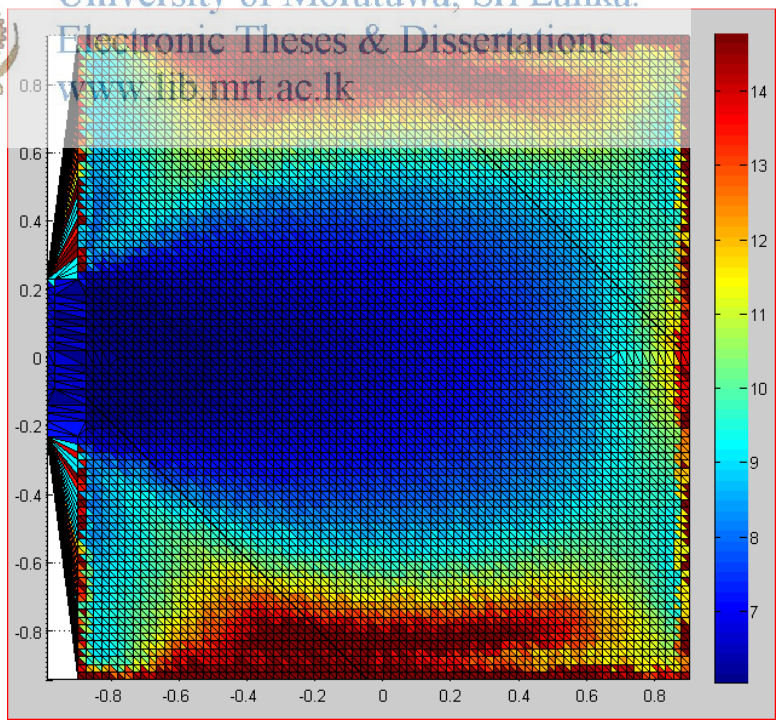

Figure 6.36: PPD_{NV} distribution on the horizontal plane at 0.6 m above the floor for ΔT= 20°C of CASE H

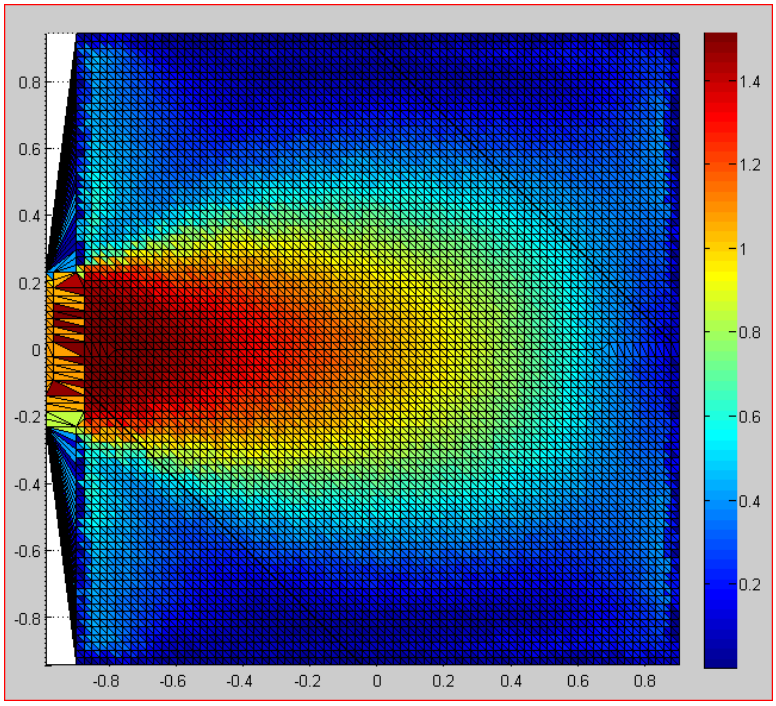

Figure 6.37Magnitude of the velocity variation on the horizontal plane at 0.6 m above the floor for ΔT= 25°C of CASE H

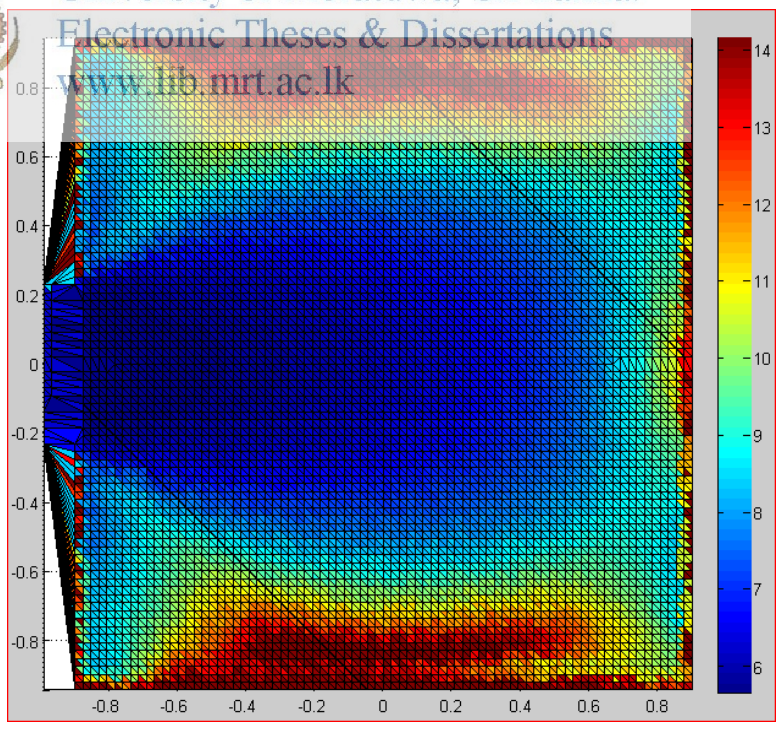

Figure 6.38: PPD_{NV} distribution on the horizontal plane at 0.6 m above the floor for ΔT= 25°C of CASE H

These velocity plots can be used to identify the areas which are difficult to ventilate by means of the buoyancy driven displacement ventilation. The velocity plots clearly show the effect of the chimney wall temperature on velocity distribution on the horizontal plane. These results will help to identify the areas which can be utilized for seating purpose in a naturally ventilated space. Further, the analysis also greatly helps building designers to examine the modifications need to the dimensions of inlet window to maximize the air flow distribution. The PPD_{NV} plots indicate the amount of area which can be naturally conditioned by means of natural ventilation.

The velocity variation relevance to 0.1 m inlet chimney height with the temperature difference for various cavity widths are shown in table 6.4 and plots in figure 6.39 respectively.

Table 6.4: Velocity variation with temperature difference for various cavity widths and 0.1 m fixed inlet height

Cavity width [m]	Temperature difference [˚C]					
	5	10	15	20	25	30
W 0.1	0.13	0.22	0.26	0.29	0.32	0.36
W 0.2	0.15	0.27	0.33	0.37	0.40	0.44
W 0.3	0.15	0.26	0.32	0.36	0.40	0.43
W 0.5	0.14	0.25	0.31	0.36	0.39	0.42

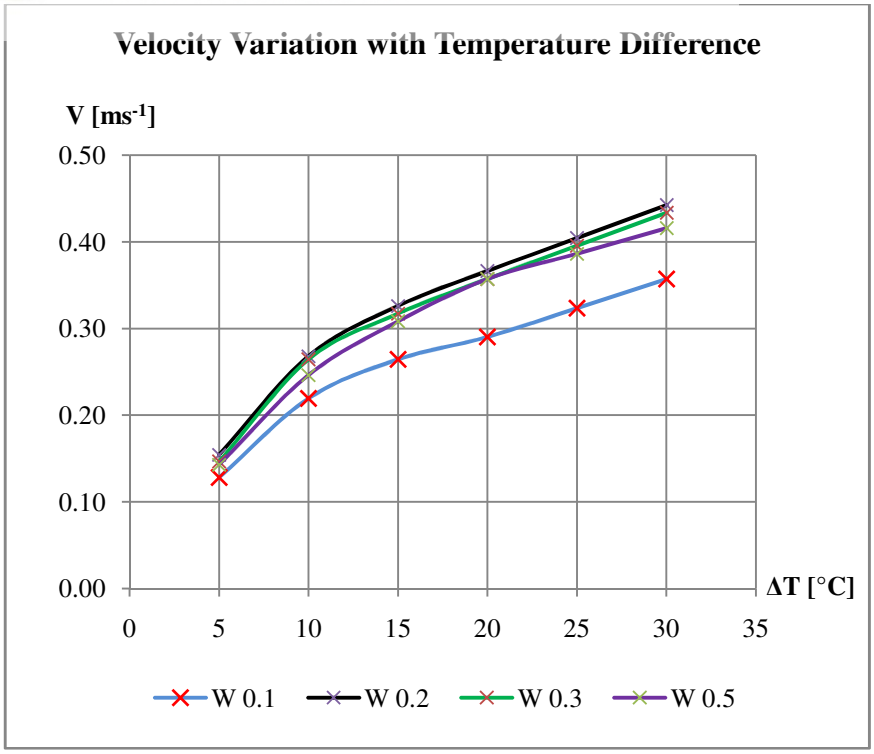

Figure 6.39: Velocity variation against temperature difference for each cavity with 0.1 m fixed inlet height

Figure 6.39 shows that mean velocity of the flow increases with the increase of the temperature difference between heated chimney wall and ambient air. A significant difference in the mean velocity can be clearly visualize for 0.2 m cavity width compared to 0.1 m cavity width, thereby meeting the optimum width for the corresponding inlet height. Beyond 0.2 m cavity width, the said variations are insignificant.

For a 0.4 m chimney inlet height, the velocity variation with temperature difference for various cavity widths are tabulated in table 6.5 and illustrates in the figure 6.40. The mean velocity values are considerably changed when cavity width changes from 0.1 m to 0.2 m and thereafter, values are slightly increases with the temperature difference.

Table 6.5: Velocity variation with temperature difference for various cavity widths and 0.4 m fixed inlet height

Cavity width [m]	Temperature difference [˚C]					
	5	10	15	20	25	30
W 0.1	0.13	0.21	0.25	0.30	0.33	0.36
W 0.2	0.16	0.29	0.35	0.42	0.44	0.46
W 0.3	0.17	0.30	0.38	0.43	0.46	0.48
W 0.5	0.19	0.33	0.42	0.46	0.48	0.51

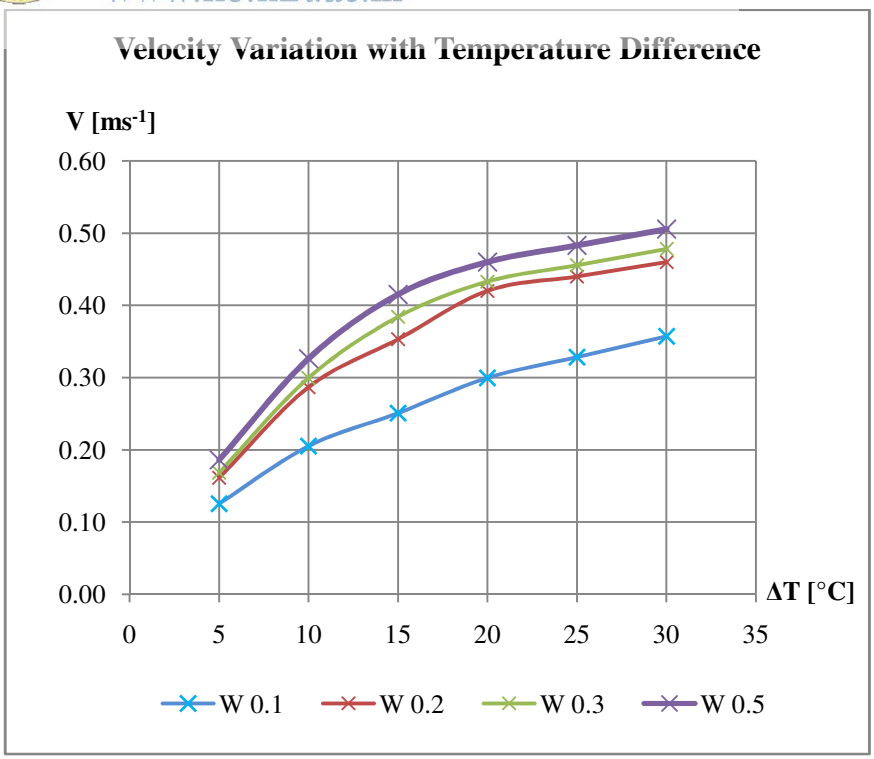

Figure 6.40: Velocity variation against temperature difference for each cavity with 0.4 m fixed inlet height

Air flow through the chimney was found to be affected by the width of the chimney and height of the chimney inlet. Air flow rates reduced as the width of the chimney widened. When the chimney width exceeded more than 0.3 m wide, it has been noticed that air flowing downwards through the chimney from its outlet. A reduction in the flow velocity was also observed when the cavity space was narrowed to less than 0.15 m, probably due to increased friction. The chimney inlet height also affected the air flow rate. As the height of the inlet was increased the velocity of the air flow increased.

Statistically it can be observed that the mean velocity of the flow maximises when the cavity width is between 0.2 m and 0.3 m. Increasing the cavity width from 0.3 m to 0.5 m shows a decline in the mean velocity of the flow which suggests that increasing the cavity width above 0.3 m may not be beneficial. However, considering the standard deviation the changes in mass flow rate may not be as significant as it appears.

The graphs also show that increasing the surface temperature increases the mean velocity of the air flow. This can be explained by the fact that with high surface temperatures, the air within the cavity gets hotter thereby reducing its density and increasing the bouncy pressure. However, considering the standard deviations, the results suggest that as the surface temperature is increased above 35˚C the increase in mass flow rate may not be significant as it appears on the graphs.

If the inlet height is reduced, and the cavity is widened, downward flow becomes significant. If the inlet height is increased and the width of the cavity is decreased, the hot air in the cavity will be replaced by cooler air from the inlet. Consequently, down flow becomes less significant. Upward flow takes place in layers close to the bounding surfaces. Outside these hot layers, in the centre, the air goes downward only when the cavity is wide.

For higher cavities, the mass flow will be greater. The height of the cavity in practice is limited to the height of the building. The observations played an important role in understanding the air flow mechanisms in the space and the cavity. The results showed the significance of a heated cavity in producing air currents. For optimum design, inlet height and cavity width are important parameters. To avoid down flow

the width of the cavity should be kept as narrow as possible within the limits specified.

According to ASHRAE 55- thermal comfort conditions, more than 70% of space falls within the range of 80% acceptable limit under the natural ventilation. In general, these results are accurate more than 95% when the temperature difference between heated surface of the wall and the ambient air is below 30^{o}C. Further, accuracy of the results tends to decrease with the increases of the temperature difference.

7 CONCLUSIONS AND RECOMMENDATIONS

7.1 Conclusions

Thesis described numerical investigations of the indoor airflows and temperature distributions in office space of buildings and the solar-assisted buoyancy-driven ventilation airflows in a simple geometry were carried out using Computational Fluid Dynamics (CFD) techniques. The numerical results obtained for the different designs were compared with the available experimental measurements and good agreement was obtained between the numerical predictions and the experimental measurements. The results obtained indicated that the CFD approach can be helpful in the preliminary design of an office spaces.

A few changes in the selected geometry were conducted based on the parametric study. The modified design of the building integrated with a chimney having a central plate 0.3 m wide cavity with distributed window over the wall was modelled and various flow situations of the buoyancy-driven ventilation were simulated.

Effect of convergence and divergence of the air flow at inlet to the window and outlet of the chimney respectively were taken in to account by modelling a surrounding environment of the room. Appropriate initial boundary conditions were applied to the model for simulation. It was assume that enclosure surface of the surrounding air of the room at rest with ambient pressure and temperature. All walls belonging to the room were assumed initially at rest on wall surfaces with environmental condition except heated surface of the chimney which was set to constant temperature which always higher than ambient temperature to make air flow through it. The conclusions for this part of the study are:

From the results obtained, it was noted that thermal comfort condition is improved up to 90% under the buoyancy driven ventilation. The PPD_{nv} (%) values indicate that only 9.3% of the occupants would not be satisfied with the thermal conditions on the horizontal plane at 0.6 m above the floor, but on the edges of the floor more than 20% of the occupants are dissatisfied with the thermal conditions. It was noticed that overall thermal conditions prevailing in the building due to buoyancy-driven ventilation are in the comfortable zone.

The calculated PPD_{NV} values indicates that most of the occupied areas of the office space are naturally conditioned and only a small percentage of less than 20% of the space is expected to be slightly uncomfortable in the region closer to the walls.

7.2 Recommendations for Future Work

The research described in this thesis has demonstrated the ability of CFD techniques to provide a fundamental understanding of the complex thermal phenomena inside office space and to analyze the ventilation strategies for such buildings. In order to give a complete picture of ventilation airflows and heat transfer in atria buildings, some extensions of the present work are recommended to be considered:

- The results of this study can be considered as being at the initial design stage of an energy efficient building that would provide a comfortable indoor thermal environment. Future research should include a study of the effects of wind speed and other climatic factors.
- Work to investigate the accuracy of CFD modelling for the buoyancy-driven flows in more complex spaces could be undertaken.
- The airflow pattern and temperature distributions in more complex buildings should be studied experimentally to provide further results the validation of CFD models. More controlled experimental studies of chimney performance are also required.

REFERENCES

Afonso, A. & Oliveira, A. 2000, "Solar chimneys: simulation and experiment", *Energy and Buildings*, vol. 32, pp 71-79.

Aris, R., 1989, "Vectors, tensors and the basic equations of fluid mechanics", Dover Publications, New York.

ASHRAE 2001, "ASHRAE Standard 55-1992 R, "Thermal environmental conditions of human occupancy", American Society of Heating, Refrigerating and Air-Conditioning Engineers, Atlanta, USA.

ASHRAE 1997, "ASHRAE Handbook Fundamentals", American Society of Heating, Refrigerating and Air-Conditioning Engineers, Atlanta, USA.

ASHRAE 2009, "ASHRAE Handbook", Chapter 9, Thermal Comfort.

Arce, J., Jimenez, M.J., Guzman, J.D., Heras, M.R., Alvarez, G. & Xaman, J. 2009, "Experimental study for natural ventilation on a solar chimney" *Renewable Energy*, vol. 34, pp 2928-2934.

Awbi, H.B. & Gan, G. 1992, "Simulation of solar-induced ventilation", *Renewable Energy Technology and the Environment*, vol. 4, pp 2016-2030.

Bansal, N.K., Mathur, R. & Bhandari, M.S. 1994, "Solar chimney for enhanced stack ventilation", *Building and Environment*, vol. 28, pp 373-377.

Barozzi, G.S., Imbabi, M.S.E., Nobile, E. & Sousa, A.C.M. 1992, " Physical and numerical modeling of a solar chimney-based ventilation system for buildings", *Building and Environment*, vol. 27, pp 433-445.

Bassiouny, R. & Koura, N.S.A. 2008, "An analytical and numerical study of solar chimney use for room natural ventilation" *Energy and Buildings*, vol. 40, pp 865-873.

Borgers, T.R. & Akbari, H. 1979, "Laminar flow within the Trombe wall channel", *Solar Energy*, vol. 22, pp 165-174.

Bouchair, A. 1994, "Solar chimney for promoting cooling ventilation in southern Algeria", *Building Services Engineering Research and Technology*, vol. 15, pp 81-93.

Boussinesq, J. 1877, "Theory the ecoulement turbullent", *Mem. Pre. par. div. Sav.,* vol. 23 , Paris.

Burek, S.A.M. & Habeb, A. 2007, "Air flow and thermal efficiency characteristics in solar chimneys and Trombe walls", *Energy and Buildings*, vol. 39, pp 128-135.

Charvat, P., Jicah, M. & Stetina, J. 2004, "Solar chimneys for ventilation and passive cooling", World Renewable Energy Congress, Denver, USA.

Chen, Z.D., Bandopadhayay, P., Halldorsson, J., Byrjalsen, C., Heiselberg, P. & Li, Y. 2003, "An experimental investigation of a solar chimney model with uniform wall heat flux", *Building and Environment*, vol. 38, pp 893-906.

Chen, Z.D. & Li, Y. 2001, "A numerical study of a solar chimney with uniform wall heat flux", In: Proceedings of the Fourth International Conference on Indoor Air Quality, Ventilation and Energy Conservation in Buildings, Human, China, pp 1447-1454.

Cheong, K. W. D., Djunaedy, E., Chua, Y. L., Tham, K. W., Sekhar, S. C., Wong, N. H. & Ullah, M. B. 2003, "Thermal comfort of an air-conditioned lecture theatre in the tropics", *Building and Environment*, vol. 8, pp. 63-73.

Deardorff, J.W. 1970, "A numerical study of three-dimensional turbulent channel flow at large Reynolds number", *Journal of Fluid Mechanics*, vol. 41, pp 453-480.

Ding, W., Hasemi, Y. & Yamada, T. 2005, "Natural ventilation performance of a double-skin façade with a solar chimney", *Energy and Buildings*, vol. 37, pp 411-418.

Eswaran, V. & Pope, S.B. 1988, " Direct numerical simulations of the turbulent mixing of a passive scalar", *Physics of Fluids*, vol. 31, pp 506-520.

Eswaran, V. & Pope, S.B. 1988, "An examination of forcing in direct numerical simulations of turbulence", *Computers and Fluids*, vol. 16, pp 257-278.

Fanger, P.O. 1970, Thermal Comfort, 1st Edition, *McGraw, Hill Book Co,* New York.

Fanger, P. O. & Toftum, J. 2002, "Extension of the PMV model to non-air conditioned buildings in warm climates", *Energy and Buildings*, vol. 34, pp. 533 - 536.

Ferziger, J.H. 1987, "Simulation of incompressible turbulent flows", *Journal of Computational Physics*, vol. 69, pp 1-48.

Gan, G. & Riffat, S.B. 1998, "A numerical study of solar chimney for natural ventilation of buildings with heat recovery", *Applied Thermal Engineering*, vol. 18, pp 1171 -1187.

Gan, G. 1998, "A parametric study of Trombe walls for passive cooling of buildings", *Energy and Buildings*, vol. 18, pp 1171-1187.

Gan, G. 2006, "Simulation of buoyancy-induced flow in open cavities for natural *ventilation", Energy and Buildings,* vol. 38, pp 410-420.

Gan, G. 2010, "Impact of computational domain on the prediction of buoyancy-driven ventilation cooling", *Building and Environment*, vol. 45, pp 1173-1183.

Givi, P. 1989, "Model-free simulations of turbulent reactive flow", *Prog. Energy Combust. Sci*., vol. 15, pp 1-107.

Gosman, A.D. & Ideriah, H.J.K. 1983, "A general computer program for two-dimensional turbulent recirculating flows", Technical report, Fluids Section, Department of Mechanical Engineering, Imperial College, London.

Harris, D.J. & Helwig, N. 2007, "Solar chimney and building ventilation", *Applied Energy*, vol. 84, pp 135-146.

Hanjalifc, K. & Launder, B.E. 1972, “A Reynolds stress model of turbulence and its application to thin shear layer flows", *Journal of Fluid Mechanics*, vol. 52, pp 609-638.

Harlow, F.H. & Nakayama, P. 1968, “Transport of turbulence energy decay rate", Technical Report Report LA 3854, Los Alamos National Laboratory, University of California.

Hinze, J.O. 1975, “Turbulence” McGraw-Hill, New York.

Hirunlabh, J., Kongduang, W., Namprakai, P. & Khedari, J. 1999, “Study of natural ventilation of houses by a metallic solar wall under tropical climate”, *Renewable Energy*, vol. 18, pp 109-119.

Ho Lee, K. & Strand, R.K. 2009, “Enhancement of natural ventilation in buildings using a thermal chimney”, *Energy and Buildings*, vol. 41, pp 615-621.

Jones, I.P. 1985, “The convergence of a simple iterative strategy for a strongly stratified flow”, Numerical methods in laminar and turbulent flow, pp 33-740.

Kavgic, M., Mumovic, D., Stevanovic, Z. & Young, A. 2008, “Analysis of thermal comfort and indoor air quality in the mechanically ventilated theatre”, *Energy and Buildings*, vol. 40, pp.1334-1343.

Khedari, J., Boonsri, B. & Hirunlabh, J. 2000, “Ventilation impact of a solar chimney on indoor temperature fluctuation and air change in a school building”, *Energy and Buildings*, vol. 32, pp 89-93.

Khedari, J., Rachapradit, N. & Hirunlabh, J. 2003, “Field study of performance of solar chimney with air-conditioned building”, *Energy*, vol. 28, pp 1099-1114.

Lam, C.K.G. & Bremhorst, K.A. 1981, “Modied form of the k - model for predicting wall turbulence", *Journal of Fluids Engineering*, vol. 103, pp 456-460.

Lane-Serff G.F., Linden P.F., Parker D.J. & Smeed D. A. 1991, “Laboratory modelling of natural ventilation via chimneys”, Proc. PLEA 91 Architecture and Urban Space, pp. 505-510.

Launder, B.E., Reece, G.J. & Rodi, W. 1975, “Progress in the development of a Reynolds Stress turbulence model”, *Journal of Fluid Mechanics*, Vol. 68, pp. 537–566.

Launder, B.E. & Spalding, D.B. 1972, Mathematical Models of Turbulence, Academic Press, London.

Launder, B.E. & Spalding D.B. 1974, “The numerical computation of turbulent flows”, *Computer methods in applied mechanics and engineering*, Vol. 3, pp. 269-289.

Li, R. & Pitts, A. 2006, “Thermal comfort and environmental modeling in atrium buildings”, PLEA2006-The 23rd Conference on Passive and Low Energy Architecture, Geneva, Switzerland.

Li, Y., & Xu, P., 2006 “Thermal mass design in buildings-heavy or light”, *International Journal of Ventilation*, vol. 5, pp. 143-149.

Martí-Herrero, J. & Heras-Celemin, M.R. 2007, "Dynamic physical model for a solar chimney", *Solar Energy*, vol. 81, pp 614-622.

Mathur, J., Bansal, N.K., Mathur, N.K., Jain, M. & Anupma. 2006, "Experimental investigations on solar chimney for room ventilation", *Solar Energy*, vol. 80, pp 927-935.

Moin, P. & Kim, J. 1982, "Numerical investigation of turbulent channel flow", *Journal Fluid Mechanics*, vol. 118, pp 341-377.

Murakami, S., Mochida, A. & Hibi, K. 1987,"Three-dimensional numerical simulation of air flow around a cubic model by means of large eddy simulation", *Journal of Wind Engineering and Industrial Aerodynamics*, Vol. 25, pp. 291-305.

Murakami, S.1997, Overview of turbulence models applied in CWE-1997, 2nd, EACWE, Italy, pp.3-23.

Nouanégué, H.F. & Bilgen, E. 2009, "Heat transfer by convection, conduction and radiation in solar chimney systems for ventilation of dwellings", *International Journal of Heat and Fluid Flow*, vol. 30, pp 150-157.

Ong, K.S. & Chow, C.C. 2003, "Performance of a solar chimney", *Solar Energy*, vol. 74, pp 1-17.

Oosthuizen, P. H. & Lightstone, M. 2009, "Numerical analysis of the flow and temperature distributions in an atrium", Proceedings of the Int. Conference on Computational Methods for Energy Engineering and Environment-ICCM3E, Sousse.

Punyasompun, S., Hirunlabh, J., Khedari, J. & Zeghmati, B. 2009, "Investigation on the application of solar chimney for multi-storey buildings", *Renewable Energy*, vol. 34, pp 2545-2561.

Rodrigues, A.M., Canha da Piedade, A., Lahellec, A. & Grandpeix, J.Y. 2000, "Modeling natural convection in a heated vertical channel for room ventilation", *Building and Environment*, vol. 35, pp 455-469.

Rogallo, R.S. & Moin, P. 1984, "Numerical simulation of turbulent flows, *Annual Review of Fluid Mechanics*", vol. 16, pp 99-137.

Rogers, M.M. & Moin, P. 1987, "The structure of the vorticity field in homogeneous turbulent flows", *Journal of Fluid Mechanics*, vol. 176, pp 33-66.

Rotta, J.C. 1951, "Statistiche Theorie nichthomogener Turbulenz", *Z. Phys*., vol. 129, pp 547-572.

Shih, T.H., Liou, W.W, Shabir, A., Yang, Z., & Zhu, J. 1994, "A new k ¡ ²eddy viscosity model for high Reynolds number turbulent flows", NASA TM 106721.

Spencer, S., Chen, Z.D., Li, Y. & Haghighat, F. 2000, "Experimental investigation of a solar chimney natural ventilation system", In: Proceedings of Room Vent, Seventh International Conference on Air Distribution in Rooms, Reading, UK, pp.813-818.

Speziale, C.G. 1987, "On non-linear k¡l and k¡² models of turbulence", *Journal of Fluid Mechanics*, vol. 178, pp 459-475.

Stamou, A., & Katsiris, I. 2006, "Verification of a CFD model for indoor airflow and heat transfer", *Buildings and Environment*, vol. 41, pp. 1171–1181.

Stavrakakis, G., Koukou, M., Vrachpoulos, M.G. & Markatos, N.C., 2008, "Natural cross- ventilation in buildings: Building-scale experiments, Numerical simulation and thermal comfort evaluation" *Energy and Buildings*, vol. 40, pp.1666-1681.

Tahir, A. & Osman, Y. 2005, "Investigating the potential use of natural ventilation in new building design", *Energy and buildings*, vol. 38, pp. 959-963.

Tennekes, H. & J.L., Lumley. 1972, "A first course in turbulence" The MIT Press, Cambridge, Massachusetts.

Tsou, J. Y. 2001, "Strategy on applying computational fluid dynamic for building performance evaluation", *Automation in Construction*, vol. 10, pp.327–335.

Versteeg, H. K. & Malalasekera, W. 2007, An Introduction to Computational Fluid Dynamics, The Finite Volume Method, Second Edition , Pearson Education Limited, UK.

Walker, C. E. & Gliksman, L. R., "Reduced scale air modeling technique for naturally ventilated Buildings", *Research in Building physics and Building Engineering*, Taylor and Francis Group.

Walsh, P. C. & Leong, W. H. 2004, "Effectiveness of several turbulence models in natural convection", *International Journal of Numerical Methods for Heat and Fluid Flow,* vol. 14, pp 633-648.

Wang, Z., Yi, L. & Gao, F. 2009, "Night ventilation control strategies in office buildings", *Solar Energy*, vol. 83, 1902-1913.

Wilcox, D. C. 1998, "Turbulence Modeling for CFD", *DCW Industries, Inc.*, La Canada, California.

Wilson S. & Hedge A. 1987, "The office environment survey: A study of building sickness", London: Building used studies limited.

Xin, W., Huang, C. & Weiwu, C. 2009, "Mathematical modeling and experimental study on vertical temperature distribution of hybrid ventilation in an atrium building", *Energy and Buildings* vol. 41, pp. 907-914.

Yakhot, V. & Orszag, S. A. 1986, "Renormalization group analysis of turbulence, Basic Theory", *Journal of Scientific Computing,* vol. 1, pp. 1-51.

Yakhot, V., Orszag, S.A., Thangam, S., Gatski, T.B., & Speziale, C.G. 1992, "Development of turbulence models for shear flows by a double expansion technique", *Physics of Fluids*, vol. 4, pp 1510-1520.

Yam, J., Li, Y. & Zheng, Z. 2003, "Nonlinear coupling between thermal mass and natural ventilation in buildings", *International Journal of heat and mass transfer,* vol.46, pp. 1251-1264.